

Alma Mater Studiorum – Università di Bologna

DOTTORATO DI RICERCA IN

Meccanica e Scienze Avanzate dell'Ingegneria

Ciclo XXXII

**Settore Concorsuale: 09/C1**

**Settore Scientifico Disciplinare: ING-IND/08**

# Modelling and Optimization of Energy Management Strategies for Hybrid Vehicles

**Presentata da:**  
Gabriele Caramia

**Coordinatore Dottorato**

**Prof. Ing. Marco Carricato**

**Supervisore**

**Prof. Ing. Nicolò Cavina**

**Esame finale anno 2020**

*To Denise and my family*

# *Abstract*

In the last decades the automotive sector has seen a technological revolution, due mainly to the more restrictive regulation, the newly introduced technologies and, as last, to the poor resources of fossil fuels remaining on Earth.

Promising solution in vehicles' propulsion are represented by alternative architectures and energy sources, for example fuel-cells and pure electric vehicles. The automotive transition to new and green vehicles is passing through the development of hybrid vehicles, that usually combine positive aspects of each technology. In this scenario, Hybrid Electric Vehicles are the most established solution, mainly for the benefits gainable in including electric machines on-board a standard combustion powertrain. Electrical auxiliary power unit can, for example, recover energy during braking phases and support the engine in high power-demanding driving conditions.

To fully exploit the powerful of hybrid vehicles, however, it is important to manage the powertrain's degrees of freedom in the smartest way possible, otherwise hybridization would be worthless. To this aim, this dissertation is focused on the development of energy management strategies and predictive control functions. Such algorithms have the goal of increasing the powertrain overall efficiency and contextually increasing the driver safety.

Such control algorithms have been applied to an axle-split Plug-in Hybrid Electric Vehicle with a complex architecture that allows more than one driving modes, including the pure electric one. The different energy management strategies investigated are mainly three: the vehicle baseline heuristic controller, in the following mentioned as rule-based controller, a sub-optimal controller that can include also predictive functionalities, referred to as Equivalent Consumption Minimization Strategy, and a vehicle global optimum control technique, called Dynamic Programming, also including the high-voltage battery thermal management.

During this project, different modelling approaches have been applied to the powertrain, including Hardware-in-the-loop, and diverse powertrain high-level controllers have been developed and implemented, increasing at each step their complexity. It has been proven the potential of using sophisticated powertrain control techniques, and that the gainable benefits in terms of fuel economy are largely influenced by the chose energy management strategy, even considering the powerful vehicle investigated. Moreover, it has also been assessed the potential of including predictive driving information within the powertrain control, showing interesting results both for the vehicle overall efficiency and pollutant emissions production reduction.

# *Acknowledgments*

First of all, I would like to express my gratitude to Prof. Ing. Nicolò Cavina, for having believed in me and given me the chance to join the challenge of a PhD course. His technical and human support have been fundamental during these years, as well as his example of how an engineer should work to be expert in his field.

A special thank also goes to Ing. Michele Caggiano, for having encouraged my work in any phase. With his curiosity and innovative thinking, he has taught me the strict correlation between high level research and industrial application.

I'm also thankful to Dr. Ing. Luca Solieri, for having given me the chance to join a European Project together with such high-level engineering partners and having always supported my activities with a critical and stimulating approach.

A human thanks also deserve all the colleagues of the Department of Industrial Engineering, for having made this PhD a journey sheared with wonderful people.

Last but not least, a thinking to the colleagues from the newly born Green Mobility Research Laboratory, it has been a pleasure to share ideas with you, knowledge and time. I hope that you will get satisfactions from your work and will always getting better.

# *Contents*

## *I. Introduction*

## *II. Overview*

<b>1</b>	<b>Hybridization</b>	<b>2</b>
1.1	Electric Hybridization	2
1.1.1	Powertrain configuration	2
1.2	HEVs' powertrain control	4
1.2.1	Heuristic Control	5
1.2.2	Sub-optimal Control	6
1.2.3	Optimal Control	7
<b>2</b>	<b>Vehicle connectivity and prediction horizon</b>	<b>9</b>
2.1	Vehicle sensors	9
2.1.1	Camera System	9
2.1.2	Radar System	9
2.1.3	Lidar System	10
2.2	Vehicle communication	10
2.2.1	V2V communication	10
2.2.2	V2I communication	11
2.2.3	V2X communication	11
2.3	Prediction Horizon	12
	<i>III. Powertrain Modelling</i>	
<b>3</b>	<b>Powertrain architecture</b>	<b>13</b>
<b>4</b>	<b>Analytic Powertrain consumption model</b>	<b>14</b>
4.1	Vehicle dynamics	14
4.2	Wheels level	14
4.3	Front axle	15
4.4	Rear axle	16
4.5	Battery model	16
<b>5</b>	<b>Model in the Loop</b>	<b>18</b>
5.1	Engine model	18
5.2	Electric motor model	19
5.3	Battery	20
5.4	Transmission	21
<b>6</b>	<b>Hardware in the Loop</b>	<b>22</b>

<b>7</b>	<b>Model Validation</b>	<b>23</b>
7.1	MiL vs experimental data	23
7.2	Analytic model vs MiL	23
<b><i>IV. Powertrain Supervisory Control</i></b>		
<b>8</b>	<b>On-line controllers</b>	<b>25</b>
8.1	Rule-based strategy	25
8.1.1	Overview	25
8.1.2	Implementation	25
8.2	Equivalent Consumption Minimization Strategy	26
8.2.1	Overview	26
8.2.2	Implementation	28
8.2.3	Battery SOC Management Strategies	29
8.3	Online controller results	32
8.3.1	RBS results	32
8.3.2	ECMS results	33
8.3.3	RBS vs ECMS comparison	34
<b>9</b>	<b>Predictive control functions</b>	<b>38</b>
9.1	Predictive State of Charge Management Strategy	38
9.1.1	Algorithm	38
9.1.2	ECMS-CS vs ECMS-predictive-CS	39
9.1.3	Battery capacity influence on ECMS-predictive-CS performance	41
9.2	Predictive NO <sub>x</sub> emission control of a Diesel-HEV	43
9.2.1	Modelling	44
9.2.2	Control	46
9.2.3	Results	47
<b>10</b>	<b>Optimal Powertrain Control</b>	<b>53</b>
10.1	Dynamic Programming	53
10.1.1	Overview	53
10.2	DP Application to PHEVs	55
10.2.1	Control variables influence on powertrain operation	57
10.2.2	Algorithm Implementation	58
10.2.3	Results vs RBS and ECMS	60
10.3	Combined optimization of Energy and HV battery thermal management	64
10.3.1	Battery cooling circuit	64
10.3.2	Battery Model	65
10.3.3	Rule based battery Thermal Management	66
10.3.4	Optimal control problem formulation	67

10.3.5	Control variables influence on powertrain operation	68
10.3.6	Algorithm Implementation	69
10.3.7	Results	71

## ***V. Hardware in the Loop Implementation***

<b>11</b>	<b>HiL testing</b>	<b>77</b>
11.1	Real-time RBS vs Real-time ECMS	77
11.1.1	Vehicle parameters	78
11.1.2	Performance comparison	79

## ***VI. Conclusions***

# ***I. Introduction***

In recent years the automotive market has seen dramatic changes in the homologation regulations, both for pollutants emissions and for fuel consumption, i.e. carbon dioxide production. To face these restrictive legislations academic researchers and automotive manufacturers have proposed different solutions, in terms of powertrain architectures, vehicle control and driver assistance systems.

Concerning the propulsion, innovative developments have regarded both the engine and the overall vehicle system. At the engine level different solutions can be cited: the engine down-sizing and down-speeding, variable valve timing and lifting, water injection, RCCI combustions. At vehicle level, instead, the most promising solution is the powertrain hybridization/electrification.

Regarding general vehicle control, promising applications of predictive control have been implemented by means of on-board and wireless vehicle connectivity for future driving conditions estimation.

To even improve the drivers' safety and the comfort, assistance systems and functionalities have been added to standard vehicles.

In this scenario, this dissertation aims to investigate the potential benefits coming from the combination of different approaches, among the aforementioned ones, with the final goal of reducing the vehicle overall energy consumption or, equivalently, to increase the tank-to-wheel global efficiency.

In the first chapter it is presented a short but necessary overview of the thesis topic, to point out which are the fundamental characteristics of hybrid electric vehicles, with a focus on their control and their possible connection to the environmental impact.

Then, the following section deals with the description of the powertrain taken into account for the research activities, showing its characteristics, the diverse approaches used to model it, and the vehicle simulation environment.

In the third chapter are detailed all the controllers, both predictive and causal (non-predictive), implemented as energy management strategies for the vehicle under study. This section can be considered the main core of this dissertation and collects all the main results obtained during this three-years-long research.

To further underline the potential benefits achieved in simulation and the stability of the implemented controllers, the fourth section shows the causal controllers testing and validation phases in a hardware-in-the-loop environment.

The main contribution of this thesis relies on the implementation of well-known energy management strategies for hybrid vehicle for a complex powertrain architecture with many degrees of freedom in providing propulsion, together with some innovative approaches to the powertrain control optimization.

## *II. Overview*

### **1 Hybridization**

As hybrid powertrain it is usually intended a vehicle architecture that includes at least one additional energy source and one or more auxiliary energy converters, that contribute directly or indirectly to the vehicle propulsion and support the conventional Internal Combustion Engine (ICE) operation [1-3].

According to the nature of the auxiliary energy source, the hybridization can be:

- Hydraulic [4], where the auxiliary energy storage system is a hydraulic accumulator and the energy converter is a hydraulic motor/pump. Usually this solution is suitable for heavy-duty application, because of the weights and sizes of the additional components.
- Pneumatic [5], in which the engine is used both as a thermal machine in standard conditions and as pneumatic machine in idle or low load conditions.
- Kinetic [6], that foresees the usage of a high-speed flywheel both to accumulate and provide the recovered energy.
- Electric [7], including a battery or super-capacitors for the energy storage and electric motor/generator as energy converter.

Considering the powertrain flexibility and the benefits achievable by adopting this solution, the electric one has become the most widespread hybridization [8].

#### **1.1 Electric Hybridization**

Hybrid electric vehicles (HEVs) usually include a conventional internal combustion engine and one or more electric machines. The energy stored on board is: chemical, flowing from the fuel tank to the engine; electrochemical flowing from the battery to the electric machines and vice versa.

The major advantage in developing HEVs consists in combining the characteristics of pure-electric and conventional ICE-based vehicles, allowing to reduce the fuel consumption. The main benefits related to HEVs are:

- the possibility to recover energy during braking phases instead of using mechanical brakes to dissipate it as heat;
- the avoidance of idling phases for the engine, switching it-off when it is not needed and restarting it using the electric machine. This functionality is commonly known as Stop/Start.;
- a better management of the power required to the engine, using the electric machine for low demanding conditions (in terms of speed and loads) or performing the so-called “load point shift”, which consists in augmenting the torque requested to the engine, in order to increase its specific efficiency, and use a part of such power to recharge the battery;
- eventually, downsize the engine and using the electric machine as booster.

##### **1.1.1 Powertrain configuration**

According to the size of the electric energy storage system and electric machines, different hybridization level can be defined [1-2]:

- Micro Hybrid, in which the electric machine is an integrated starter generator (only Stop/Start and recuperation capabilities).
- Mild Hybrid, where the small size of the electric components allows limited manoeuvres in pure-electric mode.

- Full Hybrid, which includes powerful motors and large battery sizes; in this case pure-electric mode is admissible.
- Plug-in Hybrid, the powertrain architecture is similar to full-hybrid, but the battery can be externally recharged and is typically larger.
- Range-extender electric vehicles, for which the electric propulsion is the main contribution to the propulsion and the engine is the auxiliary energy converter.

For HEVs three powertrain architectures can be defined considering their structure: series, parallel and power-split [8].

In Series HEVs, the engine can be considered as the auxiliary power unit, since it is not directly coupled to the wheels, but it only provides torque to an electric generator. For this kind of vehicles, the electric energy is always the primary mover. The energy flow principle of Series HEV is depicted in the following Fig.1.1, where ICE is the internal combustion engine, MG1 and MG2 are two electric motor/generator, BAT is the battery and the output is the mechanical power that reaches the wheels.

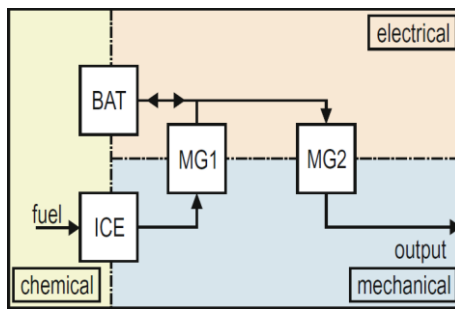


Figure 1.1. Series HEV energy flow ([8])

Parallel-HEV, instead, can have diverse configurations according to the position of the electric machine, while the engine is always mechanically coupled to the wheels through the transmission chain. In this category, all the aforementioned hybridization levels can be reached. For Parallel HEVs the energy flowing in the vehicle can be schematized as in Fig.1.2.

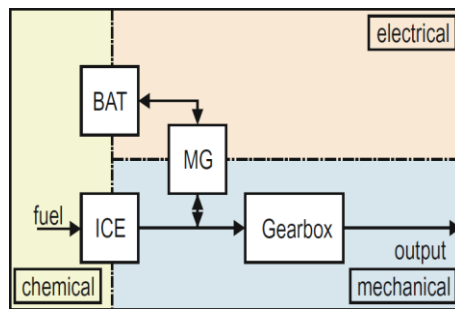


Figure 1.2. Parallel HEV energy flow ([8])

Power-split architecture, instead, foresees the possibility of managing the powertrain both in series and parallel configurations. To do so, it is needed a particular transmission technology, called planetary-gear, also mentioned as power-split device. Despite the high flexibility of such powertrains, the complexity of the vehicle control increases due to the highest number of degrees of freedom, as underlined by Fig. 1.3.

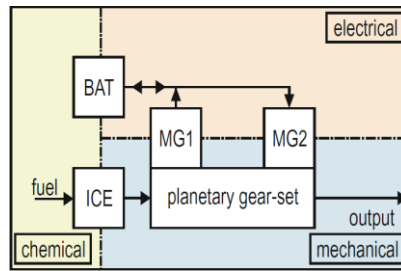


Figure 1.3. Power-split HEV energy flow (18)

In Fig.1.4 are summarized all the possible driving modes, hybridization levels and powertrain configurations that characterize HEVs [8].

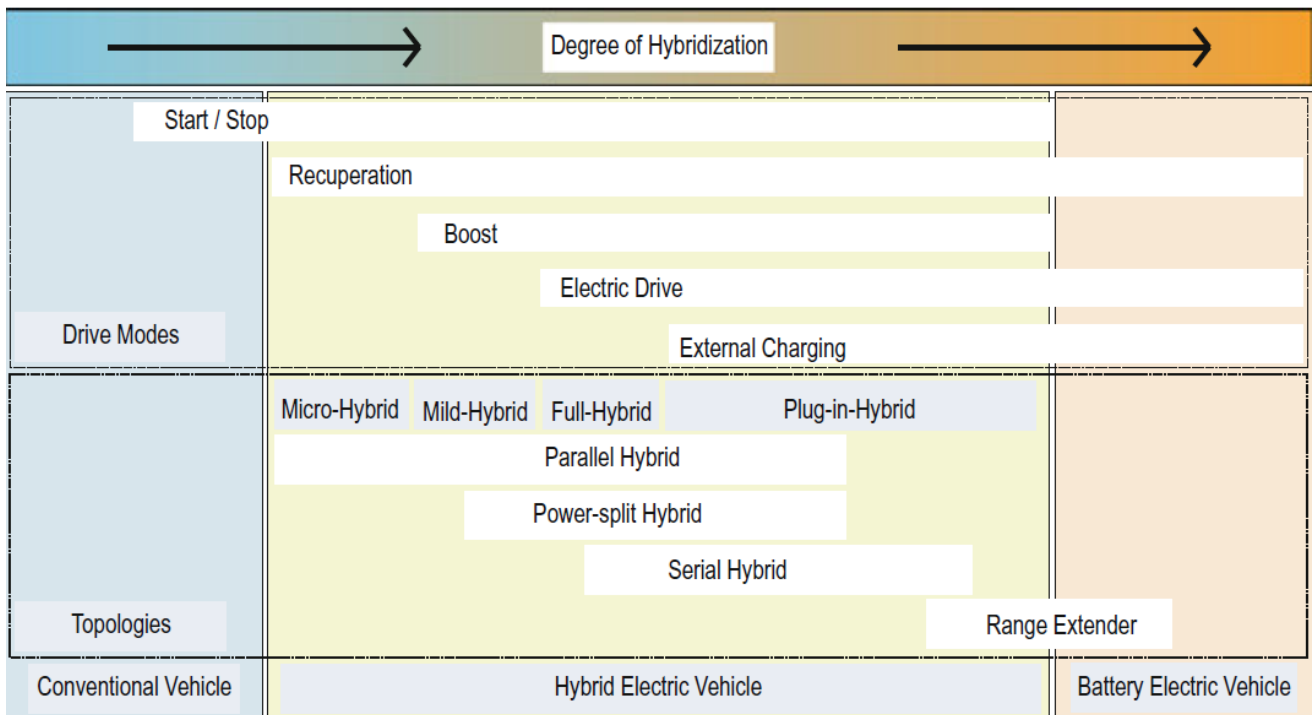


Figure 1.4. Overview of HEV characteristics (18)

## 1.2 HEVs' powertrain control

The control architecture of a HEV is usually referred to as hierarchical, since it usually includes one control unit for each main component, i.e. the engine, the electric motor, the battery and the transmission, plus a supervisory controller, usually mentioned as Hybrid Control Unit (HCU) or Vehicle Control Unit (VCU). As clarified by Fig.1.5, the HCU receives in input the driver's request and manages the lower-level controllers in order to satisfy such request according to the powertrain actual conditions. Within the supervisory controller it is implemented the Energy Management Strategy (EMS), which is the control algorithm that defines the torque distribution between the energy sources available in the powertrain.

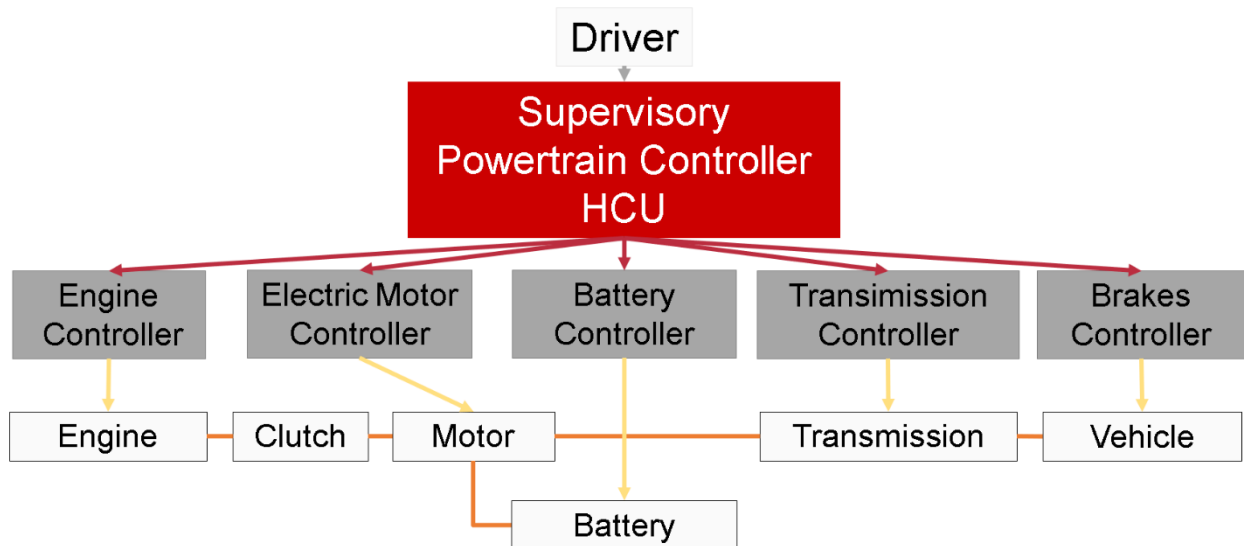


Figure 1.5. HEV's powertrain control architecture

More in detail, the HCU has to collect and respect all the constraints, both from components physical limitations and from the actual driving conditions, defining the target of the component's controllers, according to the implemented EMS. This latter has a large impact on HEV's energy consumption, since the additional degrees of freedom gained with the hybridization can be managed in order to improve the vehicle global efficiency.

The complexity of the implemented EMS depends mainly on the powertrain configuration and, most important, its development approach. There are, in fact, different ways to define the EMS for a HEV and they can be categorized according to their usage of optimal control theory. In this sense, it can be made the following distinction [1]:

- Heuristic controller, no usage of optimal control theory;
- Sub-optimal controller, local optimization of the energy management;
- Optimal controller, based on optimal control theory.

### 1.2.1 Heuristic Control

Heuristic controllers are commonly not optimization-based, but rather they include a series of rules that define powertrain management. According to the actual values of meaningful vehicle parameter, i.e. the battery state of charge and temperature, the vehicle speed and the torque requested at the wheels, ..., the EMS derives the control actions to be performed and generates the targets for the component controllers, for example the torque to be provided by each of the machines included in the vehicle.

The rules are commonly defined according to the developer experience, powertrain architecture and limitations and, in general, with the idea of maximizing the efficiency of each component.

Generally speaking, this category of EMS is fast, robust and highly real-time capable, therefore it is even the most wide-spread solution among car manufacturers. However, on the other hand, a large calibration effort is needed to tune the thresholds of the rules [9-10] and, since no optimal control theory is used in such controllers, their performances are usually quite far from optimality.

Interesting works in literature [11-13] have used optimization techniques to derive the rules to be implemented in the heuristic controller, somehow aiming to replicate on-line the optimal control policy.

### 1.2.2 Sub-optimal Control

To this EMS category belong all the controllers that make use of the optimal control theory defining and solving the problem instant by instant. Therefore, in the end, the global solution will be a sequence of local optimum solutions, which doesn't guarantee the global optimum [14].

The following control policies belong to this category:

- Equivalent Consumption Minimization Strategy (ECMS);
- Model Predictive Control (MPC);

#### *Equivalent Consumption Minimization Strategy*

ECMS-based controller derives from the Pontryagin's Minimum Principle (PMP), which is an analytic method for the minimization/maximization of a given cost-function [15]. Within the sub-optimal controller, this control strategy is the most well-known and investigated among researchers on HEVs [16]. At the basis of ECMS there is the assumption that it is possible to convert, by means of an "equivalence factor", the electrical power consumption in virtual fuel consumption. Then, the sum of the actual fuel consumption of the engine plus the virtual consumption related to the battery usage becomes the cost-function to be instantaneously minimized. Many works in literature have proven the capability of such EMS in terms of fuel economy, in most cases not so far from the optimal solution [1,16]. The main potential of such controller relies on the relatively simple implementation and reduced calibration effort, even if its performances are hugely influenced by the definition of equivalence factor, as demonstrated in the following chapters of this dissertation.

#### *Model Predictive Control*

The MPC loop is a receding horizon optimization algorithm that makes use of system predicted information. To implement it as energy management strategy of a HEV, the algorithm foresees the followings steps. Inside the loop there is a simplified vehicle model fed with historical driving data, and it is used to predict the velocity profile over the finite prediction horizon. Once the vehicle speed and acceleration have been estimated, the optimal control sequence for the time interval of the horizon can be calculated. The first element of the optimal control sequence is applied to the powertrain control, then the MPC restarts from the beginning, updating the driving historical data according to the actual feedback from the powertrain [17-18].

Following the scheme in Fig.1.6, at each step time  $k$ , the reference state  $r_k$  is given to the controller, then the optimization algorithm calculates the optimal control action sequence  $u_{k:k+N}$  for the prediction horizon. The first control action  $u_k$  is used to feed the plant, which is the powertrain in HEVs case, and the powertrain model inside the loop. The first model output  $\hat{y}_k$  is compared to the plant output  $y_k$ , the error is used to update the model. The second output of the model is used as state input for the next iteration  $\hat{y}_{k+1}$ .

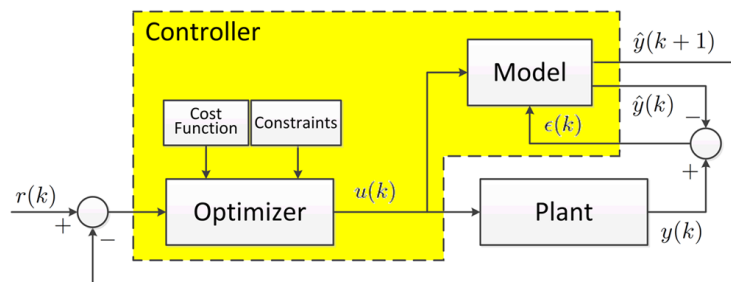


Figure 1.6. MPC loop

### 1.2.3 Optimal Control

Thinking at HEVs as complex dynamic systems that evolve over a driving mission, it is possible to define an optimal control problem in order to minimize a given cost-function, for example the fuel consumption.

Generally speaking, to perform a global optimization on a given driving mission, all the problem variables that are independent from the powertrain operation must be known a priori. Such particular characteristic makes optimization-based controllers suitable only for off-line implementation, but on the other hand they guarantee the global optimal control, being useful for benchmarking other controllers.

As optimal EMSs can be mentioned:

- Pontryagin's Minimum Principle (PMP);
- Convex Optimization (CVX);
- Dynamic Programming (DP);

#### *Pontryagin's Minimum Principle*

The Pontryagin's Minimum Principle is a theorem that aims to solve a global optimal control problem by redefining it using differential equations that represent instantaneous conditions and local minimization. To keep the global intent of the minimization, boundary conditions are imposed both for the starting and ending times, indeed it cannot be considered as a dynamic evolving system control problem [14].

The problem formulation only provides necessary conditions for optimality and, even they are not sufficient, they can be applied to search for candidates to solve the optimal control problem. The candidates that fulfil all the local conditions of the problem are identified as "extremal controls". The PMP assesses that, if an optimal control policy exists, then it is an external control and, considering that usually only one solution is admissible for the optimization problem, if there is only one extremal solution, then clearly it is the optimal control policy, while if there are more than one solution, the optimal one is the one that gives as results the lowest global cost.

The main drawback of this approach is related to the analytic formulation of the problem, which means the equations included in the optimal control problem have to be derived from a simplified system model. As a consequence, if the simplification makes the model too poor in accuracy, the system representation is not effective, and the optimal control policy found becomes sub-optimal for the real system.

#### *Convex Optimization*

In the last few years CVX approach has raised attention in the development of EMS for hybrid vehicles mainly for its computational efficiency. This optimization technique is based on the assumption that the energy management problem can be formulated in a convex form. The key points for defining a CVX problem are [19]:

- exclude from the optimization decisions regarding discrete or integer control variables, i.e. the engine on/off status and the gear-ratio;
- discretize the problem in time domain;
- model the powertrain components in a convex way [20];

The substantial advantage of this optimization algorithm, if compared to other techniques, relies on the fact the computation effort needed to solve the problem is independent from the number of system states included in the optimization. Author of [21] have also proposed to use CVX for the parametric optimization of HEVs components sizing.

## ***Dynamic Programming***

Dynamic Programming algorithm directly derives from Bellman's principle of optimality [22]. To solve a DP problem, as for the other optimal control techniques, it is necessary to know in advance the driving condition for the complete horizon. The numerical solution of the optimal control problem allows to find a global optimal solution without any simplification of the model and including its nonlinearities but, given the iterative nature of the DP, the computational effort increases with the number of variable added to the problem, both as system state variable or control variable [23]. When dealing with dynamic programming algorithm as EMS for HEVs, the problem formulation must include the following variables:

- Disturbances, which are independent from the powertrain operation, for example the vehicle speed and the road slope profiles for the chosen driving mission;
- State Variables, that are the parameters considered as representative for the powertrain status;
- Control Variables, including all the control actions that are the object of the optimal control problem solution;
- Cost-function, is the mathematical formulation of the powertrain operational cost over the mission and needs to be minimized to find the global optimal solution.

In the following chapters this optimization technique will be further discussed and implemented.

## 2 Vehicle connectivity and prediction horizon

As already mentioned in the introduction, together with the powertrain hybridization and its control optimization, interesting steps forward have been done in terms of vehicle connectivity [24] to further improve the vehicle overall efficiency by predicting in advance the future driving conditions and manage consequently the powertrain operation. The idea behind the usage of external information within the vehicle is to, somehow, limit the drivers' influence on the fuel economy, for example advising upcoming queues, stop events, traffic lights, roundabouts, and low speed zones. Moreover, if the car is capable of predictive control, data concerning the surrounding environment are fundamental input for the implemented energy management strategy.

### 2.1 Vehicle sensors

There are different technologies available in the automotive market to predict the route a-head of the vehicle, each of them with its own characteristics and capabilities. The solutions chosen to set the vehicle communication and horizon reconstruction depend on the signals or data the vehicle aims to acquire. In this sense, the following ones can be cited:

- Preceding vehicle, in terms of speed and distance;
- Stop events, such as traffic signs or road intersections;
- Weather conditions, important for the speed limitations;
- Obstacles on the route, for anti-collision features development.

According to the meaningful information that can be collected, different sensors can be installed on-board, such as:

- Cameras systems (CS);
- Radar systems (RS);
- Lidar systems (LS);

#### 2.1.1 Camera System

Cameras are not communication systems, they simply reconstruct information by “observing” the surrounding scenario. Such fundamental characteristic has led cameras to become an immediate solution for car manufacturers, together with the maturity of the sensors itself. In fact, CS are composed by a visual sensor (camera) plus hardware and software to process the acquired images in order to identify objects nearby the vehicle. Modern applications of cameras are able to detect not only the presence of other vehicles (cars, trucks, motorcycles, ecc.), pedestrian and obstacles in general, but also the presence and meaning of traffic signals [25-27]. Given the working principle of such technology, their potential can be limited by the presence of dust or dirt on the camera lens, as well as particular weather conditions, such as fog, rain and snow [28]. The fuel consumption reduction potential of CS is not widely investigated in literature and they are mainly considered for safety features [29].

#### 2.1.2 Radar System

Radars are a well-known solution for object detection in many applications, including automotive. As for CS, RS don't communicate with other parties but simply detect the presence of objects in the surrounding of the vehicle [30]. The working principle of a radar sensor is quite simple: a radio wave is emitted by the sensor and, if there is an object in the radar range, the emitted wave would be reflected, reaching back the vehicle. According to the characteristic of the reflected signal, it is possible to detect the distance between the vehicle and the object and the relative velocity. The effectiveness of such sensors highly depends on the range and

precision of the object and speed detection. As well as CS, radars are considered a reliable and robust technology and their presence is quite common in modern vehicles. By integrating information from radars and cameras systems, it is possible to overcome the weak points of the single solution [31-32]

### 2.1.3 Lidar System

Lidar is the acronym for Light Detection and Ranging and it is a technology for object detection quite similar to radars, with the only difference that in LS the emitted wave is a laser, instead of a radio wave. Lidars usually offer a detailed object detection with a higher angular range, while radars are a more mature and less expensive solution [33].

Fig. 2.1 is a representative example for vehicle sensors installation and application.

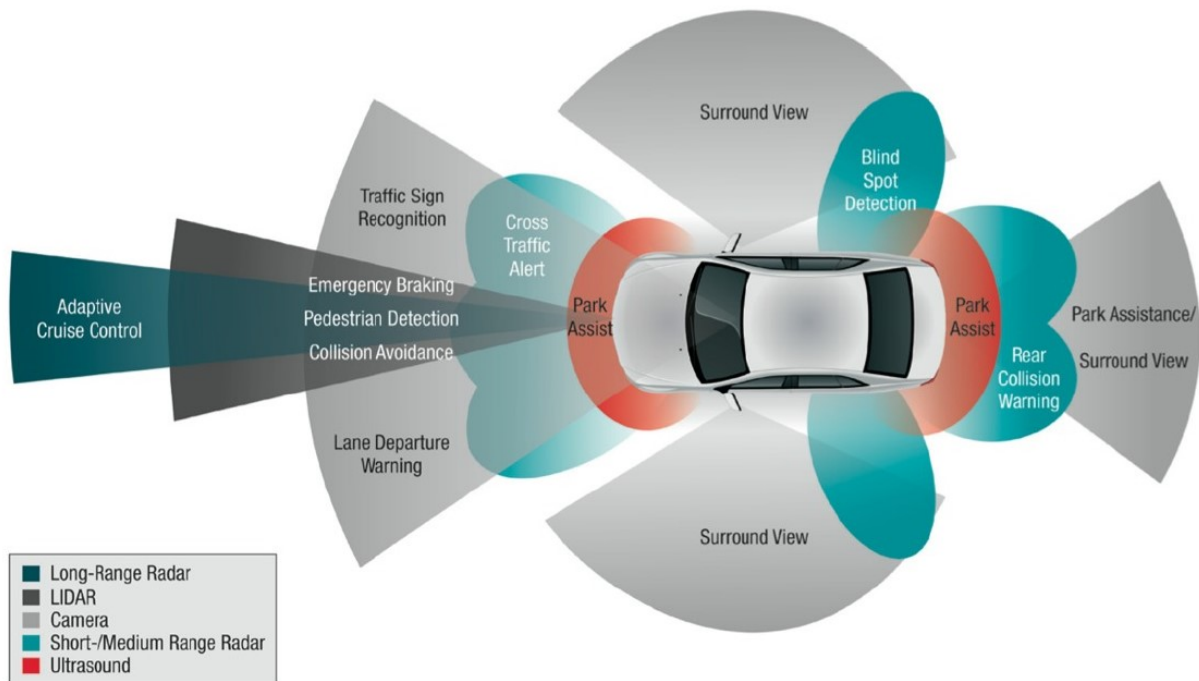


Figure 2.1. Vehicle sensors integration

## 2.2 Vehicle communication

Aiming to predict the future driving conditions, interesting solutions have been proposed in order to exchange information between the vehicle and external environment. In addition to the vehicle sensing configuration proposed in the previous paragraph, important steps forward have been made in terms of vehicle communication capabilities [34].

The most investigated solutions are:

- Vehicle-to-Vehicle (V2V) communication;
- Vehicle-to-Infrastructure (V2I) communication;
- Vehicle-to-Everything (V2X) communication.

### 2.2.1 V2V communication

The Vehicle-to-Vehicle module installed on-board provides information regarding other vehicles in the same driving environment, such as their actual speed, acceleration/deceleration and position. Moreover, the same

communication module is able to provide the same information to the other vehicles, setting up a short-range communication between vehicles. It has been shown in [35-36] a fuel economy potential between 5% and 20% compared to a standard powertrain, even if there is a significant dependency on drivers' behaviour. The main potential of this solution is related to the possibility of predicting immediate stop events, thus increasing the regenerative braking phase, as well as adding information to the standard adaptive cruise control (ACC), which is based on radars and cameras in actual applications.

### 2.2.2 V2I communication

V2I application are strictly related to V2V communication, since they basically use the same technology to communicate, but the receiver/sender is different. In this case, in fact, the vehicle communicates with a centralized data provider system, commonly mentioned as a generic infrastructure. The advantage of this approach relies on the amount and the type of data the vehicle can collect about the surrounding environment, which can impact on the fuel economy potential. A typical example of V2I communication is the possibility of knowing in advance the presence and the status of a traffic light, including its future transitions schedule. Once this information is available, a smart vehicle can manage the powertrain to approach the stop in the best way possible, in terms of safety and energy efficiency. Another application can be, for example, the prediction of traffic signals a-head that would lead to an intense deceleration, allowing a more safety approach to such critical condition [37].

In terms of potential benefits, these technologies are between 10% [38] and 40% [39] of fuel consumption reduction, considering a conventional vehicle.

### 2.2.3 V2X communication

As V2X technology is intended, in general, a communication between the vehicle and a general entity in the driving scenario, such as: pedestrian (V2P), roadside communication systems (V2R), cloud services for mobility (V2C). All these possible applications of vehicle communication are usually considered more for road safety and smart mobility concepts, than for vehicle energetic efficiency.

An example of vehicle communication systems integration is shown in Fig.2.2.

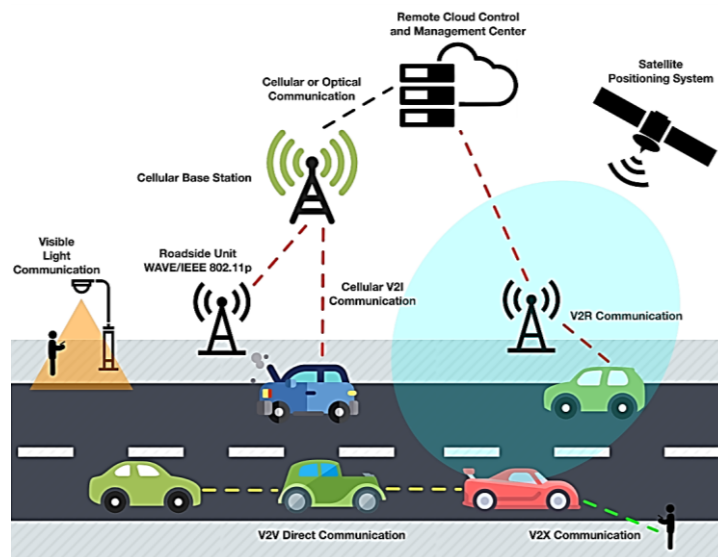


Figure 2.2. Vehicle communication technologies

## 2.3 Prediction Horizon

The prediction horizon, also mentioned as electronic horizon (eHorizon), is a reconstruction of the vehicle future driving conditions based on the combination of vehicle sensors, vehicle connectivity and road-map information [40]. Its importance varies according to the application, starting from a fuel economy and safety improvement in conventional and hybrid vehicles that have predictive control features and reaching a fundamental presence in autonomous vehicles development.

Few main potential applications of predictive horizon can be [41]:

- Driving safety and comfort enhancement;
- Fuel consumption and CO2 emission consumption;
- Adaptive cruise control;
- Autonomous driving;
- Curve warning and traffic signs recognition;

An example of how eHorizon information can be provided to the driver is shown in Fig.2.3 [42],



Figure 2.3. eHorizon information example

There are several works in literature where authors have proven the potential of predictive future driving conditions in order to improve the powertrain efficiency[43]. Zheng et al. have assessed in [44] the importance of the knowledge of road terrain in the energy management strategy of a HEV. In [45], instead, it has been proven the potential benefits related to the prediction of the future driving conditions. Authors of [46] have conducted a study that aims to underline the sensitivity of the implemented EMS to the trip estimation.

### III. Powertrain modelling

#### 3 Powertrain architecture

The powertrain architecture of the examined vehicle is depicted in Fig. 3.1. The vehicle propulsion can be provided by two different paths: the pure electrical one and the hybrid one. The former includes two identical electric machines mounted on the front axle, which can serve both as motors or generators. They are directly coupled to the front wheels by means of a fixed gear ratio.

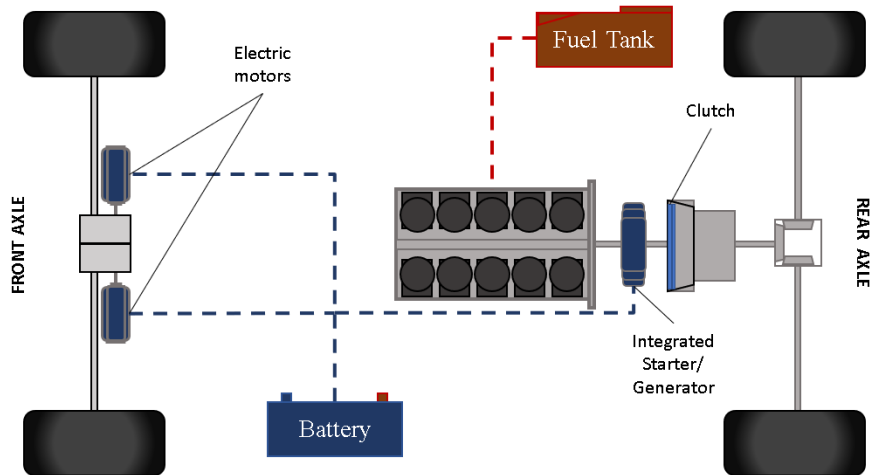


Figure 3.1 Powertrain architecture

The hybrid path, instead, includes a powerful 5.2 L gasoline engine, another electrical machine used as an integrated starter generator, a six-gear automatic transmission, and a differential gear. Depending on the selected powertrain operating mode, the two propulsion paths can work separately or in combination. If the vehicle is in pure electric mode, the propulsion comes only from the electrical machines on the front axle, so the engine is kept switched-off and the clutch is open. In this condition, a front-wheel-driving is performed (FWD). If the vehicle is in hybrid mode, all the machines available on-board work in combination to fulfil the torque request. The main powertrain specifications are listed in Tab. 3.1.

Table 3.1 Vehicle powertrain data

Battery nominal capacity (0.5C @25°C)	30 Ah
Battery nominal / max. voltage	355 / 450 V
Motor cont. / peak torque	145 / 350 Nm
Motor cont. / peak power	64 / 140 kW
Engine max. torque	533 Nm
Engine max. power	449 kW
Overall max. power (cont. / peak)	577 / 729 kW

## 4 Analytic Powertrain consumption model

The first modelling approach for the powertrain in exam is a consumption quasi-static model, which imposes a given vehicle speed at the wheels and proceeds backward through the propulsion chain to calculate the energy consumption needed to perform the given driving mission. Therefore, in the following equations, the calculation starts from the vehicle longitudinal dynamics and reaches the propulsion system.

### 4.1 Vehicle dynamics

The vehicle dynamics analytical model only takes into account the longitudinal forces acting on the car (Fig. 4.1 ). This approach is typical in control-oriented modelling of vehicle dynamics. The fundamental equation for vehicle longitudinal dynamics is:

$$m_v \frac{d}{dt} v(t) = F_{mot}(t) - F_{res}(t) \quad 4.1$$

where  $m_v$  is the vehicle mass,  $F_{mot}$  is the propulsion force, while  $F_{res}$  is the resistance force acting on the vehicle. The latter can be expressed as follows

$$F_{res}(t) = F_a(t) + F_r(t) + F_g(t) \quad 4.2$$

On the right side of Eq. 4.2 there are, respectively, aerodynamic resistance, rolling resistance, and slope-related resistance.

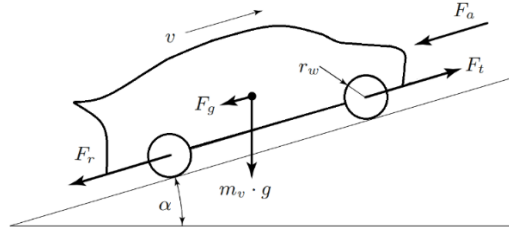


Figure 4.1 Longitudinal resistance forces acting on a moving vehicle

Since both aerodynamic and rolling resistances depend on the vehicle speed, for their modelling it has been used the *coast-down* parameters approach [47]. Therefore, the total resistance force can be re-written as

$$F_{res}(t) = f_0 + f_1 v(t) + f_2 v^2(t) + m_v g \sin \alpha(t) \quad 4.3$$

where  $f_0, f_1, f_2$  are the coast-down parameters and  $\alpha$  is the road slope.

### 4.2 Wheels level

$$F_{req}(t) = F_{res}(t) + (m_v + m_{eq,rot}) \cdot \frac{d}{dt} v(t) \quad 4.4$$

where  $F_{req}$  is the total force requested at the wheels,  $F_{res}$  is defined as in Eq. 4.3 ,  $m_v$  is the vehicle mass,

$m_{eq,rot}$  is the equivalent mass of rotative components and  $v_v$  is the vehicle speed imposed by the driving mission. Then, the torque request at the wheels is:

$$Tq_{req}(t) = F_{req}(t) \cdot r_{whl} \quad 4.5$$

with  $r_{whl}$  being the wheel radius.

### 4.3 Front axle

From the knowledge of the total torque request at the wheels, it is possible to calculate the torque request to the electrical machines on the front axle by following the transmission chain from the wheels to the motors.

$$Tq_{whl,f}(t) = Tq_{req}(t) \cdot sf(t) \quad 4.6$$

where  $Tq_{whl,f}$  is the torque to be provided on the front axle according to the factor,  $sf$ , which is the torque split factor between the front and rear-axle or, equivalently, the pure electric and hybrid paths. It is defined as:

$$sf(t) = \frac{Tq_{whl,f}(t)}{Tq_{req}(t)} \quad 4.7$$

or, equivalently,

$$sf(t) = 1 - \frac{Tq_{whl,r}(t)}{Tq_{req}(t)}$$

being  $Tq_{whl,r}$  the torque to be provided by the rear axle.

At the front differential gear, the speed is

$$n_{dif,f}(t) = n_{whl}(t) \cdot \tau_{dif,f} \quad 4.8$$

$n_{dif,f}$  is the rotational speed of the differential gear at the motors side and  $\tau_{dif,f}$  is the fixed transmission ratio. Still, at the motors' side, the requested torque is:

$$Tq_{dif,f}(t) = \frac{Tq_{whl,f}(t)}{\tau_{dif,f}} \cdot \eta_{dif,f}^a \quad 4.9$$

$$a = \begin{cases} -1, & Tq_{whl,f}(t) > 0 \\ 1, & Tq_{whl,f}(t) \leq 0 \end{cases}$$

Reaching the motors, the speed is the same as the motors shaft of the differential gear, while the torque requested is

$$Tq_{mot,f}(t) = Tq_{dif,f}(t) \cdot \eta_{mot,f}^a \quad 4.10$$

$$a = \begin{cases} -1, & Tq_{dif,f}(t) > 0 \\ 1, & Tq_{dif,f}(t) \leq 0 \end{cases}$$

being  $n_{mot,f}$  the motors' efficiency for the requested power.

#### 4.4 Rear axle

The torque to be supplied to the rear wheels is also related to the actual split factor, as it can be seen in Eq. 4.11.

$$Tq_{whl,r}(t) = Tq_{req}(t) \cdot (1 - sf(t)) \quad 4.11$$

Then it is possible to calculate the rotational speed of the engine crankshaft, which is

$$n_{ice}(t) = n_{whl}(t) \cdot \tau_{tot,r}(gr(t)) \quad 4.12$$

where the  $n_{ice}$  is the engine speed and  $\tau_{tot,r}$  is the total gear ratio considering both the actual gear ratio of the automatic transmission and the rear differential. The gear ratio depends on the currently engaged gear  $gr(t)$  and it is defined only for the rear axle, while if the vehicle is propelled only using the electrical machines on the front axle, the automatic transmission is decoupled from the crankshaft by means of a clutch.

The torque request at the engine side of the transmission is

$$Tq_{trans,r}(t) = \frac{Tq_{whl,r}(t)}{\tau_{tot,r}(gr(t))} \cdot \frac{1}{\eta_{dif,r}} \quad 4.13$$

The transmission efficiency is represented by the term  $\eta_{dif,r}$ . Therefore, the engine torque request is

$$Tq_{ice}(t) = Tq_{trans,r}(t) + Tq_{ISG_{ch}}(t) \quad 4.14$$

and, consequently, the torque request to the integrated starter generator (ISG) for recharging the battery is expressed as:

$$Tq_{ISG}(t) = Tq_{ISG_{ch}}(t) \quad 4.15$$

while the speed of this latter machine is the same as the internal combustion engine one.

#### 4.5 Battery model

The vehicle analytic model is completed by the battery model. It starts with the calculation of the global electrical power request. To this aim, the contribution related to battery thermal management,  $P_{TM}$ , can be highlighted, which takes into account the power request of the HV compressor,  $P_{cpr}$ , and the electric pump,  $P_{pmp}$ , to cool down the component. Thus

$$P_{bat}(t) = P_{mot_f}(t) + P_{ISG}(t) + P_{aux}/\eta_{DCDC} + P_{TM}(t) \quad 4.16$$

where

$$P_{TM}(t) = (P_{cpr}(t) + P_{pmp}/\eta_{DCDC}) \quad 4.17$$

in which  $P_{mot,f}$  is the power requested from the electrical motors on the front axle for traction,  $P_{ISG}$  is the power provided by the engine to recharge the battery,  $P_{aux}$  is the constant power to be supplied to the LV battery and the other auxiliaries,  $\eta_{DCDC}$  is the efficiency of the DCDC converter.

Cell electrical behaviour has been represented by an equivalent electrical circuit model (EECM) with an equivalent series resistance, as depicted in Fig. 4.2. Cell data for the open-circuit voltage as a function of battery state of charge (SOC) and for ohmic resistance as a function of the temperature have been used.

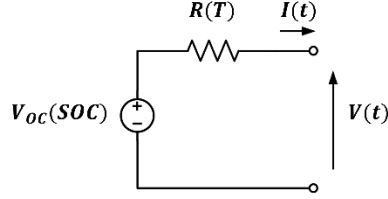


**Figure 4.2 Equivalent series resistance (ESR) model for cell electrical characterization.**

Therefore, battery voltage  $V_{bat}$  and current  $I_{bat}$  can be calculated from the following equations' system:

$$\begin{cases} V_{bat}(t) = (V_{cel,OC}(SOC) - R_{cel,int}(T) \cdot I_{bat}(t)/n_p) \cdot n_s \\ P_{bat}(t) = V_{bat}(t) \cdot I_{bat}(t) \end{cases} \quad 4.18$$

where  $n_p$ ,  $n_s$  are the number of cells in parallel and in series, respectively, and  $P_{bat}(t)$  is the battery power request coming from Eq. 4.16.

It is then possible to calculate the power losses of the battery due to resistive heating as follows

$$P_{bat,loss}(t) = V_{bat,int}(t) \cdot I_{bat}(t) = \frac{n_s}{n_p} R_{cel,int}(T) \cdot I_{bat}^2(t) \quad 4.19$$

in which  $V_{bat,int}$  is the internal voltage drop of the battery due to the presence of the internal resistance  $R_{bat,int} = R_{cel,int}(n_s/n_p)$  that causes the power dissipation  $P_{bat,loss}(t)$  when the current  $I_{bat}$  is flowing in the circuit.

Then, the battery state of charge is defined as

$$SOC(t) = SOC_0 - \frac{\int_0^t I_{bat}(t) dt / 3600}{C_{bat}} \quad 4.20$$

being  $C_{bat}$  the nominal battery capacity [Ah], and  $SOC_0$  the initial value of the state of charge (that is dimensionless and in a range between 0 and 1).

## 5 Model in the Loop

The same powertrain has been modelled in Simulink/SimScape environment. Differently from the analytic model, the Model-in-the-Loop (MiL) follows a forward-facing approach, which means there is a driver model capable of reproducing realistic acceleration and brake pedals signals. According to that, the model follows the conventional control chain present in a real vehicle. The driver request (pedals signals) is converted in torque requested at the wheels, then vehicle and components control units manage the actuators in order to provide the power to satisfy the driver request.

This modelling approach allows a more realistic simulation of the powertrain behaviour, calculating not only the energy consumption, but also all the interesting physical quantities to represent the vehicle motion, such as, for example, the actual vehicle speed and the machines behaviour in terms of torque, speed, temperature, failures.

The MiL environment is divided in different parts:

- Components, where the powertrain physical parts have been modelled using SimScape libraries, allowing a direct coupling of the rotational components.
- Controllers, in which all the control unit installed on-board a real vehicle are modelled, following the operation they would have in real-time application.
- Communication, reproducing the vehicle communication network.

All the data needed to implement the such detailed MiL derives from a real-existing vehicle prototype.

The powertrain components have been modelled using efficiency maps to calculate the energy consumption and their physical characteristics to reproduce their operation. In the following paragraphs all the data regarding the powertrain components have been normalized for confidentiality reasons.

### 5.1 Engine model

The vehicle in exam is equipped with a powerful 5.2 litres V10 gasoline engine capable of providing 540 Nm as a maximum torque and a maximum power 449 kW. As previously mentioned, the physical behaviour of the internal combustion engine (ICE) has been modelled using SimScape libraries, therefore it is considered as a generic ideal torque source. Its characteristic is reported in Fig.5.1.

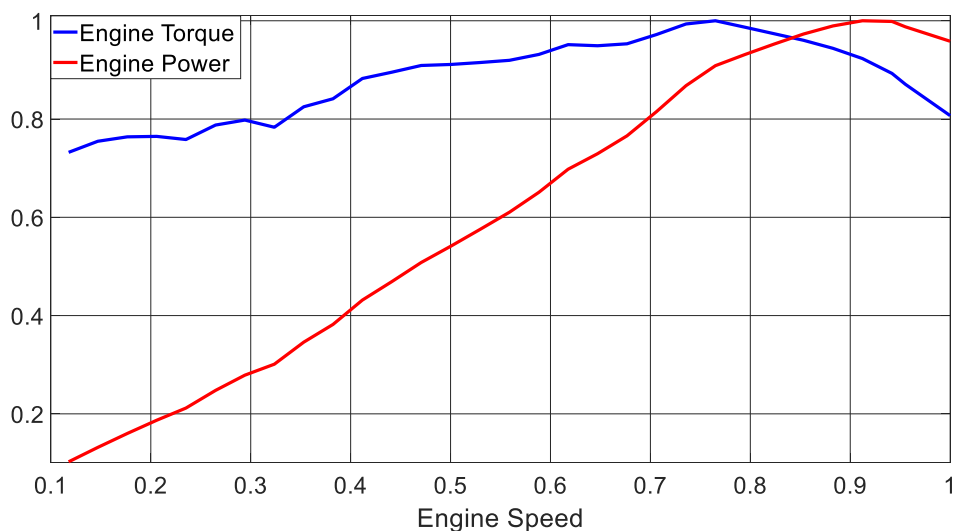
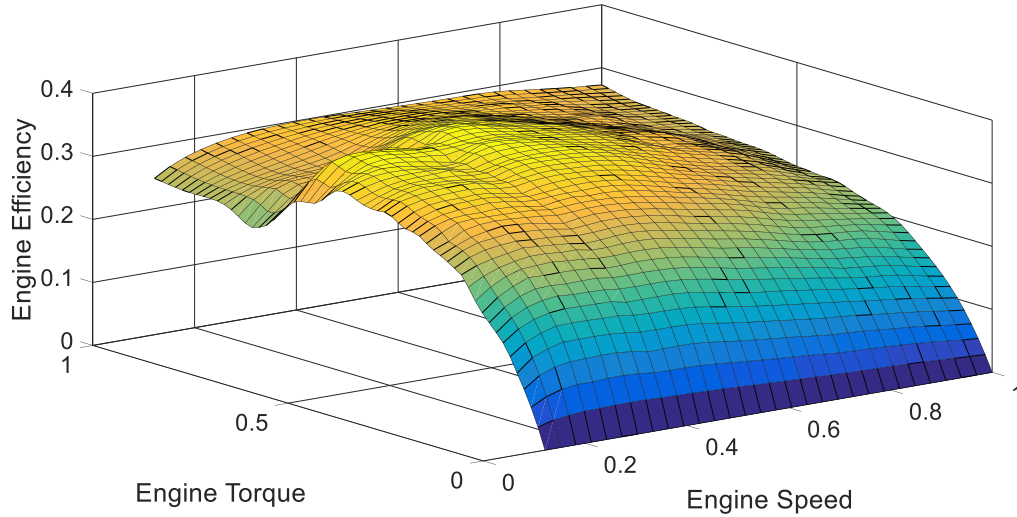


Figure 5.1. Engine Maximum Torque and Power vs Engine Speed



**Figure 5.2 Engine efficiency map**

The engine efficiency has been modelled using a map, which is function of the engine speed and torque and it is reported in Fig. 5.2. Analytically, it can be expressed as in Eq. 5.1

$$\eta_{ICE} = \frac{Tq_{ICE} * \omega_{ICE}}{\dot{m}_{fuel} * LHV_{fuel}} \quad 5.1$$

Where  $\eta_{ICE}$ ,  $Tq_{ICE}$ ,  $\omega_{ICE}$ , are respectively the efficiency, torque and angular speed of the engine and  $\dot{m}_{fuel}$ ,  $LHV_{fuel}$  are the mass fuel rate and fuel lower heating value (LHV).

## 5.2 Electric motor model

Before showing the data related to the electric propellers, it is important to underline that all the electrical machines included in the powertrain, i.e. the two electric motors/generators on the front axle (Fig. 3.1) and the integrated starter generator mounted on the crank shaft, are identical, so they have exactly the same characteristics.

The maximum torque the motors can provide as function of the motor speed is depicted in Fig. 5.3.

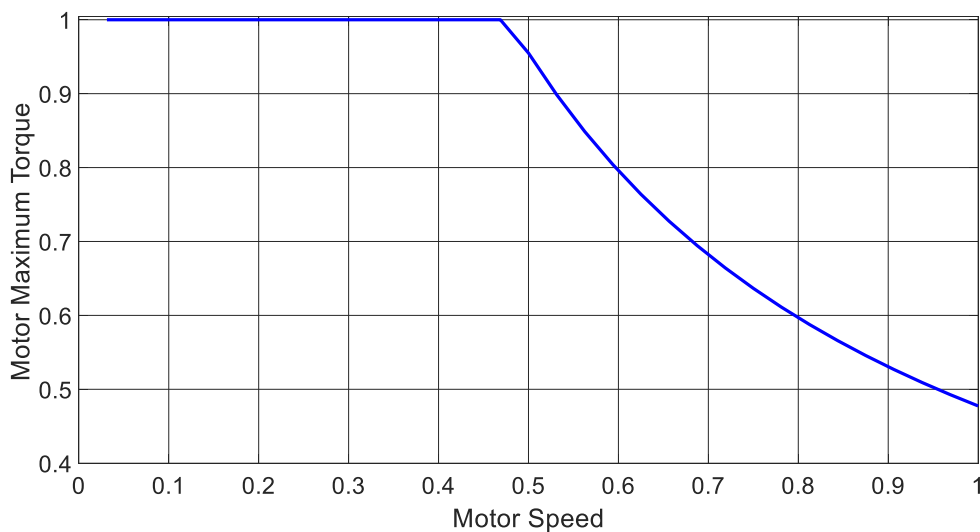


**Figure 5.3 Electric Motor Maximum Torque vs Motor Speed**

As for the engine, the motor efficiency is expressed as function of the torque and speed (Fig.5.4). The physical formulation its expressed as in Eq. 5.2, being  $\eta_{EM}$ ,  $Tq_{EM}$ ,  $\omega_{EM}$ ,  $I_{EM}$ , the efficiency, torque, angular speed and current of the motor and  $V_{Batt}$  is the voltage of the high voltage battery.

$$\eta_{EM} = \frac{Tq_{EM} * \omega_{EM}}{I_{EM} * V_{Batt}} \quad 5.2$$

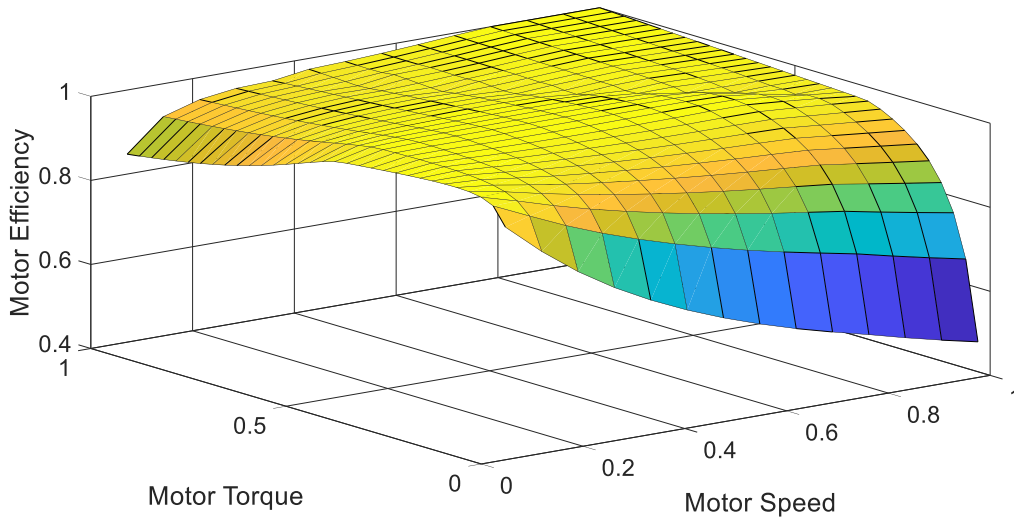


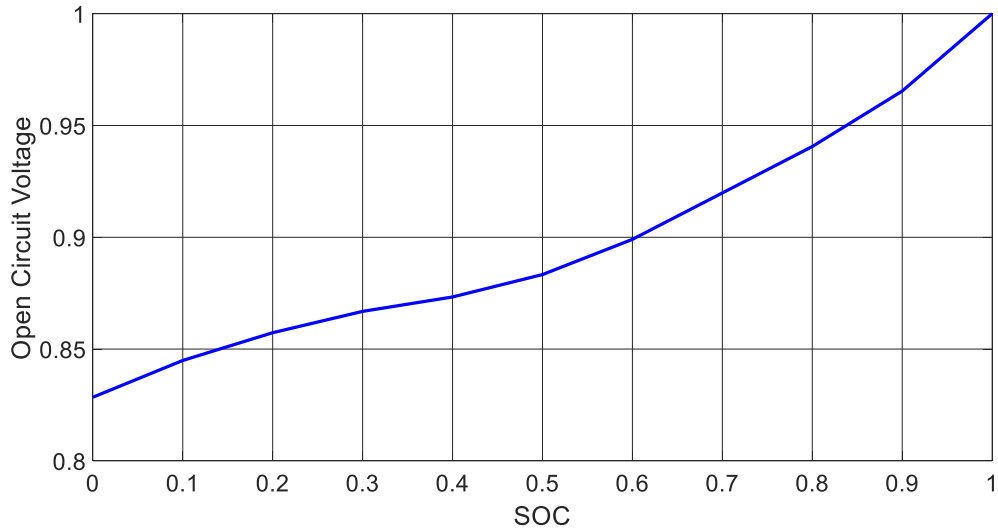
**Figure 5.4 Motor efficiency map**

### 5.3 Battery

The high voltage energy storage system, in this context mentioned simply as battery, is actually a battery pack composed by 96 electrochemical cells in series, with only one string (there are no cells in parallel). The maximum battery capacity is 30 Ah (12 kWh) and a maximum power of 140 kW . Its modelling is conceptually identical to the scheme in Fig. 4.2, but some additional information have been added in the MiL to reproduce its dependency from meaningful physical variable, such as the battery state of charge and the battery temperature.

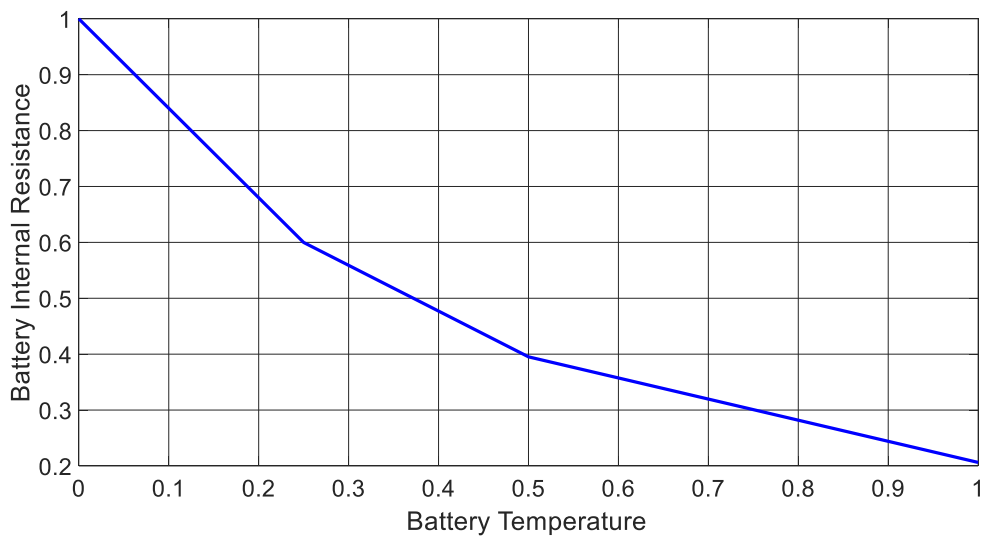
These latter, in fact, affect two main battery operational parameters, i.e. the open circuit voltage ( $V_{OC}$ ) and the internal resistance ( $R_{Batt}$ ).

Fig. 5.5 depicts the  $V_{OC}$  characteristic as a function of the SOC.



**Figure 5.5 Battery Open Circuit Voltage vs SOC**

The other fundamental parameter, the internal resistance, decreases as the battery temperature increases, as shown in Fig.5.6, where the x-axis reports the battery temperature operational range, normalized on the maximum value of the range itself.



**Figure 5.6 Battery internal Resistance vs Battery Temperature Range**

## 5.4 Transmission

The global transmission model includes a dual-clutch between the ISG and the six-gears automatic/manual transmission and a differential gear on the rear axle. No meaningful data can be shown about the gearbox, since in this case there isn't an exact scheduling of the gear-shifting, but rather a control logic that depends on the driver's request, the powertrain conditions and the transmission system actual status.

## 6 Hardware in the Loop

The Hardware in the Loop (HiL) environment, built for simulating the real-time operation of the vehicle under investigation, directly derives from the MiL illustrated in the previous chapter. In this sense, the HiL environment is strictly developed for testing the HCU operation in real-time, therefore all the signals that in the real vehicle reach the supervisory controller are modelled and, more important, the on-board diagnostic for such component is included in the loop. This approach helps to reduce the differences between the simulation and the real vehicle, allowing to detect any particular error related the robustness of the implemented control strategy before implementing it in the vehicle prototype.

The only and main difference between the MiL and HiL environments is that the latter includes three powerful computational platforms for the vehicle simulation which are:

- *SCALEXIO Processing Unit (dSpace)*, where the whole powertrain model has been deployed for real-time execution, except for the hybrid control unit (HCU). Therefore, the vehicle components and their controller are still simulated, indeed there is no real hardware for the components included in the loop.
- *SCALEXIO LabBox (dSpace)*, being the hardware that handles the communication interface. From one side, it replicates all the signals that in the real vehicle reaches the HCU, such as: CAN messages, digital and analog signals. In the opposite communication way, it takes the output of the supervisory controller and deliver the information to the processing unit.
- *MicroAutoBox (MABX) (dSpace)*, which is a rapid control prototyping unit, where the hybrid supervisory controller has been implemented for the real-time execution.

In this new vehicle configuration, the communication between SCALEXIO and MABX are physical, which means there is a cabled CAN network that replicates the communication between the vehicle components and the HCU as in the real vehicle.

To have a complete view of such complex vehicle simulator environment, the reader can refer to Fig.6.1.

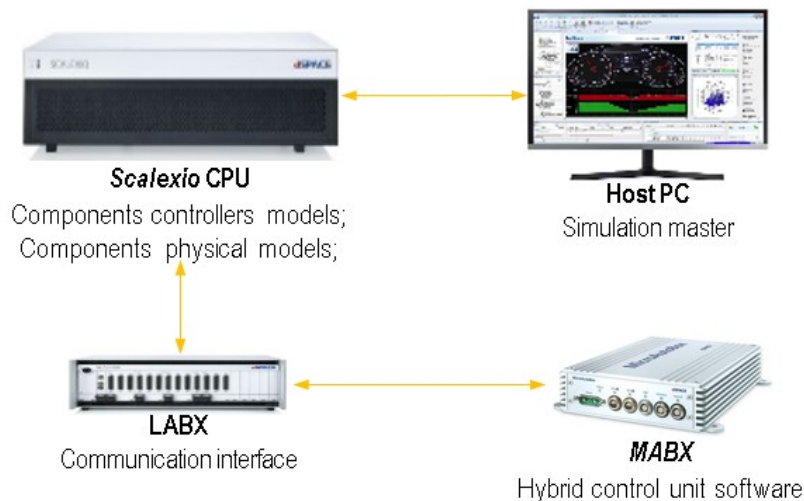


Figure 6.1 HiL setup

## 7 Model Validation

The validation of the models shown in the previous chapters has been done in two steps:

- The MiL environment has been validated against experimental data acquired on New European Driving Cycle (NEDC) test at the test-bench;
- The Analytic model of the powertrain has been developed using as reference the validated MiL simulator.

The experimental data for the validation has been provided by an industrial partner of the project, who didn't provided data on the battery state of charge trend, therefore it hasn't been possible to show it. For this reason, it has been chosen to validate the analytic model against the validated MiL data.

### 7.1 MiL vs experimental data

The MiL represents with high accuracy the real behaviour of the vehicle, considering for the validation the engine cumulative fuel consumption, speed and torque, as it can be seen in Fig. 7.1.

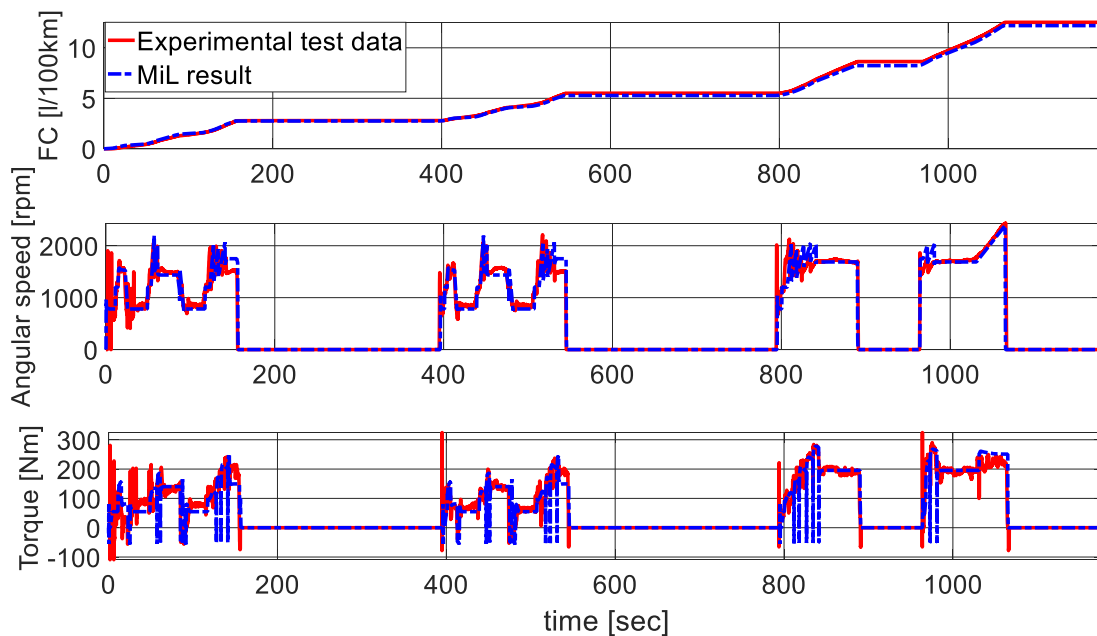


Figure 7.1 MiL validation

Except for the slight difference on the gear-shifting strategy, it can be assumed that the MiL environment represents the real vehicle behaviour with an acceptable accuracy since the overall difference in the fuel consumption is less than 3% between the model simulation and the on-board measured data. The experimental data for the validation has been provided by an industrial partner of the project, who didn't provided data on the battery state of charge trend, therefore it is not possible to show it. For this reason, the validation has been performed against the only ICE operation.

### 7.2 Analytic model vs MiL

The energy consumption, both electrical and thermal, of the analytic model has been validated against the results obtained in the model in the loop environment, which had previously been validated against experimental data.

For such validation, the reference cycle has been a Real Driving Emission (RDE) test and this choice is mainly related to the length of the cycle, which allows to have a consistent energy consumption and different operating modes of the powertrain. The speed and road altitude profile of the RDE cycle are shown in Fig.7.2.

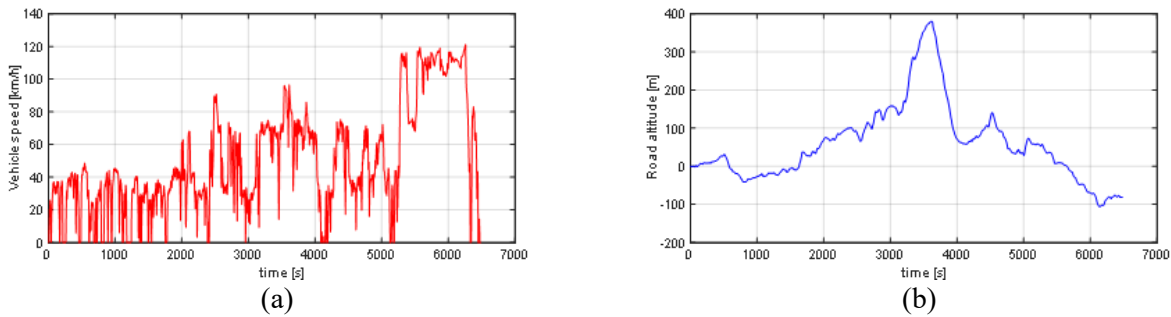


Figure 7.2 RDE cycle vehicle speed (a) and road altitude (b) profiles

The validation of the energy consumption model has been done considering the battery state of charge (SOC) evolution over the cycle and the cumulative value of the engine fuel consumption (FC).

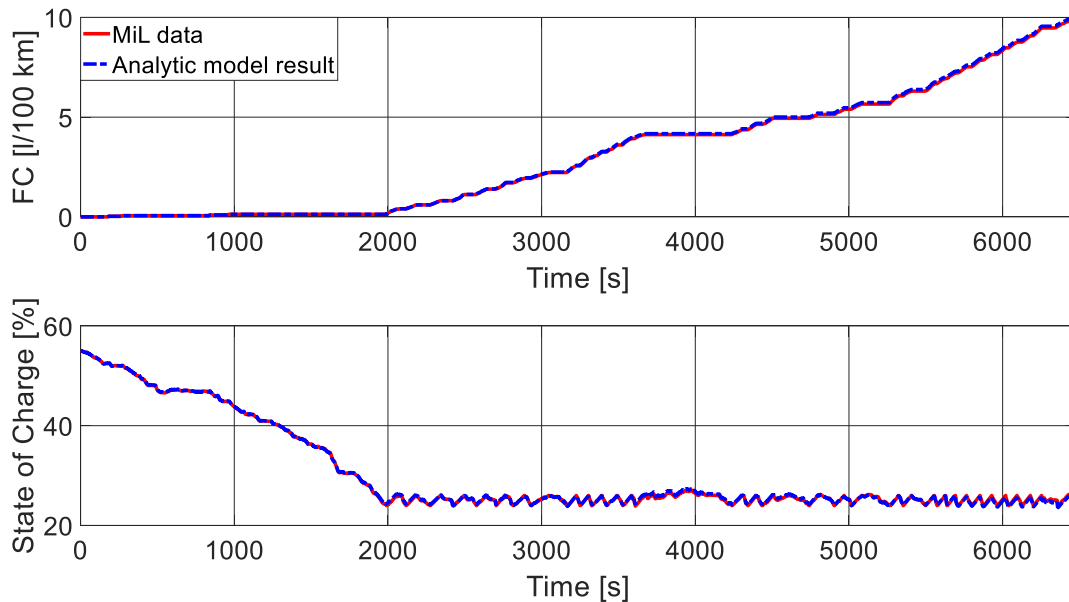


Figure 7.3 Analytic model validation

As can be noticed from Fig.7.3, the analytic energy consumption model is highly representative for the vehicle energy usage. The final value of the analytic SOC is less than the 1% lower than the reference MiL value and the same percentual difference there is between the two fuel consumptions, but in this case the analytic model value is higher than its reference.

## ***IV. Powertrain Supervisory Control***

As briefly mentioned in the overview section of this dissertation, the powertrain control of a hybrid electric vehicle is hierarchical, which means there is a supervisory controller that implements the energy management strategy and consequently manages the components controller in order to fulfil the drivers' request. In this section are collected all the EMSs implemented for the vehicle object of this project.

### **8 On-line controllers**

Causal controllers are widely known in the field of HEVs control [16], mainly for the possibility of using a control strategy that doesn't need the full (or partial) knowledge of the future driving conditions to perform the energy management. In this scenario, two main solutions can be cited: Rule-based and ECMS-based controllers. Following the classification done in the first chapter, the formers are considered as heuristic and the latter are sub-optimal strategies.

#### **8.1 Rule-based strategy**

##### **8.1.1 Overview**

The peculiarity of rule-based heuristic controllers is that they are based on thresholds and fixed rules. Automotive researchers have investigated, in this sense, diverse ways to make these controllers more effective in terms of fuel consumption. At the earliest stage of the investigation on EMSs for HEVs, heuristic controllers were developed following basic assumptions on the components, for example in [9], authors have set rules with the aim of maximizing the powertrain capabilities, indeed using as much electrical energy as possible and using the ICE at its maximum load to recharge the battery when needed. Despite these engineering assumptions make totally sense, they also make the EMS poor in flexibility, since the rules and the calibrations have no possibility to be adapted to different driving conditions.

In [48], instead, the rules are integrated in a fuzzy logic controller that has in input the battery state of charge, electric machines speed and driver request, thus considering all the powertrain components as a single complex system. Another approach, widely used by researchers for real-time prototyping and by carmakers for series production, is to derive the rules from offline optimal control policies, as proposed in [49]. The main drawback of this latter approach is that the obtained rules are particularly suitable for the driving mission chosen during the optimization, but may be less effective for other driving cycles.

##### **8.1.2 Implementation**

For the vehicle in exam, the rule-based controller (RBS) is in charge to select the operating mode between pure electric and hybrid propulsion. If the former is selected, than the drivers' request is fulfilled only by the electrical machines on the front axle, otherwise the engine is switched-on and it provides the required torque at the wheels, plus eventually a certain amount used to recharge the battery by means of the integrated starter-generator (ISG).

The parameters taken into account to decide whether to switch from a driving mode to another are:

- The battery state of charge (SOC);
- Vehicle speed ( $V_{veh}$ );
- Torque demand at the wheels ( $Tq_{whl}$ );

According to the actual value of these three variables, the RBS selects the operating mode.

There is a transition from the pure electric mode to the hybrid mode if at least one of the following conditions is satisfied:

- SOC < 24 %;
- V\_veh > 120 km/h;
- Tq\_whl > 2000 Nm.

The RBS switches from hybrid mode to pure electric if all the following conditions are true:

- SOC > 26 %;
- V\_veh < 115 km/h;
- Tq\_whl < 1800 Nm.

When the vehicle is in hybrid mode, the amount of torque the engine delivers to the ISG to recharge the battery is defined by means of a dedicated control logic based on the actual speed of the crank shaft on which both the machines are mounted.

As can be noticed, this RBS is quite simple and it is particularly related to the behaviour of a Plug-in HEV, for which it is usually considered a consistent discharge phase when the battery is charged and a following charge-sustaining phase when the SOC reaches the lower threshold.

## 8.2 Equivalent Consumption Minimization Strategy

### 8.2.1 Overview

The theory behind ECMS is well known in the energy management field for hybrid electric vehicles. It was proposed a few years ago [50] as a possible approach to optimize, with local optimization, the energy flowing through the vehicle. Different works in literature discussed and further developed this method [1-3,14-16,50-57], and in this content it has been used as starting point a particular ECMS formulation called “A-ECMS”, or Adaptive-ECMS, explained in detail in [1,55]. However, in this dissertation it has been applied to a complex powertrain that can also include pure electric driving and axle split propulsion and, moreover, different battery state of charge management strategies have been implemented and test, also including predictive information to increase the energy recovering capability of the vehicle.

The control variable that characterizes this sub-optimal controller is  $u$ , which is the torque split factor between the electrical and thermal propulsion paths, which can be defined as in Eq.8.1.

$$u(t) = \frac{T_{ELE}(t)}{T_{TOT}(t)} \quad 8.1$$

or

$$u(t) = 1 - \frac{T_{ICE}(t)}{T_{TOT}(t)}$$

where  $T_{ELE}(t)$  is the torque request to the electrical machines,  $T_{ICE}(t)$  is the torque request at the ICE and  $T_{TOT}(t)$  is the total torque request at the wheels. The main idea of ECMS is to instantaneously minimize a function that takes into account both the energy coming from the fuel and from the battery, formulated as follows:

$$\dot{m}_{eq}(t) = \dot{m}_f(t) + \dot{m}_{bat}(t) = \dot{m}_f(t) + \frac{s}{Q_{lhv}} * P_{bat}(t) \quad 8.2$$

Where  $\dot{m}_f$  is the engine instantaneous fuel consumption,  $\dot{m}_{bat}$  is the fuel consumption equivalent to the used electrical power.  $P_{bat}$  is the electrical power demanded at a certain instant,  $Q_{lhv}$  is the fuel lower heating value (energy content for mass unit) and  $s$  is the *equivalence factor*, which is used to convert the electrical power from the battery into equivalent fuel consumption. The power requested to the battery can be either positive or negative and, consequently, the equivalent fuel consumption can be higher or lower than the real one.

Defining

$$\dot{\xi}(t) = f(\xi, u, t) = - \frac{I_{bat}(\xi, u, t)}{Q_{bat}} \quad 8.3$$

Where  $I_{bat}$  is the battery current,  $Q_{bat}$  is the battery charge capacity,  $\xi$  is the battery state of charge and  $u$  is the control action, it is possible to define the Hamiltonian of the optimal control problem, which is to be minimized [56]:

$$H(\xi, u, \lambda, t) = -\lambda(t) * f(\xi, u, t) + \dot{m}_f(u, t) \quad 8.4$$

The co-state variable  $\lambda(t)$  is the solution of:

$$\dot{\lambda}(t) = -\lambda(t) \frac{\partial f(\xi, u, t)}{\partial \xi} \quad 8.5$$

In other words, the Hamiltonian is the total equivalent fuel consumption including the electric energy. To better understand the meaning of  $\lambda(t)$ , an auxiliary variable can be introduced, the equivalent factor  $s(t)$ , formulated as follow:

$$s(t) = -\lambda(t) * \frac{Q_{LHV}}{P_{bat}(t)} \quad 8.6$$

here  $P_{bat}(t)$  is the power request to the battery and  $Q_{LHV}$  is the lower heating value of the fuel. At the end, the instantaneous equivalent fuel consumption is:

$$H(\xi, u, \lambda, t) = \dot{m}_{eq}(\xi, u, s, t) = s(t) * \frac{P_{bat}(t)}{Q_{LHV}} * f(\xi, u, t) \dots + \dot{m}_f(u, t) \quad 8.7$$

The optimal control action is the one that satisfies:

$$u^*(t) = \arg \min_u H(\xi, u, \lambda, t) \quad 8.8$$

The optimal control depends on the value of  $s(t)$ , but this is unknown a priori and this makes the strategy sub-optimal.

### **Equivalence factor**

Physically, the equivalent factor  $s(t)$  represents the ‘‘cost’’ of the energy stored in the battery, so if it has a high value, then it is preferable to use the engine and recharge, while if it is low, it’s better to use electrical traction. In this work, an A-ECMS approach proposed in [1,55] has been adopted, with adaptation on feedback values. The formulation of  $s(t)$  has two contributions:

- adaptive term, which is related, in this case, to the feedback of the previous SOC (square brackets);
- penalty function that corrects the value of  $s$  when it’s near to the maximum and minimum accepted values (first curly bracket).

It is defined as follows:

$$s(t) = \left\{ 1 - k_p \left[ \frac{\xi(t) - \left( \frac{\xi_{max} + \xi_{min}}{2} \right)}{\left( \frac{\xi_{max} - \xi_{min}}{2} \right)} \right]^3 \right\} * \left[ k_a (\xi_{ref} - \xi(t)) + \left( \frac{s_{k-1} + s_{k-2}}{2} \right) \right] \quad 8.9$$

Where  $\xi(t)$  is the actual SOC,  $\xi_{max}$  and  $\xi_{min}$  are the SOC upper and lower limits defined by the developer,  $\xi_{ref}$  is the target value and  $s_{k-1}$  and  $s_{k-2}$  are the values of  $s$  used in two previous time intervals, between two adaptation steps.  $k_p$  and  $k_a$ , instead, are two gain parameters used to tune the strategy.

Focusing on the adaptive term, it can be noticed the subscript  $k$ , which indicates the current adaptation step of  $s$ . In this strategy, in fact, the adaptation is not done every simulation time step, but every update time, which is a tuning parameter and shouldn’t be too short because, otherwise, long charge or discharge phases are not

possible. In the relation above,  $s_{k-1}$  and  $s_{k-2}$  are the values of  $s$  used in two previous time intervals, between two adaptation steps.

The term  $k_a (\xi_{ref} - \xi(t))$ , instead, gives a proportional correction to  $s$  considering the difference between the reference value of the SOC and its actual value at the adaptation step.

This mathematic approach refers to ARMA (Auto-Regressive Moving-Average) models [55] and, in this case, the feedbacks are two auto-regressive terms, while the other is the moving average one. By using such solution, it is possible to lower the computational load, due to the large updating steps, reflecting in a small number of calculations. Moreover, this control policy is more robust if the driving cycle is unknown, because the trend of the SOC is corrected to have an average value as near as possible to the one desired for the whole simulation, not in the single time interval.

The contribution of the penalty function is influent when the SOC value is approaching the limits of the admissible range, because if the SOC reaches critical values for the battery operation, in terms of possible damage or high inefficiencies, a correction of  $s$  it's needed instantaneously, not at the next adaptation time.

After the calculation of the current equivalency factor, the controller evaluates possible (discrete) values of the energy split between the movers, considering the efficiencies and the actual conditions, and selects the one that minimizes the equivalent fuel consumption in Eq.8.2.

### **Torque split**

Given the complexity of the powertrain architecture, it is possible to define different torque split configurations for the same torque split factor. To be more precise, the optimization routine returns the optimal split factor  $u^*$ , which is unique, but the presence of two electrical motors on the front axle (EM) and an electrical motor just before the main clutch (ISG), leads to the possibility of obtaining the same split factor in different ways. For this work, the torque split strategy has been defined as follows:

**Table 8.1 Driving Modes**

Driving Mode	Split Factor	ICE	ISG	EM
Edrive	$u^*=1$	OFF	OFF	ON
Regenerative Braking	$u^*=1$	OFF	OFF	ON
ICE only	$u^*=0$	ON	OFF	OFF
Boosting	$0 < u^* < 1$	ON	OFF	ON
Battery Recharge	$0 < u^*$	ON	ON	OFF

### **8.2.2 Implementation**

The ECMS controller illustrated in the previous paragraph has been implemented in the model in the loop simulation environment of the real vehicle, shown in Chap. 5.

Firstly, it is needed to define a searching window that contains the values of admissible split factor for the actual conditions, considering both the powertrain physical limitations and the drivers' request. More in detail, the possible solutions of the instantaneous minimization problem must be searched considering fundamental operation parameter such as the maximum torque providable by the engine and the electrical machines, the maximum power and current the battery can deliver/absorb.

At the same time, the calculation of the equivalence factor  $s$  is done using Eq. 8.9, considering the actual value of the SOC and the tuning parameters.

Once the value of the equivalence factor and the split factor searching window are known, it is possible to calculate the value of the equivalent fuel consumption  $\dot{m}_{eq}(t)$ , as in Eq. 8.2, for all the admissible  $u$  values. The minimum of the calculated  $\dot{m}_{eq}(t)$  values returns the instantaneous optimal split factor ( $u^*$ ) that minimizes the cost function. According to the  $u^*$ , it is possible to define both the driving mode and the torque to be requested to each of the machines included in the powertrain.

A global block diagram of the ECMS controller is depicted in Fig.8.1.

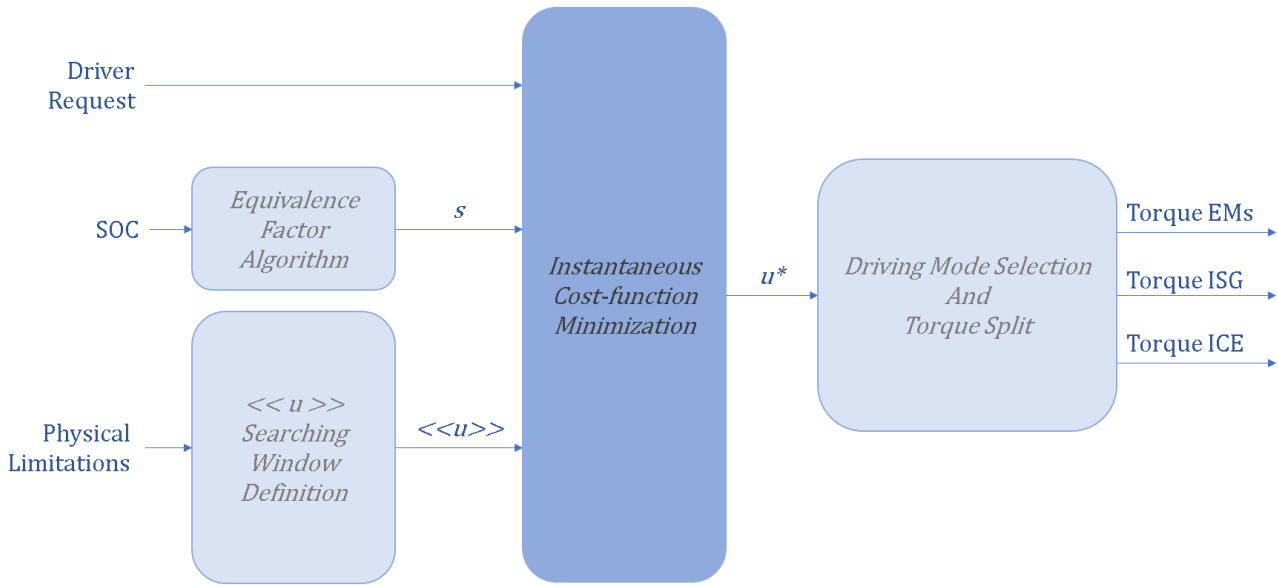


Figure 8.1 ECMS controller block diagram

### 8.2.3 Battery SOC Management Strategies

Within the ECMS control framework it is possible to define a state of charge management strategy (SoCMS), which governs the battery usage along the entire driving mission. In this context, three SoCMSs have been implemented and compared: Charge-Sustaining (CS) [1,50,55]; Charge-Blended (CB) [51,53] and Charge-Depleting/Charge-Sustaining (CD-CS).

All the proposed approaches for SoCMS are obtained by manipulation Eq. 8.9 in order to obtain different behaviour for the equivalence factor evolution over the driving cycle.

The possibility of evaluating different behaviour of the state of charge trend along the mission is mainly due to the fact the considered vehicle is a PHEV, which means it is assumed that it can “always” be recharged at the end of the driving mission.

#### **Charge-Sustaining**

For obtaining the CS policy for the SOC, the definition of the equivalence factor is exactly the same shown in Eq. 8.9. This strategy follows a target SOC value that is constant and equal to the initial state of charge, therefore the ECMS controller would keep the state of charge around such target for the entire mission, as it can be clarified by Fig.8.2, where the reference vehicle is operated along the driving cycle illustrated in Fig. 7.2.

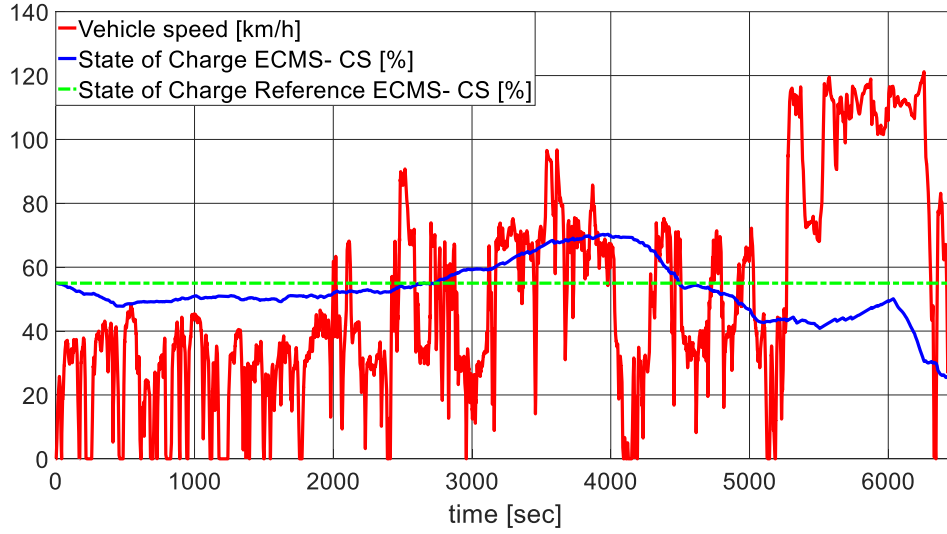


Figure 8.2 ECMS controller Charge-Sustaining

### Charge- Blended

CB is a battery charge management strategy that works similarly to the charge-sustaining mode, but follows an SOC target that linearly decreases with the driven distance, starting from the initial value of the SOC. This solution is preferable for PHEVs, since it allows to reach the end of the driving mission with a low SOC level. The formulation of the equivalence factor  $s$  is similar to Eq.8.9, as it can be noticed in Eq. 8.10, the only slight difference is related to the definition of the SOC reference value, which decreases linearly with the driven distance, as in Eq. 8.11.

$$s(t) = \left\{ 1 - k_p \left[ \frac{\xi(t) - \left( \frac{\xi_{max} + \xi_{min}}{2} \right)}{\left( \frac{\xi_{max} - \xi_{min}}{2} \right)} \right]^3 \right\} * \left[ k_a \left( \xi_{ref}(t) - \xi(t) \right) + \left( \frac{s_{k-1} + s_{k-2}}{2} \right) \right] \quad 8.10$$

Being

$$\xi_{ref}(t) = \xi_i + \frac{x}{x_f} (\xi_f - \xi_i) \quad 8.11$$

Where  $\xi_{ref}(t)$  is the SOC reference,  $\xi_i$  is the initial SOC,  $\xi_f$  is the desired SOC at the end of the driving mission,  $x$  is the actual driven distance and  $x_f$  is the supposed trip distance.

A decreasing SOC reference value is preferable for PHEVs because usually they aim to arrive with a low SOC level at the end of the mission. As for the CS, Fig. 8.3 shows the evolution of the state of charge along the mission with respect to the controller SOC reference value.

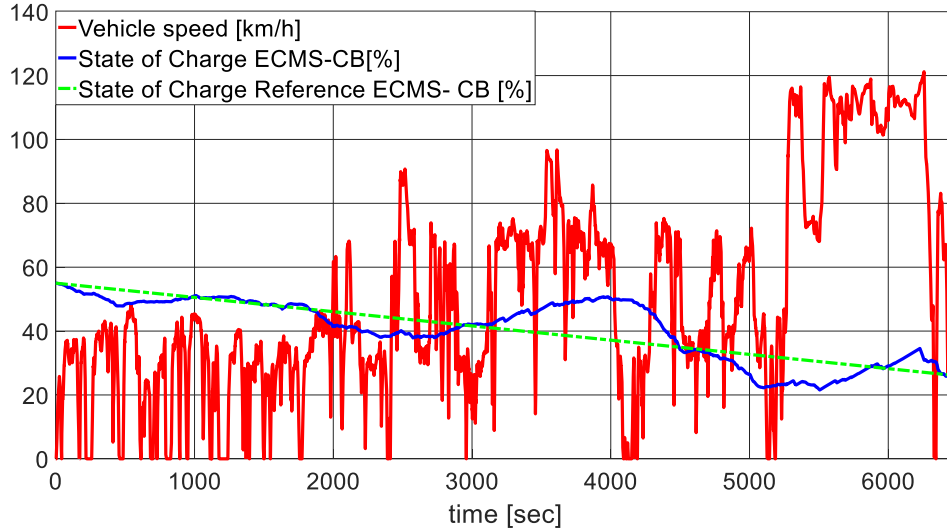


Figure 8.3 ECMS controller Charge-Blended

### Charge-Depleting/ Charge-Sustaining

For Charge-Depleting/Charge-Sustaining (CD/CS) strategy, one intends an electrical energy usage plan that firstly discharges the battery until a certain SOC value and then sustains the charge around a specific SOC target. This approach is widely used in heuristic supervisory controller for PHEVs, since commonly these vehicles have large battery capacity and can be mainly recharged from the grid, but it is usually implemented using fixed rules, while in this content it has been applied to a sub-optimal controller. The idea, and consequent benefit, of using such approach in combination with the ECMS, relies on the possibility of adapting the recharging phases to the actual powertrain conditions, avoiding pre-imposed thresholds and, moreover, leaving to the controller the freedom of switching the driving mode also if the battery state of charge is low.

In this ECMS configuration, CD/CS policy could be integrated in different ways, for example by adding a simple rule that forces the initial discharge (by varying the SOC target) until a certain value of the SOC, and then lets ECMS follows a target value (reasonably low) for the rest of the driving mission. Here this behavior has been obtained by eliminating the second term in Eq. 8.9, so that the controller has the only constraint to keep the SOC value between the given boundaries, but without following a state of charge target. This new expression for  $s$  is formulated in Eq. 8.12. The idea behind this approach is that, if the vehicle can be externally recharged at the end of the driving mission, it is worthless to add other constraints on the state of charge value, to keep it around a reference value.

Such control policy derives from two main considerations:

- Avoiding rules, less calibration effort is needed for the strategy, and the controller follows its normal algorithm.
- The initial discharge is guaranteed by the fact that, in general conditions for the given powertrain along the given driving cycle, the electric drive is always more efficient than the hybrid one, so the ECMS optimization process would select pure electric mode.

In this way, it is possible to have CD-CS behavior without forcing the driving mode and leaving to the supervisory controller the freedom to choose the best split factor in every driving condition.

$$s(t) = \left\{ 1 - k_p \left[ \frac{\xi(t) - \left( \frac{\xi_{max} + \xi_{min}}{2} \right)}{\left( \frac{\xi_{max} - \xi_{min}}{2} \right)} \right]^3 \right\} * s_0 \quad 8.12$$

The formulation in Eq. 8.12 is basically the same as in Eq. 8.9, but without the charge-sustaining capability. The parameter  $s_0$  is a gain used to tune the strategy and represents the initial cost of using electrical energy. For CD/CS SoCMS, the trend of the battery state of charge for the reference cycle is depicted in Fig 8.4.

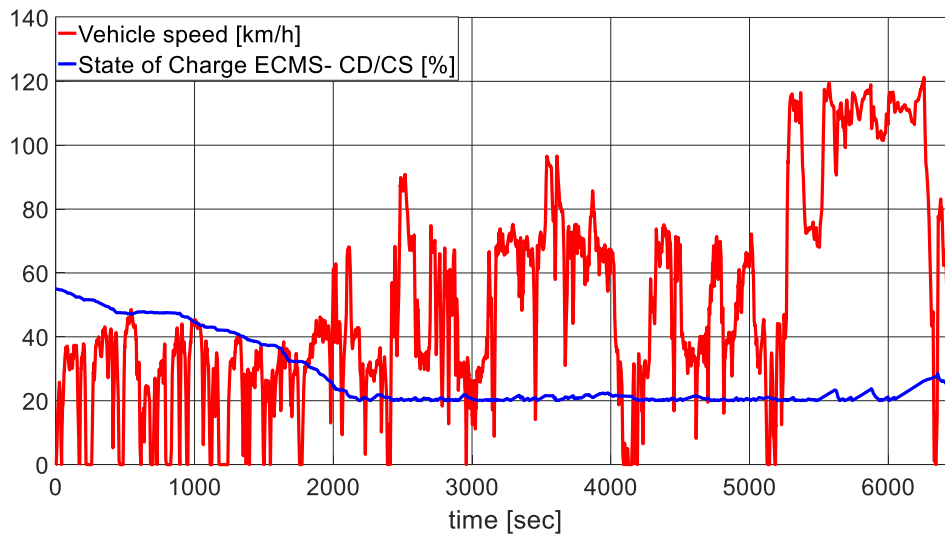


Figure 8.4 ECMS controller Charge-Depleting/Charge Sustaining

### 8.3 Online controller results

For the comparison of the performance obtained with the online causal controllers illustrated in this chapter, it has been considered only one parameter, which is the global fuel consumption of the vehicle over the driving mission, which is again the RDE cycle introduced in Chap. 7. In this case, no correction related to the electrical energy balance between the beginning and the end of the driving mission was needed, since all the controllers have ended the driving mission with the same state of charge, so the electrical energy consumption is the same for all of them. In Fig. 8.5 it can be noticed that the RBS has a CD/CS-like behaviour, since it firstly discharges the battery until a low value, and then it keeps the SOC around such minimum boundary.

#### 8.3.1 RBS results

The vehicle in exam that uses the heuristic controller to perform the reference driving mission shown in Chap.7 presents an evolution of the SOC trend over the driving mission that is shown in Fig.8.5 .

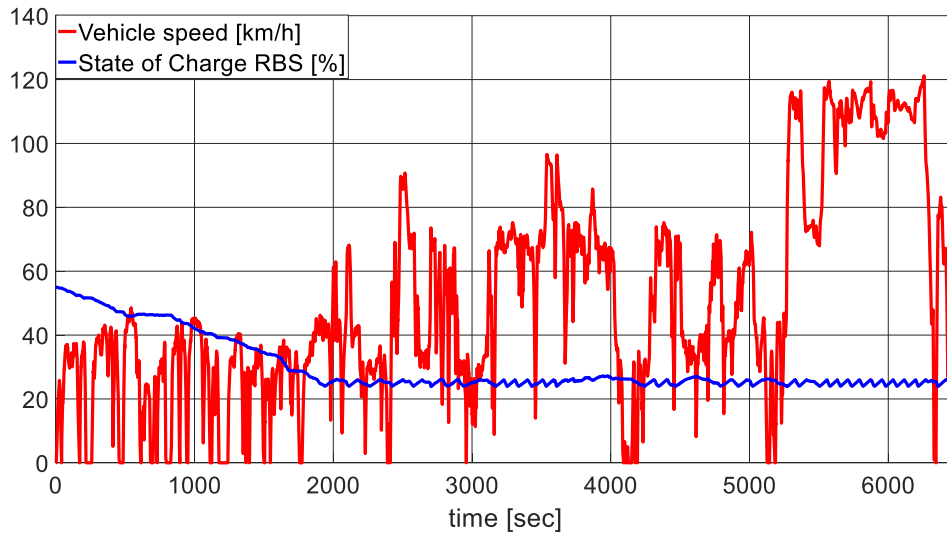


Figure 8.5 RBS results - SOC

Contextually, the fuel consumption of RBS, expressed in l/100km is reported in Fig.8.6 .

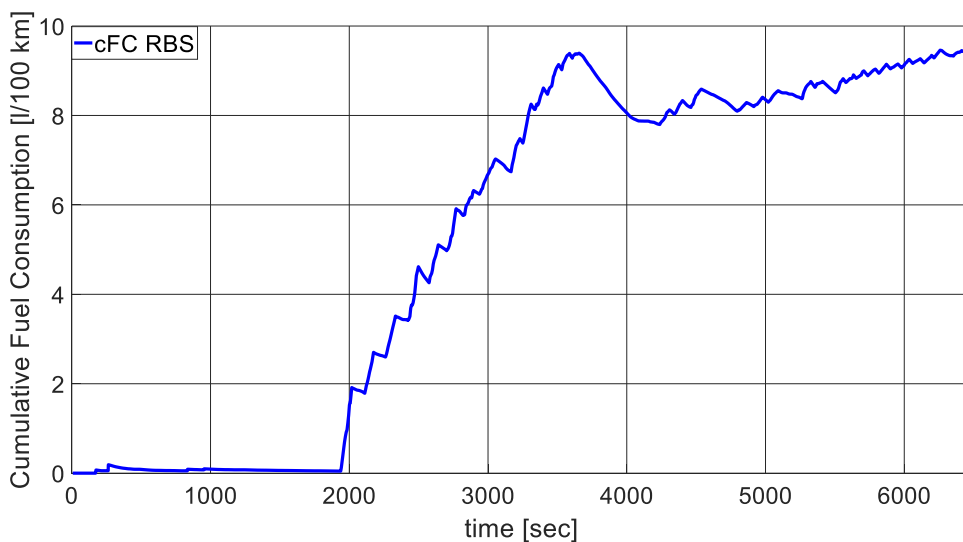


Figure 8.6 RBS results – cFC

### 8.3.2 ECMS results

The results for the ECMS controller have been reported considering all the implemented battery state of charge management strategies. Accordingly, the SOC trend over the reference cycle is reported in Fig.8.7 and the cumulative fuel consumption is depicted in Fig.8.8 .

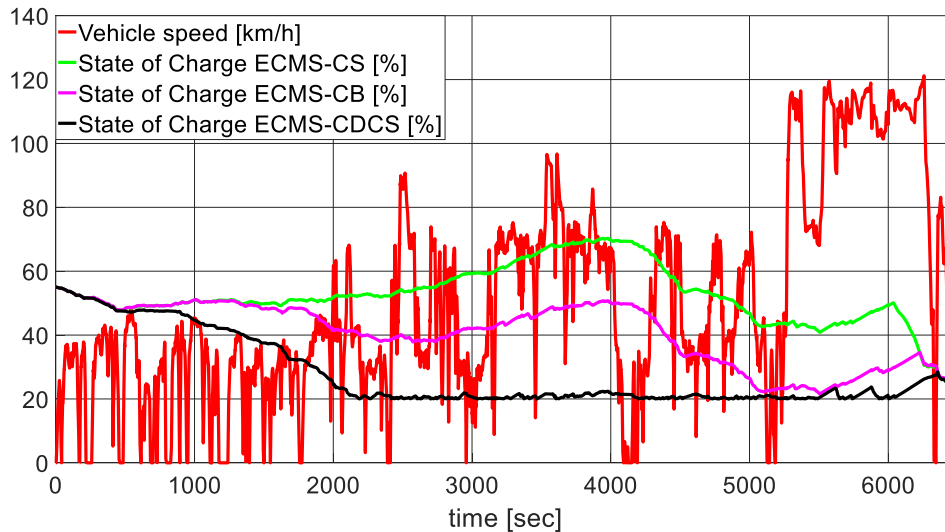


Figure 8.7 ECMS results - SOC

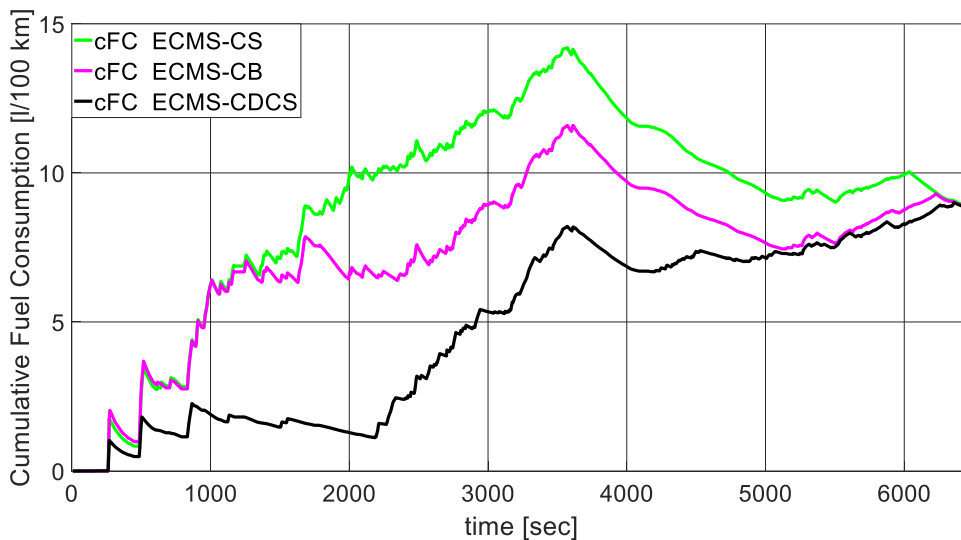


Figure 8.8 ECMS results – cFC

A charge-depleting/charge-sustaining approach, integrated within the ECMS controller, is a good solution for PHEVs, because it leaves the controller free to choose the best torque split factor, without penalizing the electrical energy use by forcing the recharge to be sustained the SOC around a pre-defined target. Anyways, this solution may not be the best if low-consumption zones are placed in the middle or at the end of the driving mission, since the SOC has already reached the lower limit, thus a further long battery discharge phase couldn't be possible.

### 8.3.3 RBS vs ECMS comparison

The comparison of the two implemented on-line controllers has been done considering both the average efficiencies of the machines included in the propulsion system and the engine fuel consumption over the driving mission. As it can be noticed from Fig.8.9, the overall average efficiencies are similar between RBS and ECMS controllers for all the propellers, which underlines that actually heuristics controller have a good efficiency in energy conversion, but the main difference, that reflects in a higher fuel consumption, is related to the conditions in which the machines are used. For the nature of the minimization algorithm, ECMS controllers are more flexible and can change the driving mode freely during the mission, according to the actual powertrain status and the driving conditions.

**Table 8.2 cFC results RBS vs EMCS**

Strategy	Fuel Consumption	Difference
	[l/100 km]	[%]
RBS	9.41	<b>0.00</b>
ECMS - Charge Sustaining	8.91	<b>-5.13</b>
ECMS - Charge Blended	8.87	<b>-5.74</b>
ECMS - Charge Depleting/Charge Sustaining	8.85	<b>-5.95</b>

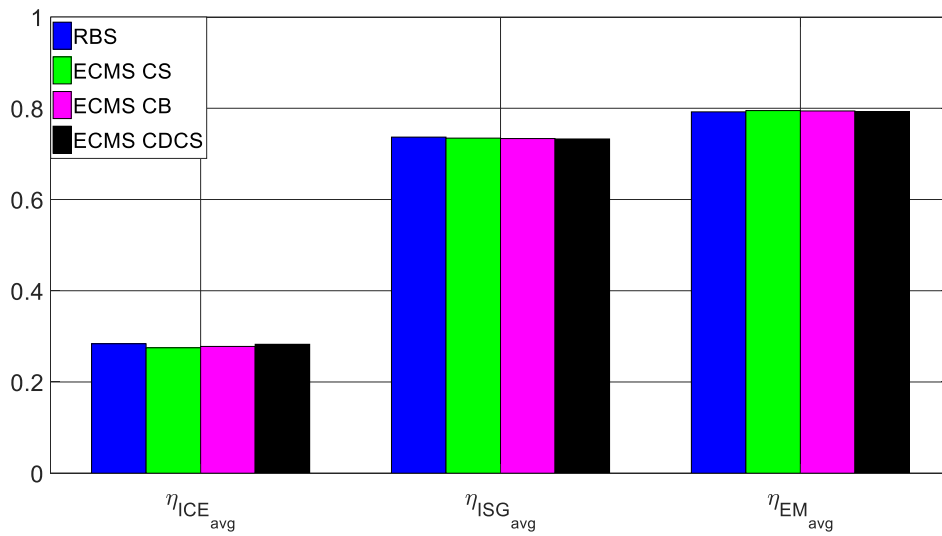


**Figure 8.9 Average Efficiencies on RDE cycle RBS vs ECMS**

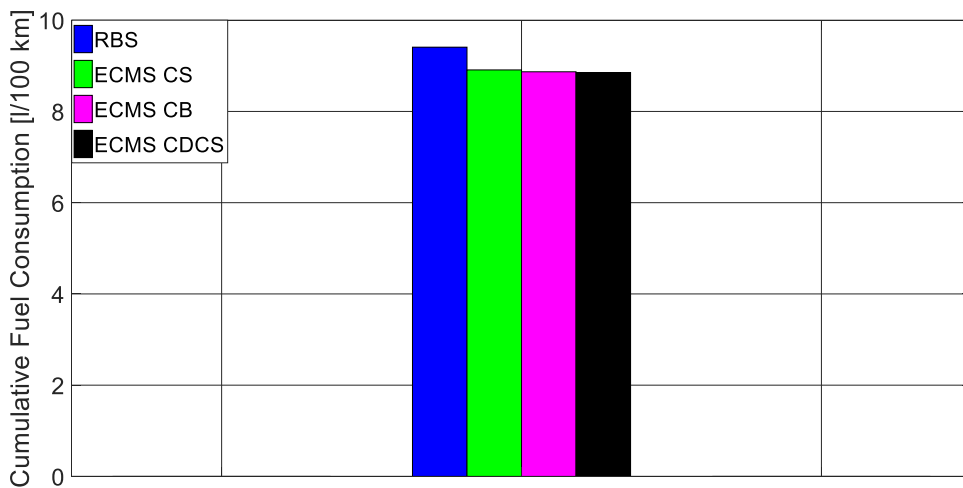


**Figure 8.10 Fuel Consumption RBS vs ECMS**

To motivate the differences in the performances of the controllers, considering the similar mean efficiencies of the machines over the cycle, it can be interesting to consider the engine usage during the cycle. It is possible to define the energy demand,  $E_{ICE}$ , to the engine as:

$$E_{ICE}(t) = \int_0^{end} Tq_{ICE} * \omega_{ICE} \quad 8.13$$

Where  $Tq_{ICE}$  is the torque provided by the engine and  $\omega_{ICE}$  is its angular speed.

Assuming such physical quantity as representative for the engine usage over the mission, it can be noticed in Fig.8.11 that the RBS controller makes a larger usage of the engine, if compared to the ECMS ones. The overall difference is around the 5% (4.5 MJ), which is a percentage similar to the fuel economy improvement shown in Tab. 8.2 and Fig. 8.10.

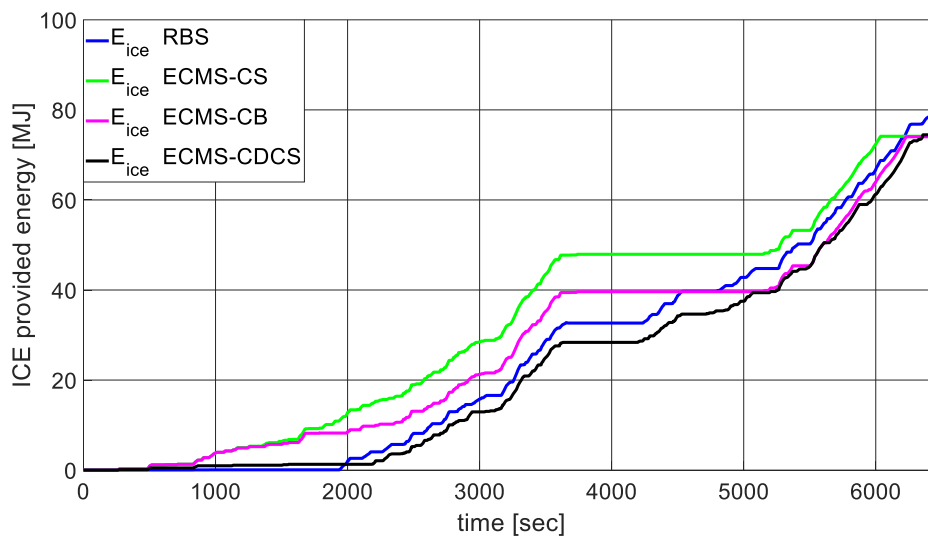
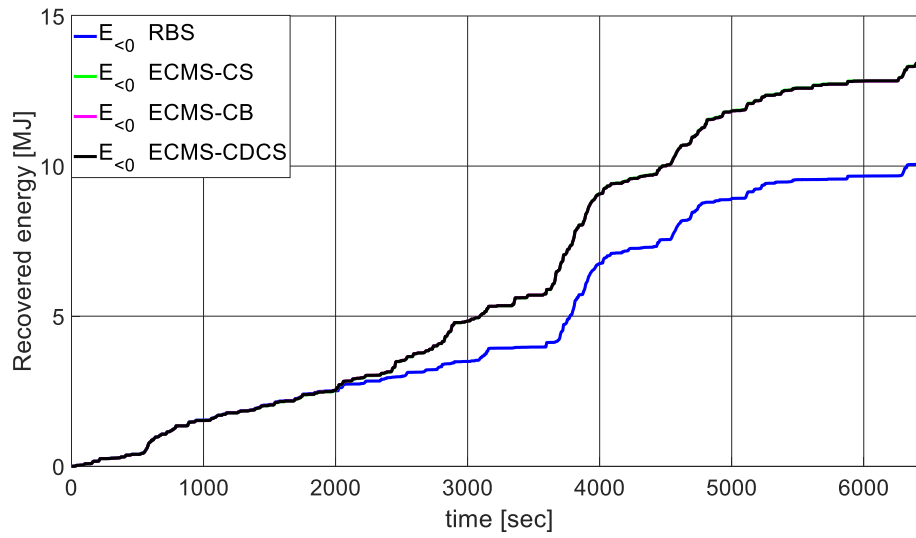


Figure 8.11 Engine provided energy on RDE cycle RBS vs ECMS

At this point, it may seem that the total amount of required energy for performing the driving cycle is different for the two controllers, since the engine provides more energy in RBS but the ending battery state of charge are the same. Even if these consideration are surely true, it is important to underline that the nature of the ECMS controller allows to recover more energy during the cycle, since the local optimization choses the torque split according to the actual required power at the wheels and, if it is negative, than choses the best recovering option, which, for the vehicle in exam, to use the electrical machines on the front axle. The RBS, instead, defines the operating mode according to the defined rules, therefore it may happen that the power request is negative, and the engine can't be switched off, but rather the recoverable energy is used mainly to keep it on using the ISG. In this case the transmission, and therefore its efficiency, is involved in the energy recuperation, leading to less net energy stored in the battery. In Fig.8.12 can be seen the trends of the recovered energy using the two controllers. The numerical difference (3.4 MJ) is similar to the one obtained in the engine usage, shown in Fig. 8.11, considering that the energy has to use the ISG, that has its own efficiency, to store the same amount of energy in the battery.



**Figure 8.12 Recovered energy on RDE cycle RBS vs ECMS**

## 9 Predictive control functions

This chapter presents two powertrain predictive control functions, for which it is assumed to know in advance, and for the entire driving mission, the vehicle speed and the road altitude profile. The aim of this section is to investigate the benefits that can come from the availability of predictive information about the route ahead the vehicle in terms of fuel economy and powertrain control in general. The first predictive function deals with the possibility of optimizing the energy recuperation when a ECMS controller is implemented in the vehicle (Par. 8.2), while the second control function is related to a generic Diesel hybrid electric vehicle and the goal is to optimize the usage of the aftertreatment system (Par.9.2).

### 9.1 Predictive State of Charge Management Strategy

For the implementation of a predictive state of charge management strategy for an optimal recuperation, the vehicle speed profile and road altitude profile have been considered known. The reference cycle for this section has been the one introduced in Chap. 7. The main aim of the proposed predictive SoCMS is to free enough battery capacity to store as much energy as possible during long recuperation phases [54].

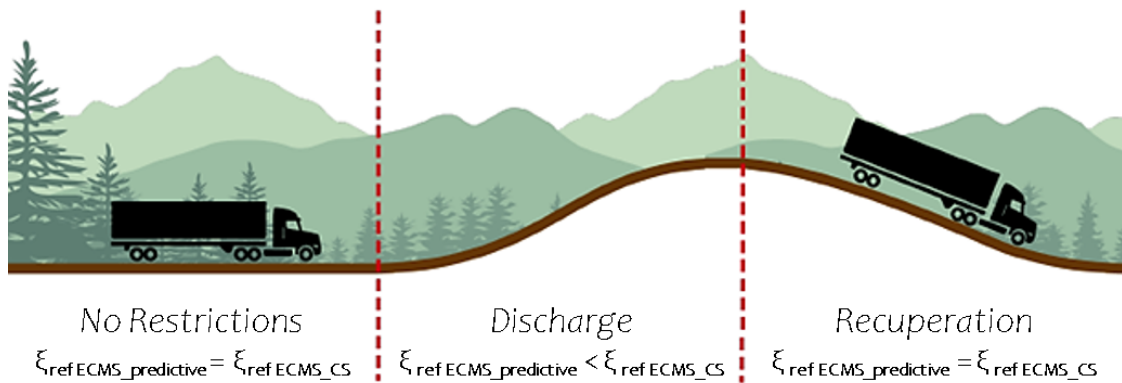


Figure 9.1 Predictive SOC target ideal modification

The predictive function influences the battery state of charge by modifying the SOC reference value along the driving mission, according to the presence of recuperation phases detected in the route ahead by means of predictive data.

#### 9.1.1 Algorithm

Predictive information is used in an algorithm that modifies the SOC reference value ( $\xi_{ref}$ ) of a CS state of charge management strategy (Eq. 8.9), as shown in Fig. 9.1.

##### 1° Step- Data preparation

Road altitude profile is filtered to eliminate noise (since it is a recorded signal, it presents some noise). After that, it is converted into road slope signal.

##### 2° Step- Global energy request calculation

Vehicle speed profile and road slope profile are used to calculate the energy request at the wheels to drive the cycle, using the simplified vehicle dynamics model mentioned in Par 4.1.

##### 3° Step- Recuperation phase detection

Energy request profile is used to find the recuperation phases in the cycle and the amount of energy that can be recuperated in each phase.

#### 4° Step- SOC reference modification

At this point, the energy recoverable for each phase is converted into equivalent battery state of charge, then these values are used to lower the SOC reference. Since even the energy profile is already calculated, the SOC reference is lowered only for the space segments just before every recuperation phase. Each segment space length is exactly the one the vehicle needs to consume the energy it will recover in the following recuperation phase.

In this study, only the CS strategy has been combined with predictive information, because:

- CB mode already lowers the SOC reference value along the distance, so the combination with the aforementioned algorithm is worthless.
- CD-CS strategy always has enough battery capacity to store energy in recuperation phases, since it sustains the charge once it reaches the lower battery limit;

### 9.1.2 ECMS-CS vs ECMS-predictive-CS

As for the comparisons in the previous chapter, the performance of the ECMS with and without predictive function for the battery state of charge management are compared using the evolution of the state of charge, the cumulative fuel consumption and the average efficiencies of the machines available on-board the vehicle.

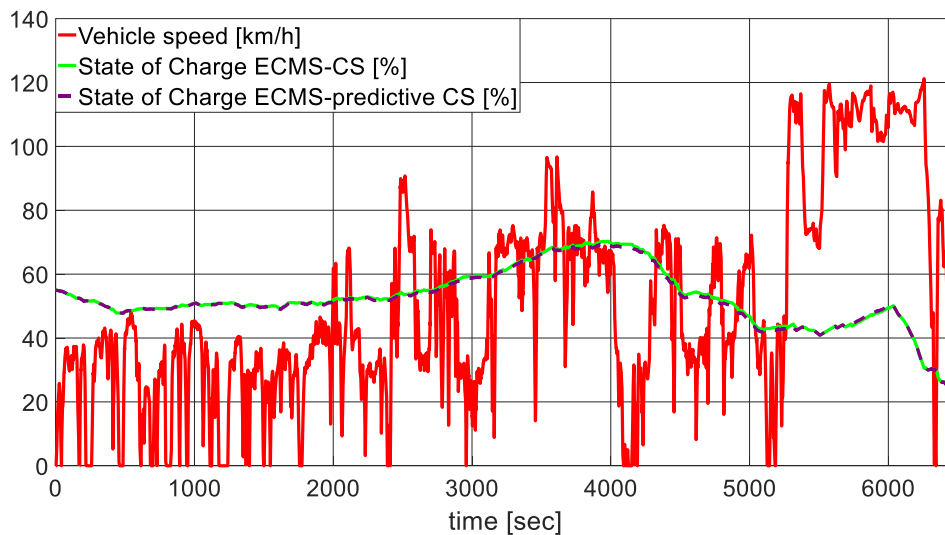


Figure 9.2 ECMS-CS vs ECMS-predictive\_CS – SOC

Figures 9.2 and 9.3 show behaviours for the controllers that substantially equivalent, and it is confirmed by the numerical data collected in Tab.9.1 And by Fig. 9.4, where average efficiencies are depicted.

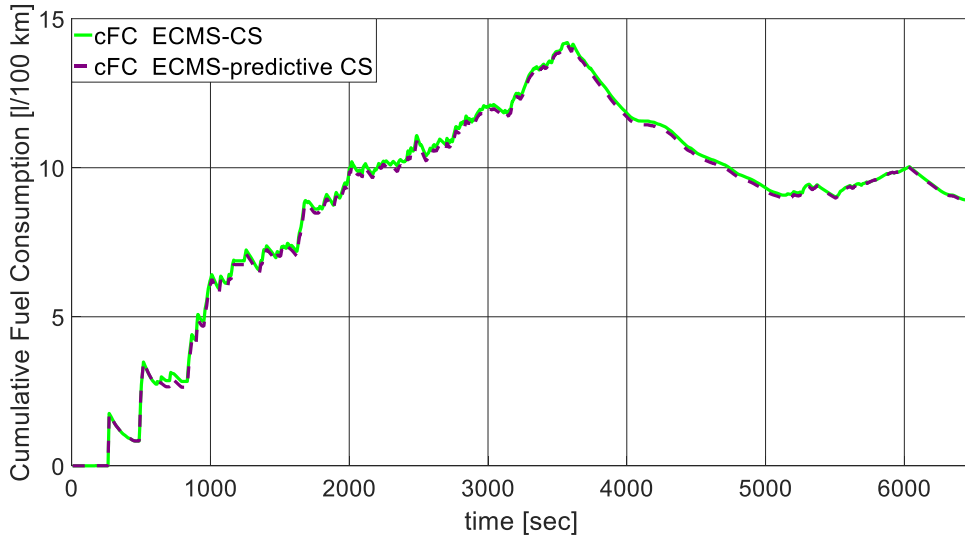


Figure 9.3 ECMS-CS vs ECMS-predictive\_CS – cFC

Table 9.1 Fuel Consumption comparison ECMS-CS vs ECMS - predictive CS

Strategy	Fuel Consumption	Difference
	[l/100 km]	[%]
ECMS - CS	8.91	0.00
ECMS – predictive CS	8.88	-0.34

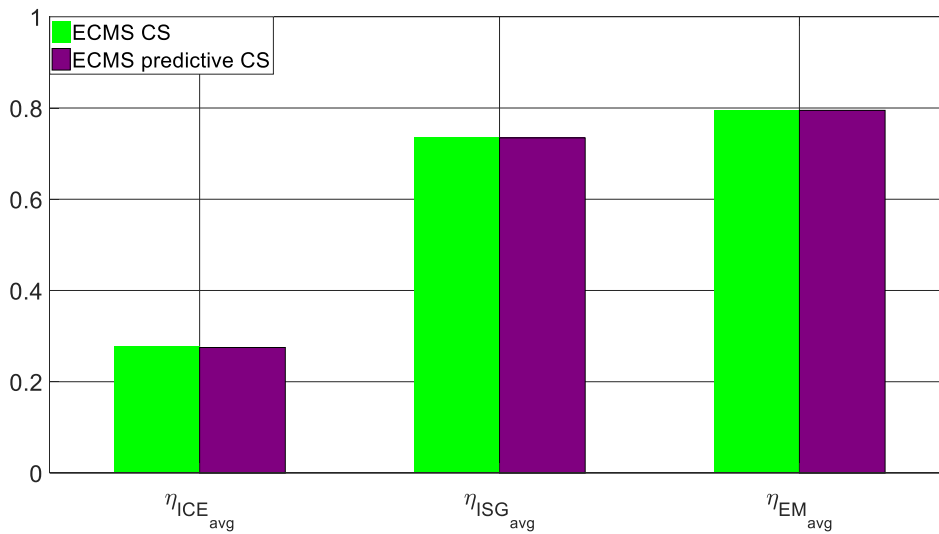


Figure 9.4 Average Efficiencies on RDE cycle ECMS-CS vs ECMS - predictive CS

Considering the limited benefits gained with the usage of predictive information for the battery levelling along the route, it may seem that the proposed function is worthless. However, since the aim of the shown predictive control is to partially empty the battery capacity in order to recover as much energy as possible during the regenerative braking phases, the reachable benefits by using such approach are strongly influenced by the total battery capacity, which is, for the vehicle under study, quite large.

To prove the dependency of the performance of the ECMS-predictive CS from the battery capacity, a sensitivity analysis has been conducted considering smaller battery sizes, and it is presented in detail in the following paragraph.

### 9.1.3 Battery capacity influence on ECMS-predictive-CS performance

This section aims to demonstrate that the battery total capacity has an influence on the proposed predictive state of charge management strategy. To do so, the comparison between ECMS -CS and ECMS-predictive CS has been done considering smaller battery capacities: 15 Ah and 6Ah, respectively 0.5 and 0.2 times the original size.

#### 15 Ah battery capacity

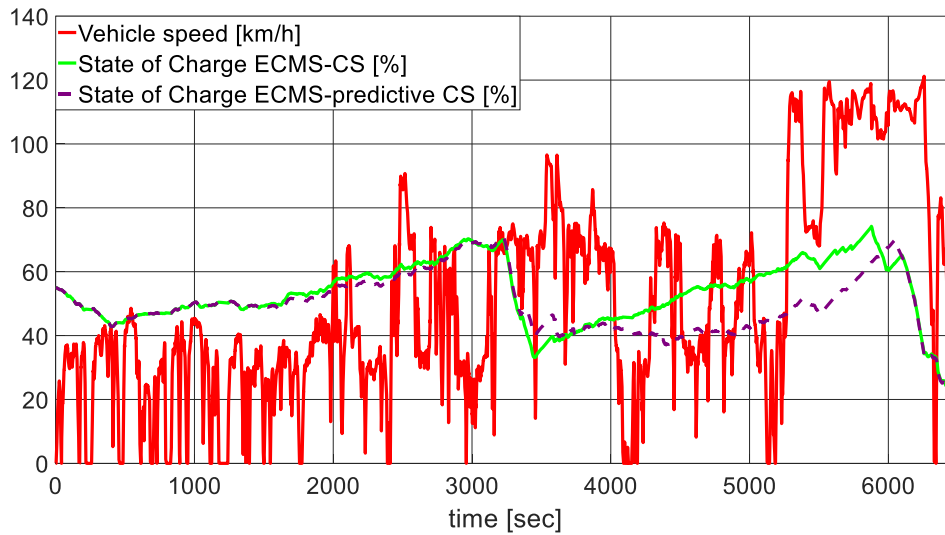


Figure 9.5 15Ah-ECMS-CS vs ECMS-predictive\_CS – SOC

Just considering a half of the original battery size, it is already possible to appreciate the difference between the behaviours of the two ECMS controllers. The predictive SoCMS behaves differently starting from the middle of the driving mission to the end. Contextually, also the benefits of using predictive information, in terms of fuel economy, are more appreciable, as confirmed by the numerical results collected in Tab 9.2.

Table 9.2 15Ah-Fuel Consumption comparison ECMS-CS vs ECMS - predictive CS

Strategy	Fuel Consumption	Difference
Battery capacity: 15 Ah	[l/100 km]	[%]
ECMS - CS	9.84	0.00
ECMS – predictive CS	9.78	-0.61

#### 6 Ah battery capacity

With a battery capacity of 6Ah, the different decisions the two controllers take along the driving mission are evident from the SOC trends, as depicted in Fig.9.6. In this case, in fact, there are diverse zones where the recoverable energy, if compared to the energy in the battery, is consistent.

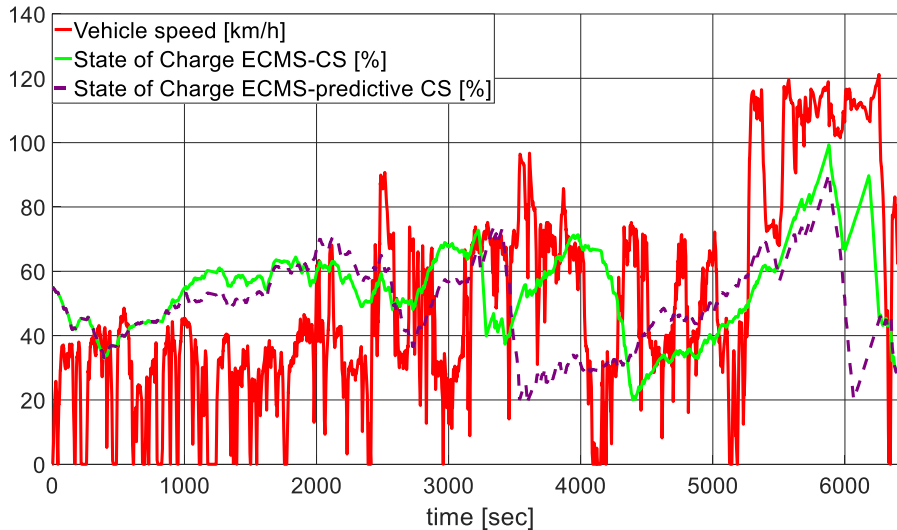


Figure 9.6 6Ah-ECMS-CS vs ECMS-predictive\_CS – SOC

The different behaviour of the predictive controller with respect to the standard ECMS – CS controller reflects in a different performance in terms of fuel consumption, as can be seen in Tab. 9.3.

Table 9.3 6Ah-Fuel Consumption comparison ECMS-CS vs ECMS - predictive CS

Strategy	Fuel Consumption	Difference
Battery capacity: 6 Ah	[l/100 km]	[%]
ECMS - CS	10.26	0.00
ECMS – predictive CS	10.15	-1.07

To further explain why the benefits of predictive information are more appreciable in the SOC levelling if considering small battery capacity, Figure 9.7 shows the SOC target modification for the considered battery sizes. The recoverable amount of energy corresponds to large percentages of the battery total energy if the capacity is limited. Due to this reason, the SOC target value is decreased differently for different battery capacities. In the case of the baseline 30Ah battery, the SOC target modification is so small that the effect is barely appreciable. On the contrary, if a 6Ah battery capacity is considered, the effect is noticeable, since the reference value of the ECMS controllers is highly modified by the predictive function.

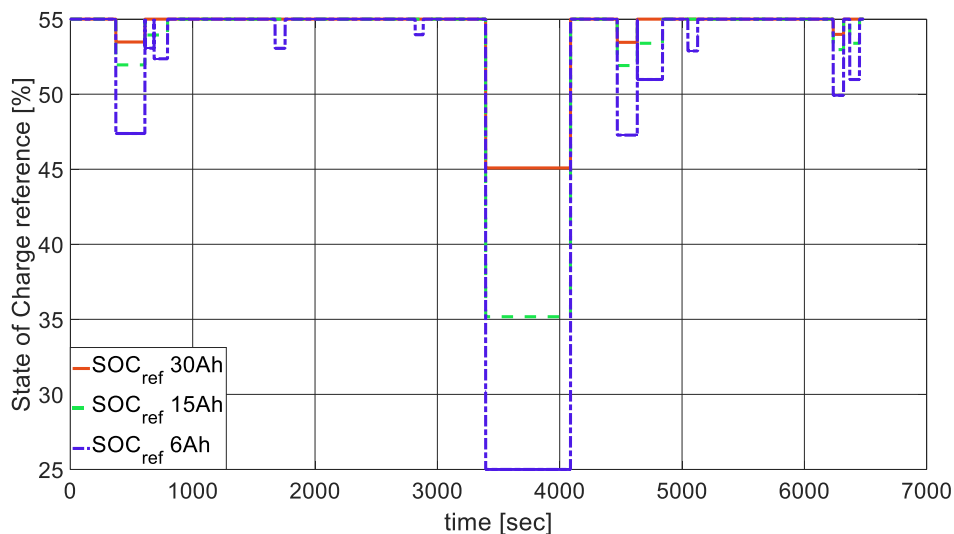


Figure 9.7 SOC target modification for different battery capacities

Moreover, considering that the ECMS charge-sustaining capability is given by an analytic function that acts like a slow PI controller, if the target modification is small, the control actions taken by the predictive controller are not so different from the standard ones. On the contrary, large target modifications lead to significant changes in the controllers' behaviours, reflecting in appreciable differences in the SOC trends and global fuel consumptions.

## 9.2 Predictive NOx emission control of a Diesel-HEV

With the aim of assessing the benefit of adding predictive information to powertrain control in order to better control the pollutant emission, in this test case it has been considered a different powertrain architecture and propulsion, considering a Diesel-based engine. However, also in this case, as in Par. 9.1, the external inputs are still the same, the vehicle speed and road slope profile. Such similarity depends on the goal of the section, which is to underline the potential benefits that can be obtained by including long-term predictive information (long-term e-horizon function) within the supervisory controller.

This section deals with the development of a predictive NOx emissions control function for a diesel hybrid electric vehicle, equipped with an electrically heated after-treatment system composed by a Diesel Oxidation Catalyst (DOC), a Diesel Particulate Filter (DPF), and a Selective Catalytic Reactor (SCR). Such function makes use of an a-priori-known vehicle speed trajectory that would be made available by the electronic horizon provider, and it presents two main sections. The first one predicts the aftertreatment system temperature and the NOx emissions both at the engine out and at the tailpipe over the prediction horizon. The second section defines the powertrain and after-treatment control policy, with the objective of minimizing after-treatment electric heating energy and SCR urea consumption, while respecting the legal NOx limits for the given mission. Furthermore, if the estimated pollutant production exceeds the limits even if the aftertreatment system is operated in the highest efficiency conditions, the predictive control function redefines the torque demanded to the internal combustion engine (and the one requested to the electric motor) to match the legal limits.

The aim of this predictive control function is to keep the NOx emissions within the legal limits, while minimizing urea usage and electrical energy consumption related to the aftertreatment system operation.

The control algorithm receives as input the speed and torque profiles of the engine for the next driving mission. Such information are supposed to be available on-board once the energy management strategy receives the information about the route ahead, and computes the optimal torque/power split factor between the electrical and thermal machines. Even if the electrical catalyst heating is mainly designed for the DOC system, but it is supposed the aftertreatment components are close to each other, so that there is a considerable effect even on SCR temperature. Figure 9.8 can give an overview of the algorithm structure of the predictive aftertreatment control function.

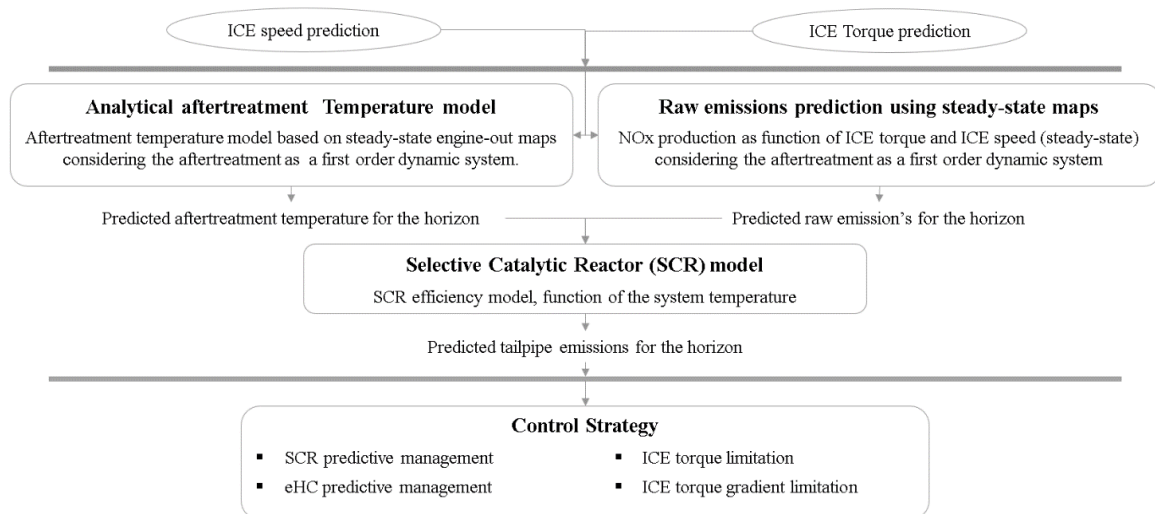


Figure 9.8 Predictive Aftertreatment control function algorithm structure

## 9.2.1 Modelling

### *Aftertreatment System Temperature Model*

As widely known, temperature plays a key role in the emissions reduction efficiency of an aftertreatment system. In this paper, the aftertreatment system temperature has to be intended as the average value of the SCR hardware, which is the parameter that mostly influences the efficiency of that component.

The methodology partially derives from the solution found by authors of [14], where a similar approach is used to model a temperature sensor positioned on the aftertreatment system before the DOC.

Firstly, a quasi-static exhaust gases temperature model has been designed by using steady-state maps. Therefore, the instantaneous engine-out temperature is only function of the engine speed and load.

$$T_{exh\_ss} = f(n_{eng}, bmep) \quad 9.1$$

Where  $T_{exh\_ss}$  is the exhaust gasses temperature,  $n_{eng}$  is the ICE rotational speed and  $bmep$  is the brake mean effective pressure of the engine. Then the aftertreatment temperature is evaluated by summing the responses of two first-order systems to the  $T_{exh\_ss}$ .

The combination of the two dynamics is needed since each of them represents a specific physical behavior of the aftertreatment system. More in detail, in the following the two contribution are referred to as fast and slow dynamics.

$$T_{aft\_fast} = \frac{(1-b)d}{1-bz^{-1}} T_{exh\_ss} \quad 9.2$$

Here  $z$  is the  $z$ -transform variable,  $b$  is the filtering quantity and  $d$  is a weighting gain. This term represents the heat exchange between the exhaust gases and the aftertreatment line as a physical system.

$$T_{aft\_slow} = \frac{(1-c)(1-d)}{1-cz^{-1}} T_{exh\_ss} \quad 9.3$$

Where the  $z$  is the  $z$ -transform variable,  $c$  is the filtering quantity and  $d$  is a weighting gain (as in Eq.2). The slow dynamics represent the thermal inertia of the aftertreatment line as a physical system.

Therefore, considering Eq. 9.2 and Eq.9.3 in the superposition principle, the predicted aftertreatment temperature is:

$$T_{aft} = T_{aft\_fast} + T_{aft\_slow} \quad 9.4$$

### *NOx Emissions Production Model*

Emissions production has been modelled using experimental steady-state maps based on engine load and speed. In this context, they haven't been corrected to consider transient phenomena [59], but only to take into account cold-start related emission. "Cold-start" refers to the conditions in which the engine is restarted when the SCR temperature is below its light-off value (190°C). The additional contribution to the emissions

production related to this specific scenario is due to the null conversion efficiency that the SCR system has when its temperature is below the activation limit.

According to this definition, the instantaneous production can be defined as:

$$\dot{m}_{NOx} = f(n_{eng}, bmep) + d\dot{m}_{NOx\_CS} \quad 9.5$$

Where  $\dot{m}_{NOx}$  is the actual emission and  $d\dot{m}_{NOx\_CS}$  is the additional contribution due to cold start events, if needed. The decision of adding the cold-start terms depends on the aftertreatment temperature and the contribution is proportional to the difference between the actual temperature at the engine re-start and SCR light-off temperature. The value obtained with this modelling is representative of the emissions production at the engine-out, while the tailpipe emissions are obtained considering the presence of SCR and eHC systems. The selective catalytic reactor has been modelled considering its efficiency as a function of the system temperature, assuming a light-off temperature equal to 190°C. If also the electrically heating feature is used, then the cold-start related contribution is eliminated since, as it will be clarified in the next paragraph, the look-ahead nature of the function allows using the aftertreatment electrical heating in a predictive way, so that at the engine restart the SCR system is already warm enough to be efficient.

#### Models validation

The validation of the aftertreatment temperature and raw emissions production modelling has been done against experimental data, results have been normalized for confidentiality reasons. The reference cycle for the validation has been WLTC, since the experimental data were already available at the beginning of this activity.

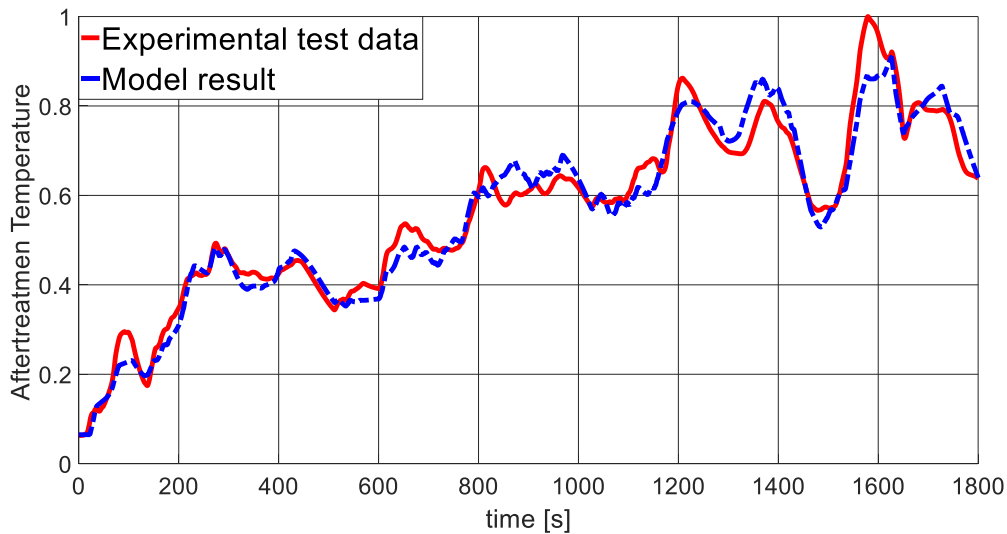


**Figure 9.9 Aftertreatment Temperature model validation**

Figure 9.9 shows that the aftertreatment temperature is estimated quite well considering that the modelling is zero-dimensional and control oriented, therefore it needs to be fast, which is usually detrimental for the accuracy. Instead, the raw emissions production model is highly representative for the experimentally measured data (Fig9.10).

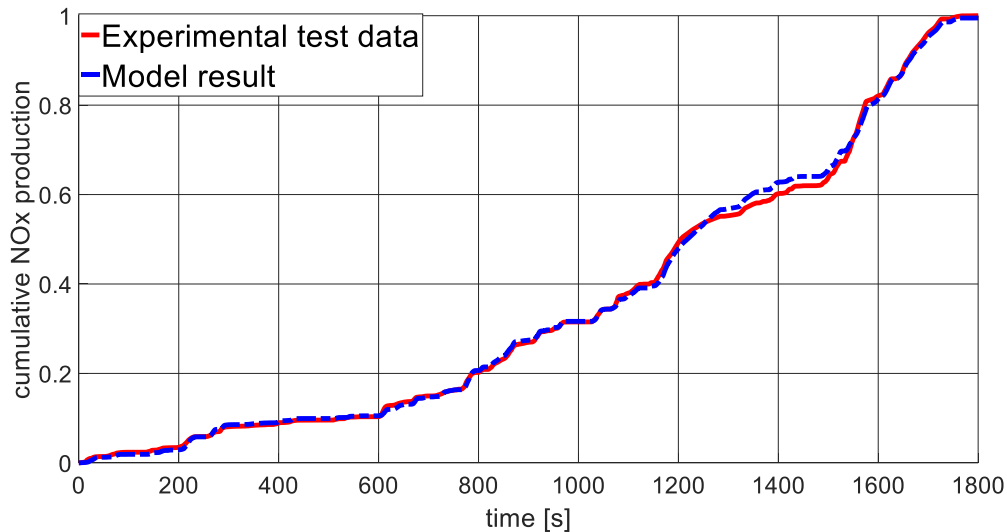


Figure 9.10 NOx production model validation

### 9.2.2 Control

The emission control is here meant as the strategy to be followed in order to ensure the NOx cumulative production over the driving mission will respect the legal limitations (to be always intended at the tailpipe), while reducing as much as possible the SCR and eHC usage. In general, when a prediction horizon is considered, it is assumed that the driving mission won't change in the future. Anyways, to take also into account small changes that can occur along the route, the emissions legal limitations are corrected with a safety factor  $k_s$ , as clarified in the following.

It is important to remark that the designed function has, by means of emissions production modelling, the capability to predict the NOx production over the mission before it starts. This is possible knowing in advance the engine torque and speed profiles, considered as predictive information. The control strategy foresees three different cases:

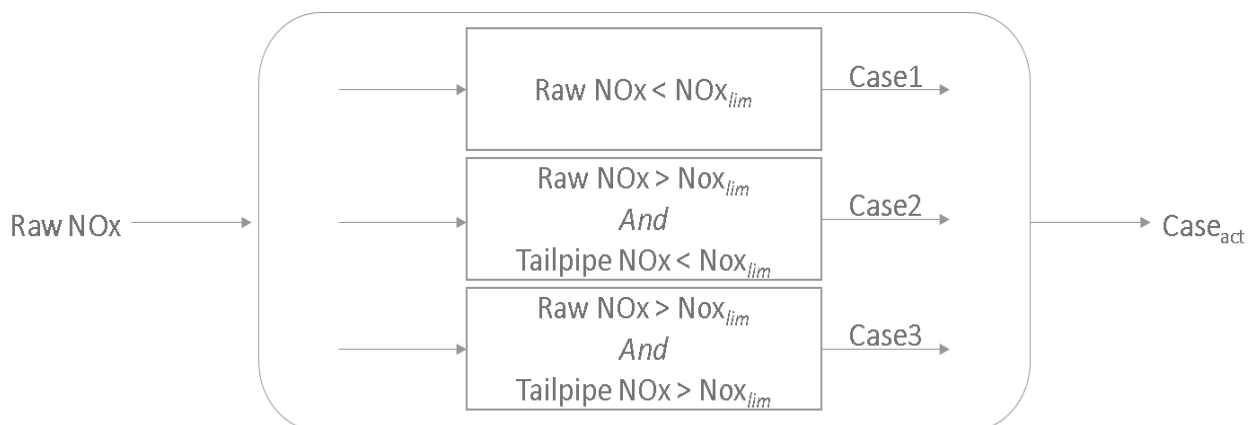


Figure 9.11 Strategy possible cases

- “**Case 1**”, the raw NOx emissions, at the engine-out and reported at the tailpipe without SCR and eHC activation, respect the limitation;
- “**Case 2**”, the raw NOx emissions don't respect the limits, but tailpipe emissions are within the limits (using SCR and eHC systems);
- “**Case 3**”, Tailpipe NOx emissions exceed the limit imposed by the regulation.

According to the actual case ( $Case_{act}$ ) of the driving mission, i.e. the prediction horizon, the control function can make different choices:

- $Case_{act} = \text{Case 1}$ , here the controller asks to the Engine Control Unit (ECU) to minimize the SCR operation and to disable the eHC system, for the whole driving mission;
- $Case_{act} = \text{Case 2}$ , the function will calculate the exact position over the horizon from where on it is possible to minimize the usage of the SCR, while remaining within the legal NOx emission limitations;
- $Case_{act} = \text{Case 3}$ , in this case the algorithm foresees the possibility of limiting the engine torque absolute value and gradient to avoid high emissions phases, in order to respect the limits.

**Table 9.4 Predictive emission control strategy possible actions**

$CASE_{act}$	Control Strategy			
	SCR	eHC	ICE Torque	ICE Torque gradient
1	Minimum	Off	Unconstrained	Unconstrained
2	On/Minimum	On/Off	Unconstrained	Unconstrained
3	On	On	Limited	Limited

The SCR “minimum” usage request has to be intended as an advice to the ECU. This latter would still manage the SCR system following its standard strategy, but assuming a very low NOx production at the tailpipe. Therefore, when possible and for the maximum time allowed, the AdBlue usage will be reduced.

At this point, a clarification for Case3 is probably needed. Since the vehicle has a hybrid powertrain, when the function asks for a torque gradient limitation of the ICE, it assumes that the battery has enough energy to provide the additional using the electrical machine, to still match the overall driver request. Therefore, such torque gradient limitation request is verified by the Hybrid Control Unit (HCU), that decides if it is possible to satisfy it or not, according to the driver demand and the battery state of charge level.

As briefly mentioned before, the control function also foresees the possibility of predictively requiring the eHC activation. In fact, combining the predictive knowledge of the engine switch-on events with the predicted aftertreatment temperature trend, it is possible to know in advance when it is needed to heat-up the aftertreatment system. Consequently, the function can ask to the ECU to switch-on the eHC before the engine firings, in order to avoid cold starts emissions, since the SCR system will be already warm enough to be efficient. However, this functionality has not been further investigated since data on the eHC system were not available, therefore the proof of the capability of the predictive function in terms of predictive catalyst heating hasn’t been possible in this content.

The outputs of the described control function have two different targets: the ECU and the Hybrid Control Unit (HCU). More in detail, the engine control unit will be asked for managing the SCR (On/Minimum) and the eHC (On/Off) according to the function calculations, while the HCU will receive the limitation on the engine torque gradient in order to respect the emissions limitation (only for Case 3).

The objective of respecting the NOx legal limitations is always considered, while the goal of reducing urea consumption and CO<sub>2</sub> emissions can be reached only in Cases 1 and 2.

### 9.2.3 Results

Considering as reference driving cycle the RDE cycle introduced in Cap. 7, the input for the aftertreatment temperature and NOx production is the predicted usage of the internal combustion engine over the mission, supposed to be known as this control function has been developed to be integrated in a predictive energy management capable of optimizing the energy usage, therefore calculating when it is worth to use the engine rather than performing a pure electric drive. Therefore, the function input are the ICE speed and torque profile over the chosen route. The trends of these two parameter are reported in Fig.9.12. As can be noticed, the engine is not always used but rather has a switching behaviour, which would hardly influence the aftertreatment temperature.

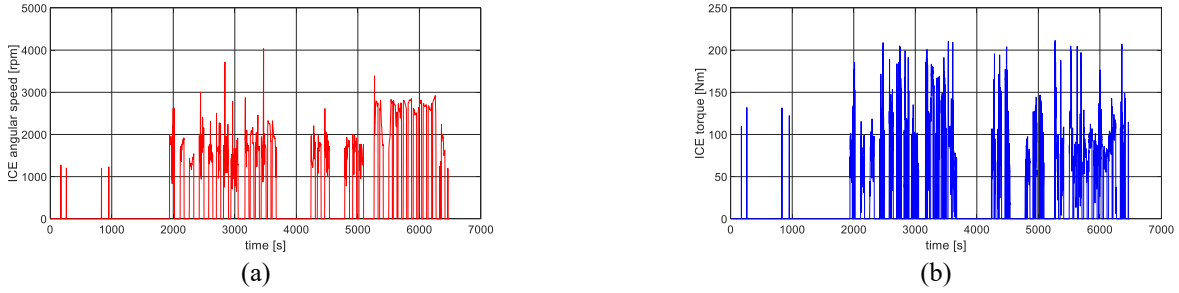


Figure 9.12 Predictive Aftertreatment control function Input

According to the shown input, the predicted aftertreatment temperature trend obtained by using the model shown in Par 9.2.1, is depicted in Fig.9.13.

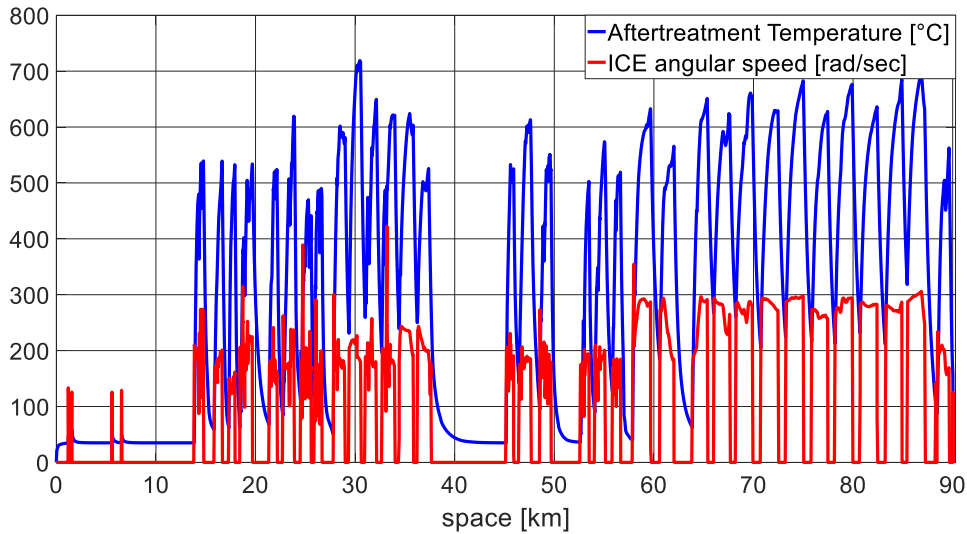


Figure 9.13 Aftertreatment Temperature prediction

Before showing the NO<sub>x</sub> production estimation, it is important to mention that in this function have been considered two limitations for the pollutant emission production, the first one can be referred to as legal limitation, since it is simply the Euro 6 limits for NO<sub>x</sub> production in Diesel vehicles [80 mg/km], multiplied by the total space driven during the driving mission, which is predictable since the speed profile is given.

$$NO_{x\_leg\_lim} = NO_{x\_lim} * s \quad 9.6$$

Where  $NO_{x\_leg\_lim}$  is the cumulative value of the limit,  $NO_{x\_lim}$  is the limit imposed by the regulation and  $s$  is the total distance (in km).

The additional limitation considered within the function and called function limitation,  $NO_{x\_fun\_lim}$ , is a virtual limitation, more restrictive than the legal one, imposed to ensure the NO<sub>x</sub> production won't exceed in any case the legal limit of 80 mg/km. The function limitation is obtained by the legal one by means a of safety factor  $k_s$ , chosen equal to 0.8, as in Eq. 9.7.

$$NO_{x\_fun\_lim} = NO_{x\_leg\_lim} * k_s \quad 9.7$$

Considering these two limitations, the NO<sub>x</sub> production estimation both at the engine-out and at the tailpipe can be calculated. The results on the reference driving mission are depicted in Fig.9.14.

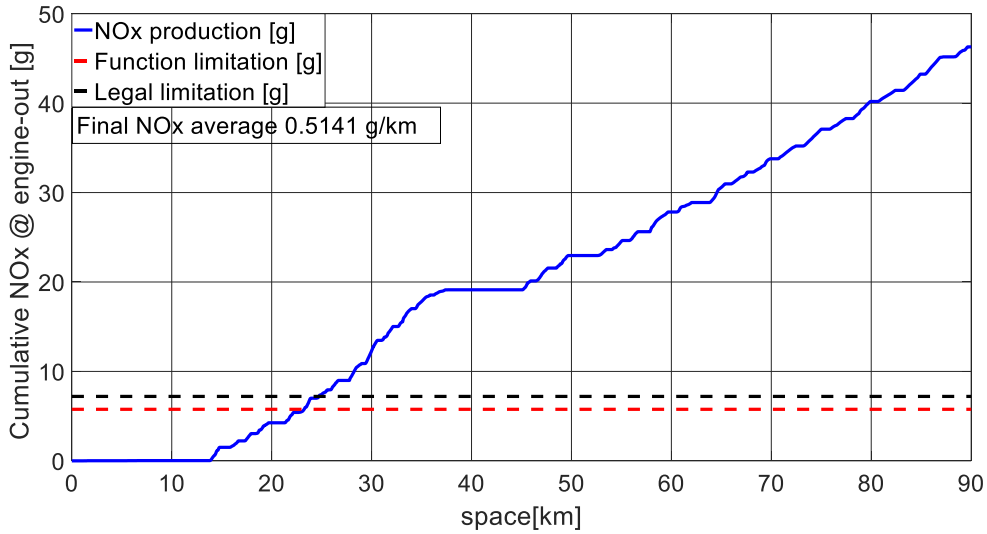


**Figure 9.14 Cumulative NOx production @ engine - out estimation**

The emission production estimation at the tailpipe have been done considering an SCR conversion efficiency that depends on the aftertreatment actual temperature, as from the scheme in Fig. 9.8, for the whole driving mission, without any predictive aftertreatment control. The trend obtained is depicted in Fig.9.15.

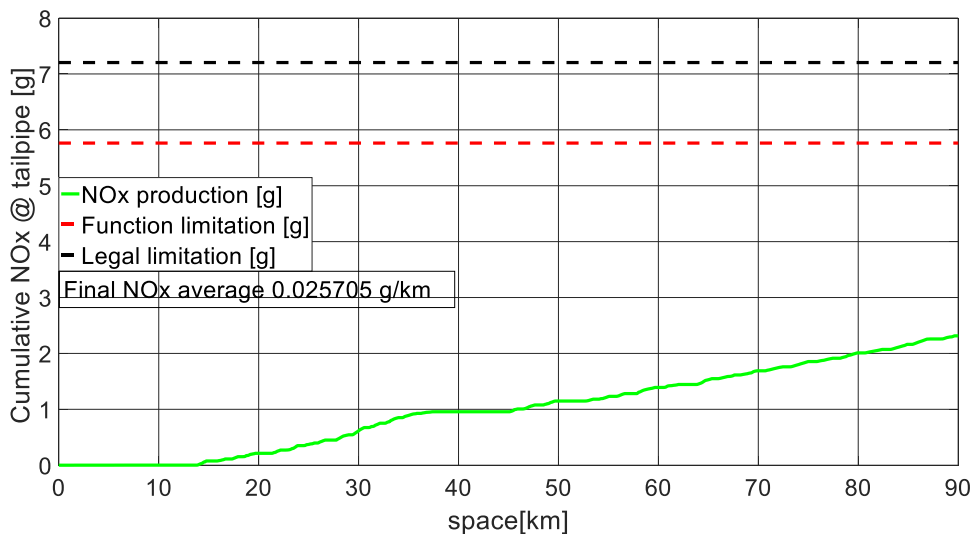


**Figure 9.15 Cumulative NOx production @ tailpipe estimation**

### Case 2

According to the rules defined in Tab.9.4, the chosen driving mission belongs to Case2.

As foreseen by the strategy for Case2, there would be a certain position over the route, from which on it would be possible to minimize the SCR system usage while respecting the function NOx cumulative limitation.

Figure 9.16 shows that the strategy requires the SCR to be active until km 84.2, where the system usage can be minimized while respecting the cumulative emissions limitation. Unfortunately, the lack of experimental data doesn't allow a clear quantification of the AdBlue usage reduction. It is anyways possible to assess that for the 6.52 % of the total distance, the SCR consumption is minimized and, moreover, it happens in the high-speed portion of the mission, which would require a consistent urea injection if the SCR system was active. The SCR request outputted by the function needs a clarification: when it is set to 1, the function leaves to the

ECU the freedom of using the system without constraints, while if it is set to 0, it means the function is suggesting to the ECU to avoid injecting more AdBlue than the minimum value, because it would be useless, since the NOx emissions limitation won't be exceeded.

Another information provided by Fig. 9.16 is that, in Case2, the control function matches exactly the imposed function limitation since the average NOx production is 0.064 [g/km], which is also the value of the virtual constraint.

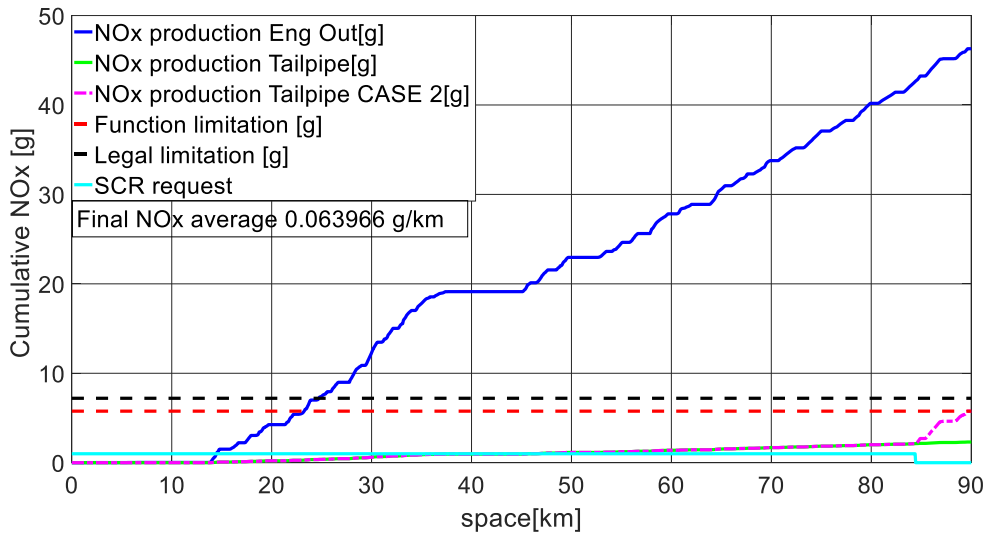


Figure 9.16 Predictive emission control strategy decisions for Case2

### Case 1

To investigate also the control decisions taken from the predictive control function on a driving mission that belongs to Case1, it has been considered a limited portion of the same cycle.

Here the suggestion to the ECU is to minimize as much as possible the SCR usage since, from the NOx productions estimations, it is possible to assess that the limit won't be exceeded. For such test-case the chosen portion of the cycle is 0-1990 [s], for which the inputs are as reported in Fig.9.17.

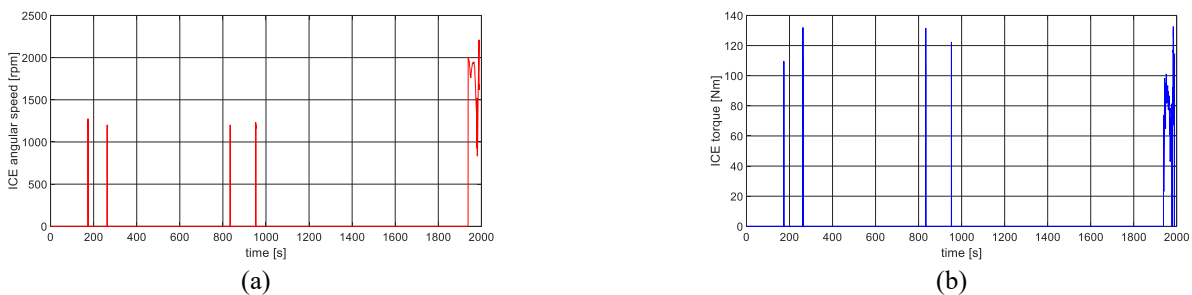


Figure 9.17 Predictive Aftertreatment control function Input (Case1)

As it can be noticed from the Fig.9.18, the NOx production at the tailpipe (dot-dashed magenta line) are equal to the ones predicted at the engine-out (blue line), considering null the contribution of the SCR system (cyan line), for which the activation request is constantly zero over the considered cycle portion.

The green line, representing the NOx production at the tailpipe if the SCR system is always active when needed, it's quite far from the limitation, both the legal and the function ones, meaning that the injected AdBlue would be somehow useless, since the NOx production at the engine-out would be already compliant with the regulation limit.

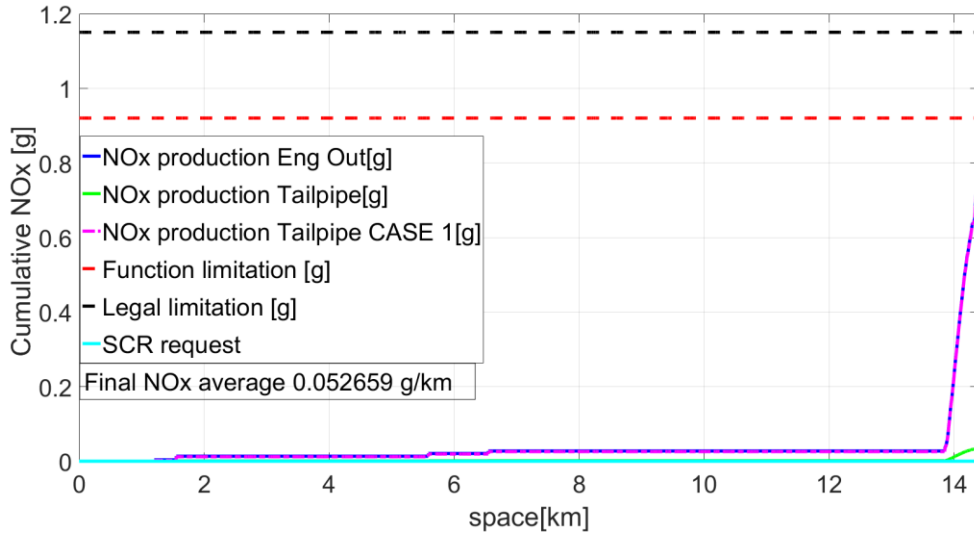


Figure 9.18 Predictive emission control strategy decision for Case 1

### Case 3

For driving mission belonging to Case3, which means that the NOx production limitation won't be respected even using the SCR for the whole duration of the trip, the proposed control strategy proposes to the supervisory controller to limit the engine torque gradient.

To show the behavior of the function in this case, the considered cycle portion is between 5262.5 and 5308 seconds, since it is needed an "aggressive" portion of the cycle, which means the engine speed and torque are significantly high, to be sure that also the tailpipe emissions, considering the SCR system always active, exceed the function limitation. With this aim, the input of the function is reported in Fig.9.19.

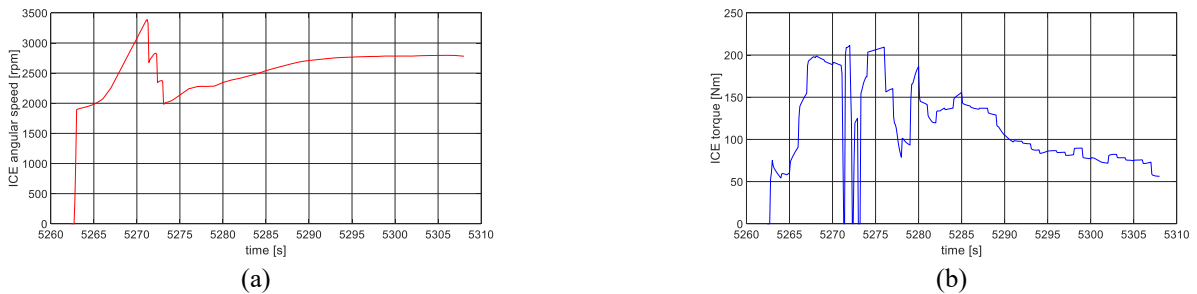
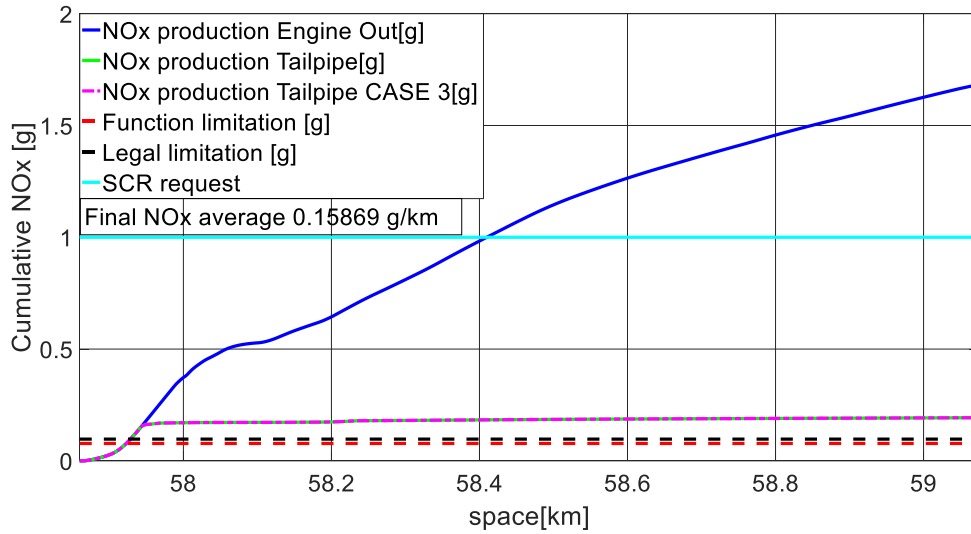


Figure 9.19 Predictive Aftertreatment control function Input (Case3)

The results for Case3 are reported in the following figure, without any limitation on the engine usage. It is possible to see that the NOx production estimation exceeds both the legal and function limitation, therefore, on that particular driving mission, the pollutant emissions wouldn't be compliant with the actual regulation. In order to match the imposed limitations, as reported in Tab. 9.4, the implemented predictive aftertreatment control function has the capability of calculating the internal combustion engine torque limitation needed in order to reduce the NOx production to be compliant with the constraints.



**Figure 9.20 Predictive emission control strategy decision for Case3**

In this particular scenario, Case3, it can be seen the additional capability of the proposed predictive function, which is the engine torque gradient limitation in order to match the function limitation.

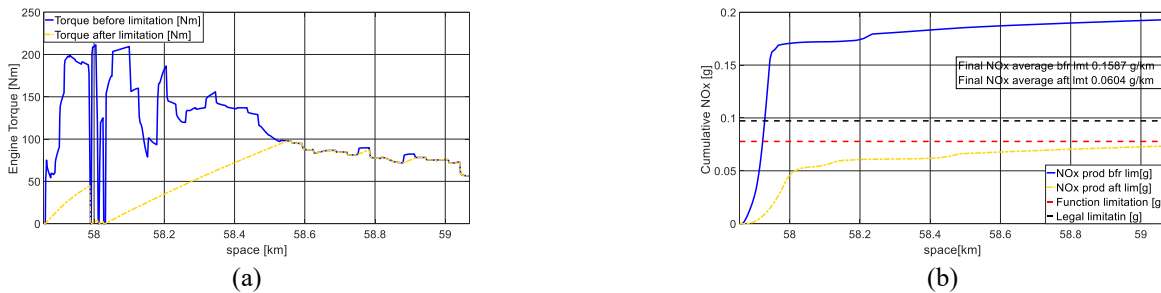


**Figure 9.21 Torque gradient limitation (a) and consequent NOx production reduction (b) for Case3**

As Fig.9.21 shows, the torque limitation (a) helps to reduce the NOx production (b) and, therefore, to respect the function constraints. The yellow line in Fig.9.21 (a) represents the limited engine torque, and it clarifies why this control policy can be considered only if the powertrain can drive in pure electric or, at least, has a large electric boosting capability since, if the electrical part won't be able to fill the gap given by the engine torque limitation, the driver request won't be satisfied.

## 10 Optimal Powertrain Control

Considering a generic multivariable dynamic system evolving over a time horizon, an optimal control problem can be formulated in order to find the optimal sequence of control inputs that minimizes a given cost-function, which is usually related to the cost of the system operation.

Thinking to a powertrain that performs a given driving mission, it is possible to define an optimal control problem to optimize its operation in order to obtain the best performance in correlation with the objective which could be, for example, the minimum fuel consumption [1,23], the minimum lap-time on a track [60] or the minimum of the pollutant emissions production [61].

Usually, when dealing with an optimal control problem, the following characteristics are always present:

- *Boundary Conditions*, that defines the initial and final state desired for the dynamic system;
- *Constraints* on the values the variable included in the problem can assume;
- *Cost-function*, to be minimized in order to find the optimal control law.

Different algorithms have been proposed over the years by automotive researchers with the aim of solving optimal control problems applied to hybrid powertrains using, as mentioned in Par.1.2.3, optimization techniques called: *Dynamic Programming* [1,62-63], *Pontryagin's minimum principle* [14-15,64-65] and *Convex Optimization* [66-68].

In this content the Dynamic Programming has been investigated in detail and applied to the reference vehicle detailed in Chap.3 to find the optimal control law to be applied to the powertrain in order to reach the best possible fuel economy.

### 10.1 Dynamic Programming

#### 10.1.1 Overview

##### *Theory*

As Dynamic Programming (DP) [69] is intended a direct, or numerical, method to solve multistage optimal control problems (OCP). It is considered the only optimization technique able to provide a solution to any OCP without limitation on the problem complexity. Since it performs a global optimization, it is non-causal [1], which means the problem variables that are independent on the system evolution (in the following mentioned as *Disturbances*), must be known *a priori* for the entire optimization horizon.

Such algorithm derives from the Bellman's principle of optimality, that can be stated in different ways, for example:

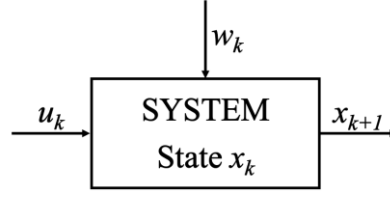
*“if the optimal solution for a problem passes through an intermediate state  $(x_1, t_1)$ , then the optimal solution to the same problem starting at  $(x_1, t_1)$  must be the continuation of the same path [70].”*

Or, equivalently

*“An optimal control policy has the property that no matter what the previous decision (i.e., controls) have been, the remaining decisions must constitute an optimal policy with regard to the state resulting from those previous decisions [71].”*

Considering Bellman's principle, it can be assessed that, from a generic stage of the problem domain to the end, the optimal control policy corresponds to the remaining part of the global optimal solution.

To express such complex concept in mathematical formulations, a generic discrete-time dynamic system (Fig. 10.1) can be considered.



$$x_{k+1} = g_k(x_k, u_k, w_k) \quad k = 0, 1, \dots, N - 1$$

Figure 10.1 Generic discrete-time dynamic system

Being

- $k$ , discrete-time index, or stage;
- $N$ , given time horizon;
- $x_k \in S_k$ , system state vector at time  $k$ , can be measured at time  $k$ ;
- $u_k \in U_k(x_k)$ , control input vector at time  $k$ ;
- $w_k$ , disturbance vector at time  $k$ , a random variable;
- $g_k(\bullet, \bullet, \bullet)$ , function capturing system evolution at time  $k$ .

Assuming that all the intermediate states of the system's evolution are known, the aim is to find an optimal control input policy that minimizes a given cost-function  $J$ , which can be formulated as shown in Eq. 10.1.

$$J = \underbrace{g_N(x_N)}_{\text{terminal cost}} + \underbrace{\sum_{k=0}^{N-1} g_k(x_k, u_k, w_k)}_{\text{cumulate cost}} \quad 10.1$$

The terminal cost is a constraint to ensure the desired state of the system at the final stage, while the stage cost is related to the actual system status.

Now let  $\mu_k$  map the state  $x_k$  to control input  $u_k$

$$u_k = \mu_k(x_k), \quad u_k \in U_k \forall x_k \in S_k \quad 10.2$$

The following definition may then be introduced

$$\pi := \{\mu_0(\bullet), \mu_1(\bullet), \dots, \mu_{N-1}(\bullet)\} \quad 10.3$$

where  $\pi$  is called *admissible policy*. Given an initial system state  $x_0$ , the states  $x_1, \dots, x_N$  are unknown and the disturbances  $w_0, \dots, w_N$  are random variables. It is then possible to define the *expected cost* associated with an admissible policy  $\pi$  as:

$$J_\pi(x_0) := g_N(x_N) + \sum_{k=0}^{N-1} g_k(x_k, \mu_k(x_k), w_k) \quad 10.4$$

Let  $\Pi$  be the set of all admissible policies. Then,  $\pi^*$  is called an *optimal policy* if:

$$J_{\pi^*}(x_0) \leq J_\pi(x_0), \quad \forall \pi \in \Pi \quad 10.5$$

The optimal cost is defined as  $J^*(x_0) := J_{\pi^*}(x_0)$ . Thus,  $J^*(\bullet)$  is a function that maps initial states to optimal cost.

Therefore, the output of the optimization algorithm returns the optimal control policy  $\pi^*$  defined as:

$$\pi^* = \{u^*_0, u^*_1, \dots, u^*_{N-1}\} \quad 10.6$$

In other words, the DP algorithm proceeds backwards starting from the final state, choosing at each stage the control actions that minimize the cost-to-go function from the actual stage to the end, finding in this way the optimal control policy that minimizes the global cost.

The backward optimization is divided in two stages:

- *Initialization*, where a cost is associated to desired final state of the system:

$$J_N(x_N) = g_N(x_N), \quad \forall x_N \in S_N \quad 10.7$$

- *Recursion*, where the cost-to-go matrix is minimized to find the optimal control action at actual stage:

$$J_k(x_k) = \min_{u_k \in U_k(x_k)} [g_k(x_k, u_k, w_k) + J_{k+1}(f_k(x_k, u_k, w_k))] \quad 10.8$$

$$\forall x_k \in S_k, \quad k = N - 1, \dots, 0$$

### ***Applications in Automotive***

Over the years, DP has been largely used in automotive research for different applications. Authors of [72] have used dynamic programming to optimize the energy management of hybrid electric vehicles, while the work [73] proposes an optimization of the battery thermal management using this optimization technique. In [1] the author uses the optimal control policy to benchmark a real-time sub-optimal controller.

Other interesting works use DP in combination with other optimization algorithm, for example in [67] it has been used in a two layer optimal control, in combination with convex optimization, to optimize the non-linear control variable, such as the gear selection and the ICE status, making the problem of energy management convex and, therefore, solvable using CVX.

In [74], instead, Dynamic programming has been applied in order to optimize the vehicle speed profile over a given route in a given time, while authors of [75] have improved the capability of cruise controller application by applying DP over a receding horizon, in order to optimize both the vehicle speed and the gear-shifting, showing interesting results in terms of achievable fuel economy.

## **10.2 DP Application to PHEVs**

The application of the described generic algorithm to the considered complex dynamic system, i.e. the plug-in hybrid electric powertrain, needs an association between algorithm variables and specific problem variables.

In this section the DP has been implemented to find the optimal powertrain control in order to minimize the vehicle fuel consumption, indeed, to optimize the EMS for the vehicle.

The following variables have been chosen to define the problem formulation:

### ***Disturbances***

The disturbances vector  $w$ , which collects the variables that are independent of the vehicle state, which are the speed  $v$  and the road slope  $\alpha$  profiles.

$$w_k = \begin{bmatrix} v_k \\ \alpha_k \end{bmatrix} \quad 10.9$$

### State variables

The state variables,  $x$ , chosen for defining the system state are the battery state of charge,  $SOC$ , the currently engaged gear,  $gr$ .

$$x_k = \begin{bmatrix} SOC_k \\ gr_k \end{bmatrix} \quad 10.10$$

### Control variables

The chosen variables for the powertrain operating control are:

- the torque split factor  $sf$  between the electrical and hybrid paths. When it is equal to 1, the total amount of torque requested at the wheels is provided by the two electric motors on the front axle and the engine is switched off. Otherwise, if  $sf$  is equal to 0, the engine provides the torque requested at the wheels and the electrical machines on the front axle are used only for regenerative braking;
- the additional torque  $lps$  (that means *load point shift*) requested to the engine to recharge the battery. This control variable is used in combination with the  $sf$  to define the total amount of torque the engine has to provide and, multiplied by -1, to calculate the torque of the integrated starter-generator (ISG);

In symbols,

$$u_k = \begin{bmatrix} sf_k \\ lps_k \end{bmatrix} \quad 10.11$$

### Cost function

The cost function associated to the powertrain energy management problem is the sum of the instantaneous fuel consumption at each stage, plus the final cost related to the battery state of charge target for the end of the driving mission. To be more precise, there is no running cost for the electrical energy usage, but only a constraint, defined using the terminal cost  $J_{fin}$ , that forces the controller to reach a specific state of charge at the end of the cycle ( $SOC_{fin}$ ).

$$J_{\pi}(x_0) = J_{fin}(SOC_{fin}) + \sum_{k=0}^{N-1} \dot{m}_{fuel,k}(x_k, u_k, w_k) \quad 10.12$$

Subject to

$$SOC_{min} \leq SOC_k \leq SOC_{max}$$

$$Tq_{ice} \leq Tq_{ice_{max}}$$

$$Tq_{em} \leq Tq_{em_{max}}$$

$$Tq_{em} \geq Tq_{em_{min}}$$

$$Tq_{isg} \geq Tq_{isg_{min}}$$

where the  $SOC$  is the battery state of charge and  $Tq_{ice}$ ,  $Tq_{em}$ ,  $Tq_{isg}$  are, respectively, the torque requests to the engine, electric motors and integrated starter-generator.

### 10.2.1 Control variables influence on powertrain operation

According to the value of the chosen control variables, the supervisory controller defines the EMS for the vehicle in a certain instant of the driving mission. To better understand how such variables affect the energy flow among the powertrain, in Fig.10.2 have been reported the powertrain layout with a mention of the components influenced by each control variable.

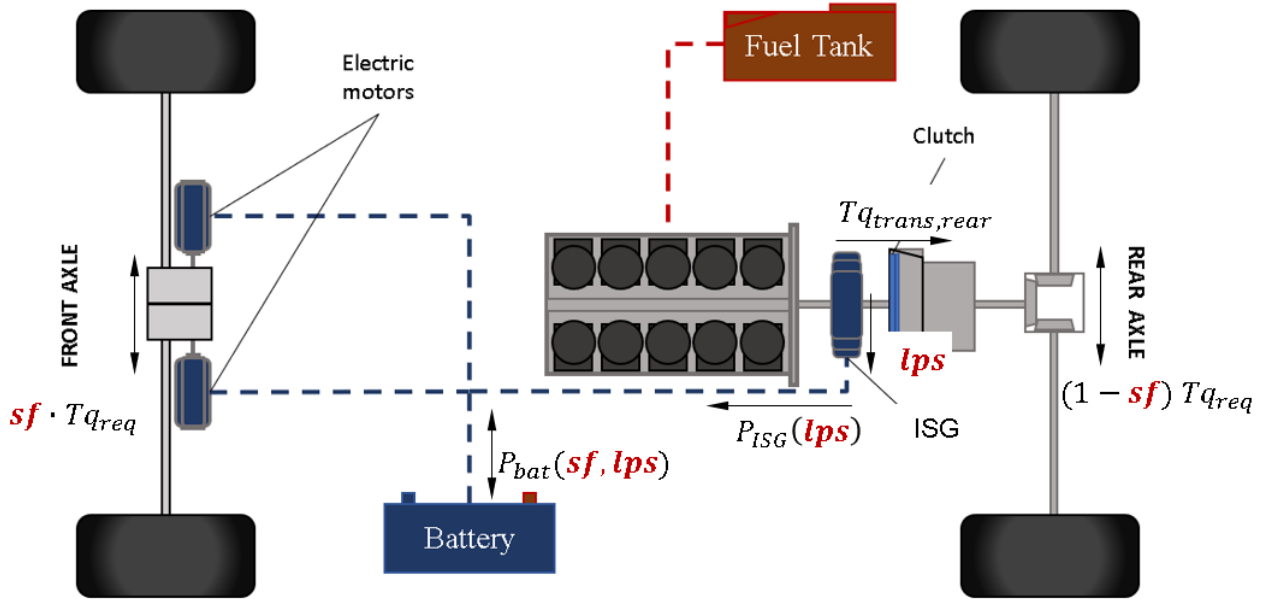


Figure 10.2 Control variable for target PHEV

Remembering the powertrain analytic model illustrated in Chap.4, the control variables appear in the definition of:

- The torque split between the electrical and thermal paths ( $sf$ )

$$Tq_{whl, front} = sf \cdot Tq_{req} \quad 10.13$$

and

$$Tq_{whl, rear} = (1 - sf) Tq_{req} \quad 10.14$$

- The total torque requested to the engine ( $sf$ ,  $lps$ )

$$Tq_{ice}(t) = lps + Tq_{trans, rear} = lps + Tq_{whl, rear}(sf) \cdot \tau_{trans} \quad 10.15$$

- The battery power request ( $sf$ ,  $lps$ )

$$P_{bat} = P_{mot_f}(sf) + P_{ISG}(lps) + P_{aux}/\eta_{DCDC} + P_{TM} \quad 10.16$$

## 10.2.2 Algorithm Implementation

For the backward optimization algorithm, it has been chosen a discrete approach, therefore all the variables of the problem can only assume discrete values.

### *Variables Discretization*

In this section, it is presented the discretization chosen for each of the problem variables. With regards to the state variables, the discretization's are:

- *Battery state of charge*

$$SOC_k = [0.25:0.001:0.95];$$

- *Actual engaged gear*

$$gr_k = [1:1:6];$$

and for the control variables:

- *Torque split factor*

$$sf_k = [0:0.5:1];$$

- *Engine additional torque for battery recharge*

$$lps_k = [0:5:200];$$

The term *discretization* here means the minimum step the algorithm can take to span a variable vector. In this sense, the algorithm is considering that the problem variables can only be part of the fixed range and, moreover, assumes the discrete values defined by the vectors shown above. The more the discretization step is small, the more the accuracy of the optimal solution increases but, contextually, it increases the computational load. The choice of using only three steps to discretize the split factor variable derives from a sensitivity analysis performed in order to investigate the influence of each variable on the global optimum cost, that have shown a flat behaviour with respect to  $sf$  discretization, as can be seen in Fig.10.3 .

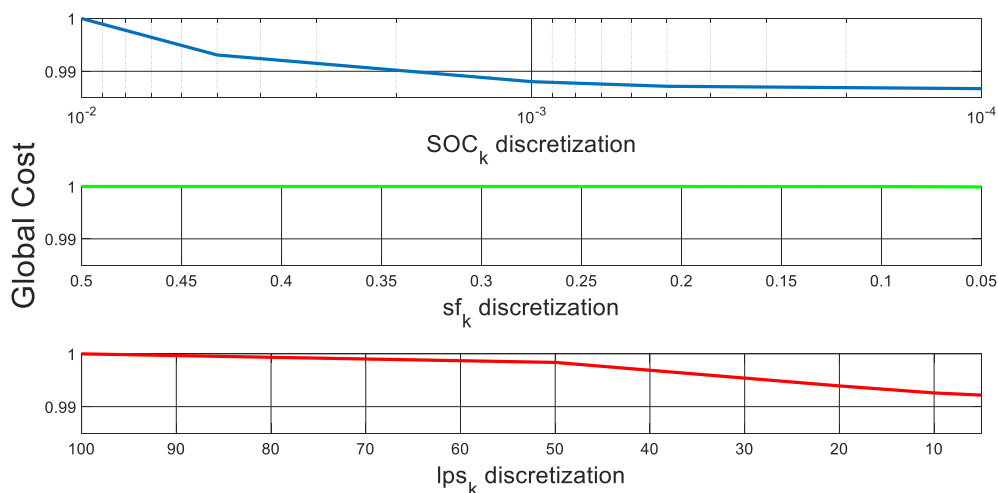


**Figure 10.3 Sensitivity of the Global Cost to variables discretization**

For the  $lps$  discretization it has been chosen the minimum step, 5, which is even the one that leads to a lower global cost.

Regarding the *SOC*, instead, it has been made a trade-off between the optimization time and the global cost, since the optimization time for the chosen step is 3750 seconds, while with the lowest step considered the simulation time is 20512 seconds. For the maximum step, 0.01, the time needed for the optimization is 1737 seconds, but the global cost is slightly higher. The chosen step has a global cost near the minimum and an acceptable computational time.

From Fig. 10.3 it seems the system has a slow sensitivity with respect on the variable discretization. For the *sf* and *lps* the behavior can be explained considering that the engine is definitively powerful, therefore the optimization algorithm mostly chooses an On/Off behaviour, rather than a torque splitting one and when the engine is on, the load point shift is often high to reach higher efficiencies zones.

Concerning the *SOC*, the sensitivity analysis has been conducted only on discretization that are already small enough to have a good accuracy, for two main reasons:

- the results of the optimization have to be implemented in a more complex simulation environment (MiL) to assess the benefit of optimal control. A large discretization on such important state variable may lead to important differences between the analytical model and the model-in-the loop;
- the battery capacity is quite high, therefore a small percentage of the state of charge is a consistent amount of energy, therefore a poor accuracy in the discretization could affect the definition of the optimal control policy.

### ***Backward Optimization***

The evaluation for all the possible combination is performed using concatenated iteration loops, one for each problem variable, that can be schematically represented as follows:

```

for time= N-1:-1:0
    % analytic longitudinal vehicle dynamics
    for sf=0:0.5:1
        for lps=0:5:200
            %analytic components model
            % cost-to-go matrix updating with actual stage cost
            for SOC=0.25:0.001:0.95
                for gr=1:6
                    %cost-to-go-matrix minimization
                    %control variables optimal combination for the actual states
                    variables combination
                end
            end
        end
    end
end

```

At the end of the optimization algorithm, the optimal control variables for each time stage and each possible combination of the state variables are saved in “results matrixes”, one for each control variable, with 3D dimension (1 dimension for the stage+2 dimensions for the states).

### ***Forward Implementation***

The forward implementation of the optimal control policy has been done using the MiL environment of the vehicle, in order to have a more realistic behaviour of the powertrain in terms of components control. Such

approach has been possible since the state variables have been discretized, therefore small changes in the powertrain state evolution with respect to the backward optimization can be handled.

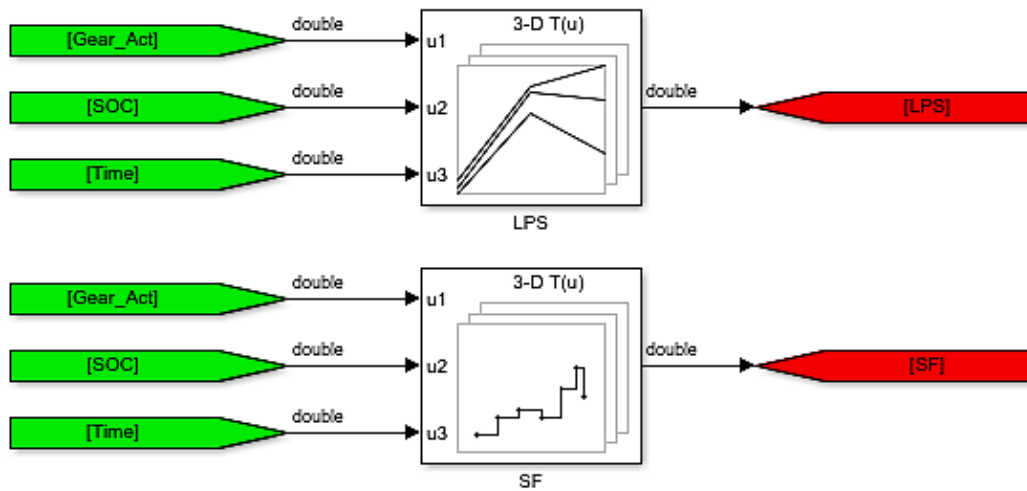


Figure 10.4 Forward implementation of the optimal control policy

Since the Mil has been implemented in Simulink, the optimal control matrixes have been loaded using 3D look-up table where the breakpoints are the vectors previously defined in this paragraph.

### 10.2.3 Results vs RBS and ECMS

Before showing the results, a mention is needed on the performances shown in the following paragraphs. Since, as hybrid electric vehicle, the considered powertrain has two possible energy sources and, therefore, two different energy consumptions, it has been chosen to find a single parameter for comparing the controllers' performances. The proposed correction is purely based on energetic considerations, therefore it isn't aligned with homologation standard. In this case, the idea, is to consider a more "neutral" approach to the fuel consumption, including just the energy provided by each energy storage systems, i.e. fuel tank and battery, along the driving mission. Moreover, using such policy, it is possible to make the results independent from the driving mission type, by taking into account just the efficiencies of the machines.

#### *CO<sub>2</sub> correction*

The CO<sub>2</sub> production has been chosen as the assessment parameter for comparing the global energy consumption related to the applied control strategies.

The CO<sub>2</sub> production is evaluated directly from the fuel consumption, calculated within the MiL, by means of a conversion factor whose value is  $k_{CO_2} = 2370 \text{ g}_{CO_2}/L_{fuel}$ . In order to evaluate the effective fuel consumption of the engine it has been used a look-up table that maps the fuel mass rate as a function of the engine speed and torque.

For having a comparison on a single parameter, that takes also into account the electrical energy balance of the battery between the beginning and the end of the driving mission, the CO<sub>2</sub> production has been corrected considering the following approach.

The energy requested at the wheels can be delivered both by the ICE or the EMs, therefore two different situations can occur: energy balance at the end of the cycle,  $\Delta eC$  (expressed in KJ), is positive or negative, i.e. the battery SOC at the end is higher or lower than the initial value. In the first scenario, it is assumed that the positive difference of the electric energy is covered by the engine (recharging the battery using the ISG), consuming more fuel than actually required. It is possible to calculate the virtual fuel consumption (to be subtracted to the actual one) using the average efficiencies of the machines on the thermal path, as shown in Eq. 10.17

$$\Delta m_{fuel} \cdot LHV_{fuel} \cdot \bar{\eta}_{ICE} = \frac{\Delta eC}{\bar{\eta}_{ISG}} \quad 10.17$$

where  $LHV_{fuel}$  is the lower heating value of the fuel equal to 42500 KJ/Kg, and  $\bar{\eta}_{ICE}$  and  $\bar{\eta}_{ISG}$  are the average efficiencies calculated directly in Simulink. Instant by instant, the engine efficiency is calculated by dividing the mechanical power provided by the engine for the chemical power of the injected fuel.

In the other case, with negative electrical energy balance, the difference is considered as a further request of torque addressed to the EMs on the front axle instead of using the ICE. Therefore, it is possible to calculate the additional fuel consumption to be added to the actual one, in order to compensate the battery balance. The formulation is defined by Eq. 10.18.

$$\Delta m_{fuel} \cdot LHV_{fuel} \cdot \bar{\eta}_{ICE} = \Delta eC \cdot \bar{\eta}_{EM} \quad 10.18$$

It is important to underline that this correction is formulated considering the physics of the powertrain since there is no regulation that can be followed for the chosen driving cycles.

### Results comparison

The results shown in the following regard the driving mission introduced in Chap 7. As it can be seen from Fig.10.5, the full knowledge of the driving mission allows the DP-based controller to manage the SOC in a completely different way with respect to the other two causal controllers. This different behavior reflects in a better fuel economy, as it can be noticed in Fig.10.6.

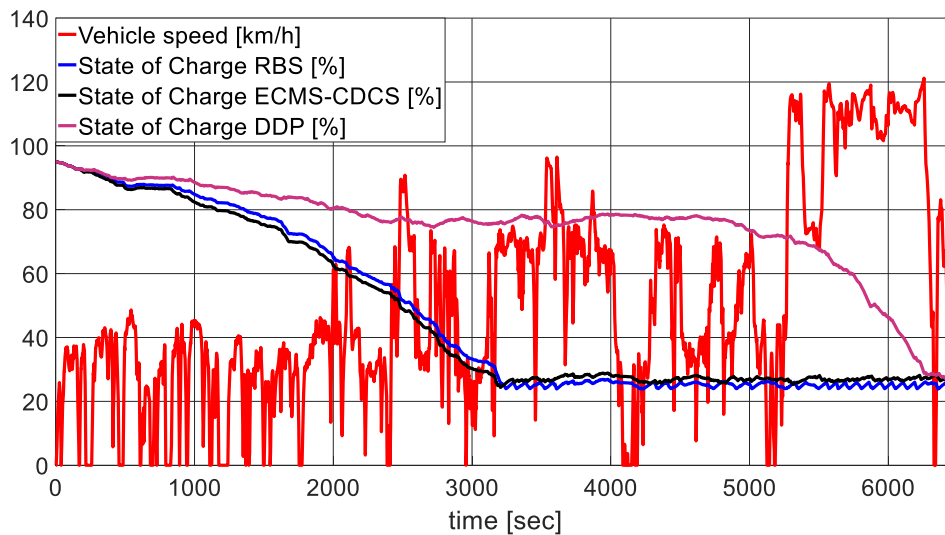


Figure 10.5 DDP vs ECMS-CDCS vs RBS – SOC

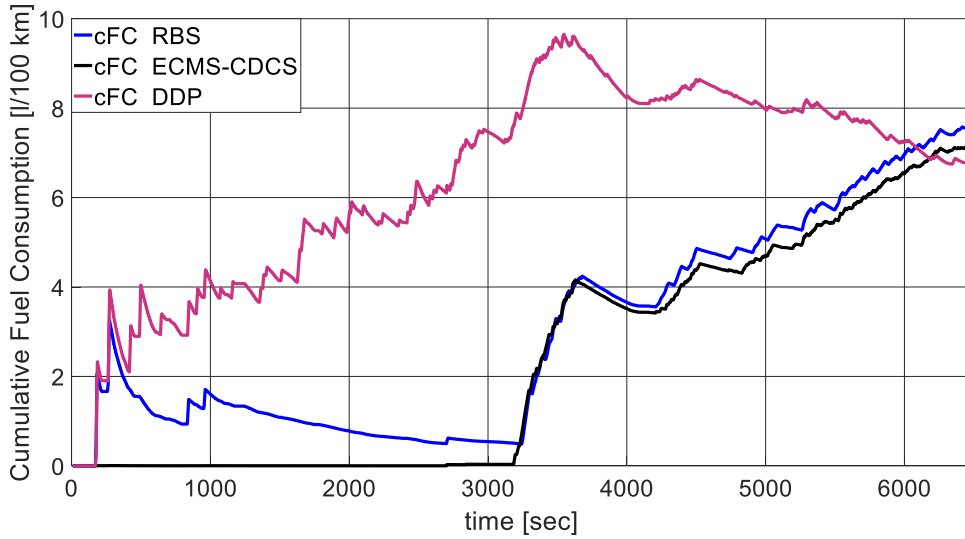


Figure 10.6 DDP vs ECMS-CDCS vs RBS – cFC

Considering the afore mentioned correction to balance the electrical energy in the battery between the beginning and the end of the driving mission, the numerical results that summarize the controllers' performance over the given driving mission are collected in Tab.10.1.

Table 10.1 Corrected CO2 comparison DDP vs ECMS CDCS vs RBS

Strategy	Corrected CO2	Difference
	[g/km]	[%]
RBS	251.76	0.00
ECMS – CDCS	237.05	-5.85
DDP	229.78	-8.73

As can be noticed, using the DP-based controller in a MiL simulation, thus considering all the complexities that can't be expressed within the analytic model, allows a further improvement of almost the 3% with respect to the sub-optimal controller introduced in Par. 8.2 and more than the 8% with respect to the baseline RBS controller.

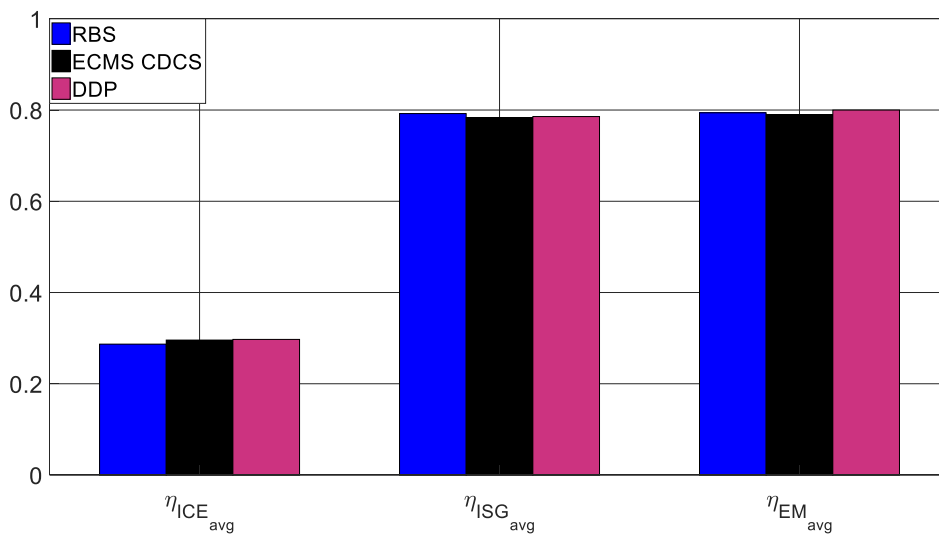


Figure 10.7 Average Efficiencies on RDE cycle DDP vs ECMS CDCS vs RBS

The machines' average efficiencies over the cycle are comparable for all the controllers, which underlines that RBS is not inefficient in the management of the components, but rather far from optimality in terms of energy management, because the fixed rules are not adaptive with respect to actual driving conditions. As it has already been shown in Par. 8.3.3, a large contribute to the fuel consumption reduction is due to the better management of the recuperation phases, which is more efficient in the case of the ECMS and DDP controller.

**Results on others RDE cycles,**

**Table 10.2 Corrected CO2 comparison DDP vs ECMS CDCS vs RBS - RDE2**

<b>RDE-2</b>	<i>Strategy</i>	SOC <sub>fin</sub>	CO <sub>2</sub>	Corrected CO <sub>2</sub>	<b>Difference</b>
		[%]	[g/km]	[g/km]	[%]
	<i>RBS</i>	25.00	206.27	281.31	<b>0.00</b>
	<i>ECMS – CDCS</i>	28.00	188.31	255.93	<b>-9.02</b>
	<i>DDP</i>	27.27	181.48	253.29	<b>-9.96</b>

The RDE-2 cycle is similar to the one shown in detail in the previous paragraph and, as can be seen from Tab.10.2 , the performance of the sub-optimal controller is somehow near to the optimal powertrain control in fact, the percentual difference on the corrected fuel consumption with respect to the DDP controller is less than 1%.

**Table 10.3 Corrected CO2 comparison DDP vs ECMS CDCS vs RBS - RDE3**

<b>RDE-3</b>	<i>Strategy</i>	SOC <sub>fin</sub>	CO <sub>2</sub>	Corrected CO <sub>2</sub>	<b>Difference</b>
		[%]	[g/km]	[g/km]	[%]
	<i>RBS</i>	25.33	224.00	312.90	<b>0.00</b>
	<i>ECMS – CDCS</i>	26.64	19200	272.20	<b>-13.00</b>
	<i>DDP</i>	27.12	169.10	249.00	<b>-20.42</b>

For the third RDE cycle, instead, it has been considered an inverted driving cycle, which mean the low-speed zone is placed at the end of the driving mission, as in Fig.10.8. In this case it is possible to see that, for unknown driving cycles, the ECMS controller is definitely more performant than RBS, as confirmed by the quantitative results reported in Tab.10.3.

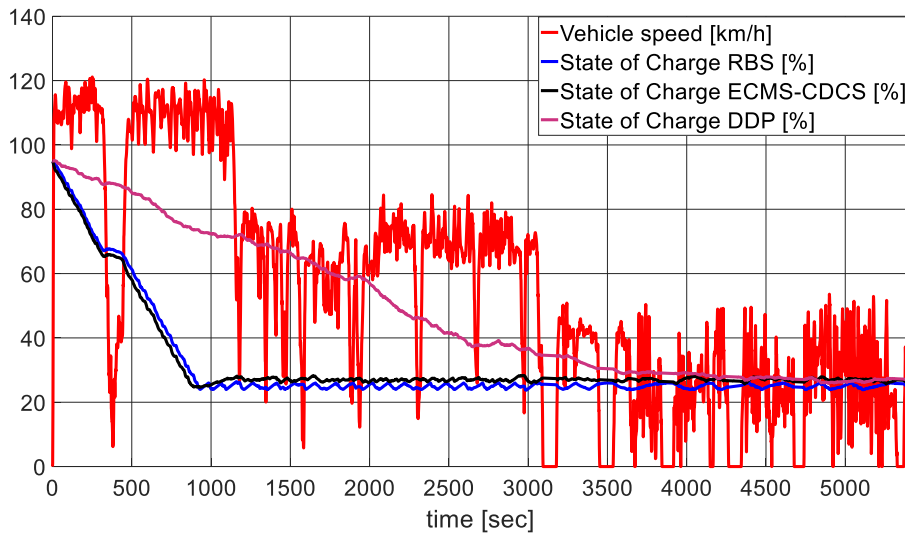


**Figure 10.8 RDE3: DDP vs ECMS-CDCS vs RBS – SOC**

Even if RBS and ECMS-CDCS have the same charge-depleting/charge-sustaining behaviour, the one obtained with the sub-optimal controller leads to an higher efficiency in the engine usage, as shown in Fig.10.9 . The DDP controller, instead, reaches a large gain in fuel economy both for the engine usage efficiency and the knowledge of the driving mission, which allows a different usage of the electrical energy stored in the battery, resulting in a different SOC evolution on the cycle, as noticeable in Fig. 10.8.

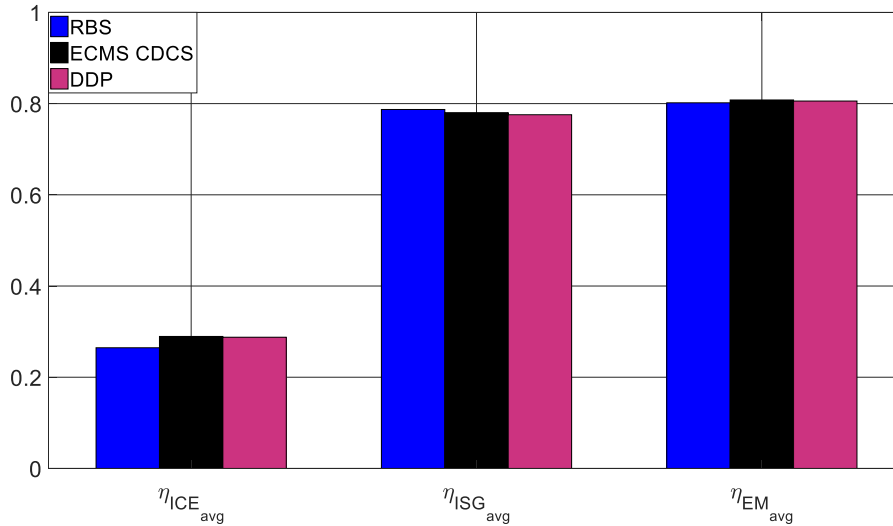


Figure 10.9 Average Efficiencies on RDE3 cycle DDP vs ECMS CDCS vs RBS

### 10.3 Combined optimization of Energy and HV battery thermal management

This section proposes a combined optimization algorithm that simultaneously optimizes the energy management and HV battery thermal management of the reference vehicle. There are two aims in combining the optimization:

- Include in the Energy Management optimization the energy consumption related to the battery cooling and adding the battery temperature as a state variable, therefore considering also the efficiency of the battery with respect to such variable, see Fig.5.6;
- Optimize the Thermal Management control over a given driving mission.

#### 10.3.1 Battery cooling circuit

The battery cooling circuit is depicted in Fig.10.10.

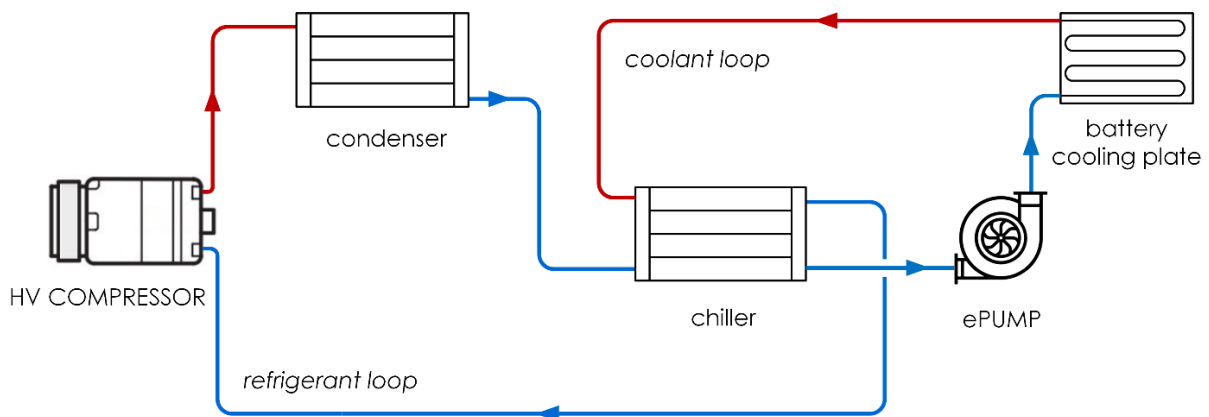


Figure 10.10 HV Battery cooling circuit

As it can be seen, it comprehends two different loops: the refrigerant and the coolant one.

In the first one, a high-voltage compressor is used, which is then directly supplied by the HV battery. The heat transfer, in which both the refrigerant and the coolant are involved, takes place at the common heat exchanger, usually named as *chiller*. In the other loop, the coolant (a water-glycol mixture) absorbs the heat generated within the battery pack by flowing through a cooling plate. An electrical (low-voltage) pump is used in the coolant loop.

Technical data regarding the main actuators, namely the compressor and the pump, are listed in Tab10.4.

**Table 10.4 Data regarding battery cooling circuit actuators**

Pump nominal speed	7000 rpm
Pump nominal volume flow	20 L/min
Pump nominal power	100 W
Compressor nominal speed	3000 rpm
Compressor max power	~4 kW

To include the contribution of the battery cooling, the analytical model illustrated in Par. 4.5 has been updated as follows.

### 10.3.2 Battery Model

Starting from Eq.4.16, which is re-written in Eq.10.19

$$P_{bat}(t) = P_{mot,f}(t) + P_{ISG}(t) + P_{aux}/\eta_{DCDC} + P_{TM}(t) \quad 10.19$$

where

$$P_{TM}(t) = u_{TM}(t) \cdot (P_{cpr}(t) + P_{pmp}/\eta_{DCDC}) \quad 10.20$$

and where  $P_{mot,f}$  is the power requested from the electrical motors on the front axle for traction,  $P_{ISG}$  is the power provided by the engine to recharge the battery,  $P_{aux}$  is the constant power to be supplied to the LV battery and the other auxiliaries,  $\eta_{DCDC}$  is the efficiency of the DCDC converter, and, newly introduced  $u_{TM}$ , which is the control signal of the battery cooling circuit actuators. The rest of the electrical battery model is the same as in Par. 4.5.

Focusing on the battery cooling circuit model, for the sake of simplicity, the refrigerant loop has not been modelled. Therefore, a heat transfer efficiency  $\eta_{chl}$  of the chiller has been introduced in order to evaluate the power request of the compressor from the heat absorbed by the coolant

$$P_{cpr}(t) = \frac{\dot{Q}_{cool,k-1}(t)}{\eta_{chl} \cdot COP} \quad 10.21$$

where  $COP$  is the coefficient of performance of the refrigeration circuit (refrigerant loop in Fig.10.10).

The thermal balance applied to the coolant yields to:

$$\Delta T_w(t) = \frac{\dot{Q}_{cool,k-1}(t)}{\rho_w \dot{V}_w \cdot c_{p,w}} \quad 10.22$$

being  $\rho_w$ ,  $\dot{V}_w$ ,  $c_{p,w}$  the mass density, the volume flow and the specific heat capacity of the coolant. Therefore, the temperature of the coolant at the outlet of the battery cooling plate is simply evaluated as:

$$T_{w,out}(t) = T_{w,in} + \Delta T_w(t) \quad 10.23$$

where  $T_{w,in}$ , namely the temperature of the coolant at chiller outlet, has been considered constant due to the aforementioned hypothesis on coolant loop modelling. The coolant-battery convective heat exchange can be modelled as:

$$\dot{Q}_{cool}(t) = h_w A_{cool} \cdot \Delta T_{ML,cool}(t) \quad 10.24$$

being  $h_{cool}$  the heat transfer coefficient [ $W/(K \cdot m^2)$ ] of the coolant,  $A_{cool}$  the area of the cooling surface, and  $\Delta T_{ML,cool}$  the mean logarithmic temperature difference related to the heat exchange at the battery cooling plate and expressed as follows:

$$\Delta T_{ML,cool}(t) = \frac{\Delta T_1(t) - \Delta T_2(t)}{\ln\left(\frac{\Delta T_1(t)}{\Delta T_2(t)}\right)} \quad 10.25$$

where

$$\Delta T_1(t) = T_{bat}(t) - T_{w,in}$$

$$\Delta T_2(t) = T_{bat}(t) - T_{w,out}(t)$$

Once that both the heating ( $P_{b,loss}$ ) and cooling ( $\dot{Q}_{cool}$ ) contributions have been evaluated in Eq. 4.19 and Eq. 10.24 respectively, the thermal balance applied to the HV battery may be solved as shown in Eq. 10.26 in order to calculate the temperature of the component

$$T_{bat}(t) = T_{b,0} + \frac{1}{m_b \cdot c_{p,b}} \int_0^t (P_{b,loss}(t) - \dot{Q}_{cool}(t)) dt \quad 10.26$$

where  $m_b$  and  $c_{p,b}$  represent, respectively, the mass and the specific heat capacity of the battery pack. The latter has been assumed to be constant due to its limited variations within battery working temperature range and its value has been obtained by calibration, as further explained later. At this point, the thermal management control variable  $u_{TM}$  has been added as control variable in the optimal control problem, while the battery temperature,  $T_{bat}$ , has been added as state variable.

### 10.3.3 Rule based battery Thermal Management

The standard battery thermal management implemented in the vehicle is rule-based (TM-RBS), or heuristic, and it is based on intuitive rules and correlations involving various parameters, mainly temperatures. One guiding principle of such a strategy is to preserve the temperature of thermal-stressed components within a restricted range of fixed values. Therefore, upper and lower temperature thresholds are set after a calibration phase, which can turn out to be an expensive and time-consuming task because the choice of the optimal values is influenced by the architecture of the examined cooling system.

Moreover, in order to avoid performance de-rating and especially premature ageing of the component, the physical constraint represented by the upper limit of the battery operating temperature range has been

considered, as well. In this case, the thermal characterization of the battery under study led to set the upper thermal limit  $T_{bat_{max}} = 40^{\circ}\text{C}$ , which has been confirmed to be a reasonable value by literature [76]. As a consequence, because of the standard strategy relies on fixed threshold values, the latter are usually lower than the one related to the aforementioned thermal constraint because highly demanding working conditions have to be taken into account in advance by setting a high safety margin.

The decision on whether to switch-on and off the battery thermal management is made according to the actual value of the component temperature:

- $T_{bat} > 27^{\circ}\text{C}$  implies the TM-RBS is switched- **ON**;
- $T_{bat} < 25^{\circ}\text{C}$  implies the TM-RBS is switched- **OFF**.

The idea of including the battery thermal management within the optimization loop relies on the hypothesis that an optimal battery thermal management would lead to an overall energy saving over the cycle, as happens for the only energy management optimization.

### 10.3.4 Optimal control problem formulation

The combined optimization of energy and battery thermal management is similar to the one defined in Par. 10.2, with the adjoint of the variables newly introduced in the previous paragraph.

#### *Disturbances*

Since the disturbances vector  $w$  is not influenced by the powertrain definition, it is the same as in Par. 10.2.

$$w_k = \begin{bmatrix} v_k \\ \alpha_k \end{bmatrix} \quad 10.27$$

#### *State variables*

For the state variables, it includes not only  $SOC$  and  $gr$ , strictly related to the energy management, but also  $T_{bat}$ , which depends on the chosen thermal management control.

$$x_k = \begin{bmatrix} SOC_k \\ gr_k \\ T_{bat_k} \end{bmatrix} \quad 10.28$$

#### *Control variables*

The control variables to be optimized to solve the combined optimal control problem are again the torque split factor and the load point shift for the energy management, plus  $u_{TM}$ , which is the control of the actuator for the thermal management and it can 0, if no thermal management is needed or 1, if the battery needs to be cooled down.

In symbols,

$$u_k = \begin{bmatrix} sf_k \\ lps_k \\ u_{TM_k} \end{bmatrix} \quad 10.29$$

#### *Cost function*

It has been chosen to still minimize only the energy consumption, that in this case includes also the energy needed by the thermal management, therefore the cost function is the same as in Par. 10.2. Again the only final

cost imposed is to reach a given battery state of charge at the end of the driving mission, while no penalization has been imposed to the final thermal state of the battery, the only limitation is to have a battery temperature within the admissible range, and this has been imposed as a problem constraint.

$$J_{\pi}(x_0) = J_{fin}(SOC_{fin}) + \sum_{k=0}^{N-1} \dot{m}_{fuel,k}(x_k, u_k, w_k) \quad 10.30$$

Subject to

$$SOC_{min} \leq SOC_k \leq SOC_{max}$$

$$T_{bat_{min}} \leq T_{bat_k} \leq T_{bat_{max}}$$

$$Tq_{ice} \leq Tq_{ice_{max}}$$

$$Tq_{em} \leq Tq_{em_{max}}$$

$$Tq_{em} \geq Tq_{em_{min}}$$

$$Tq_{isg} \geq Tq_{isg_{min}}$$

### 10.3.5 Control variables influence on powertrain operation

The adjoint control variable to optimize the battery thermal management is shown in Fig.10.11. From an energetic point of view, it has effects only on the battery, since it modifies the power requested according to the actual decision on the operation of the cooling circuit, as in Eq. 10.31:

$$P_{bat} = P_{mot_f}(sf) + P_{ISG}(lps) + P_{aux}/\eta_{DCDC} + P_{TM}(u_{TM}) \quad 10.31$$

Where

$$P_{TM} = u_{TM}(P_{cpr}(t) + P_{pmp}/\eta_{DCDC}) \quad 10.32$$

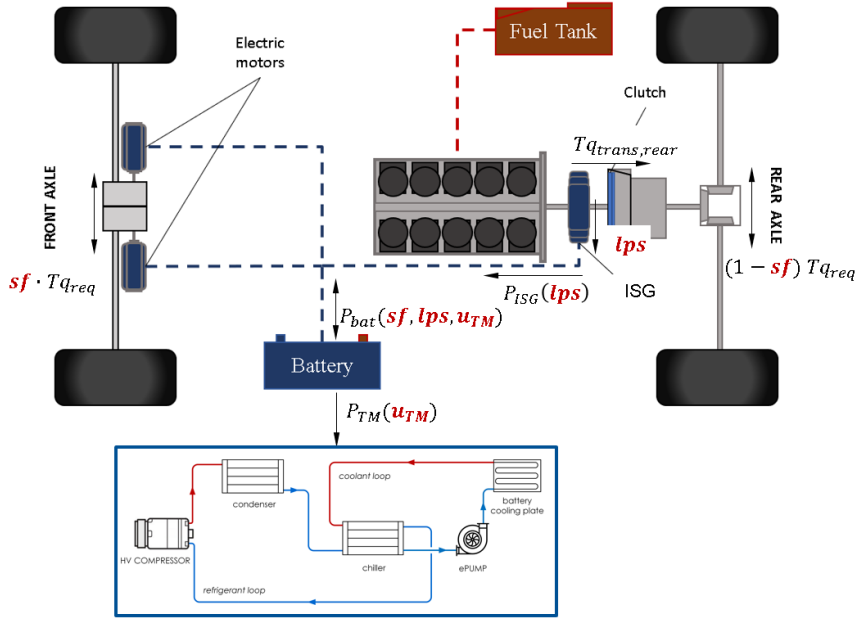


Figure 10.11 Control variable for combined optimization of PHEV

The effect of the other two control variables have been already introduced in Par. 10.2.1.

### 10.3.6 Algorithm Implementation

The basis of the optimization algorithm is the same as the one shown in Par. 10.2.2

#### Variable Discretization

In this section, it is presented the discretization chosen for each of the problem variables. With regards to the state variables, we have:

- Battery state of charge

$$SOC_k = [0.25: 0.001: 0.95];$$

- Actual engaged gear

$$gr_k = [1: 1: 6];$$

- Battery temperature

$$T_{bat,k} = [0: 1: 40];$$

and for the control variables

- Torque split factor

$$sf_k = [0: 1];$$

- Engine additional torque for battery recharge

$$lps_k = [0: 50: 200];$$

- Circuit control for battery cooling

$$u_{TM,k} = [0: 1]$$

The unitary step for the battery temperature state has been chosen because of the size of the range to be span, since a higher discretization would have led to a definitely high dimension of the optimal control problem. For the thermal management control variable  $u_{TM}$ , instead, it has been chosen to maintain On/Off behaviour of the system. In this case the  $sf$  and  $lps$  have been discretized differently since the combined optimization have more dimensions and, therefore, a higher computational time is needed.

### **Backward Optimization**

For the backward optimization, two additional iterative cycles have been added, one for each additional problem variable.

```

for time=N-1:-1:0
    % analytic longitudinal vehicle dynamics
    for sf=0:1
        for lps=0:50:200
            for Tbatt=0:1:40
                %analytic components model
                % cost-to-go matrix updating with actual stage cost
                for SOC=0.25:0.001:0.95
                    for gr=1:6
                        for uTM=0:1
                            %cost-go-matrix minimization
                            %control variables optimal combination for the
                            actual states variables combination
                        end
                    end
                end
            end
        end
    end
end

```

In this case, the output matrixes containing the results of the optimal discretized control problem have four dimensions, three for the state variables and one for the stage variable, which is the time.

### **Forward Implementation**

As it has been done in Par.10.2.2, the forward implementation of the optimal control policy has been made in Simulink using 4D look-up tables, where the additional state variable is the high voltage battery temperature and the third look-up table contains the optimal values for the thermal management control variable  $u_{TM}$ .

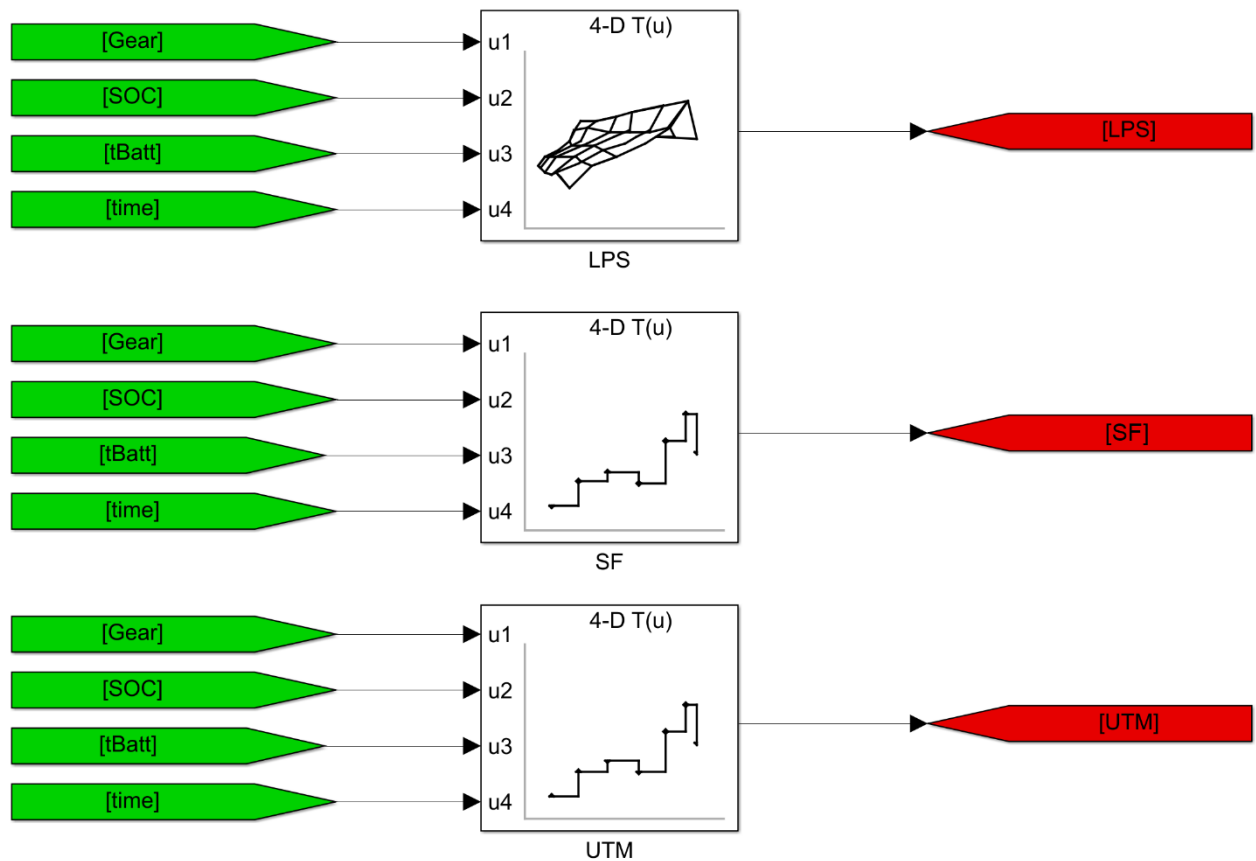


Figure 10.12 Forward implementation of the combined-optimal control policy

The output of the LPS and SF matrixes are used to define the energy management strategy to be applied to the powertrain, while the output of UTM matrix controls the battery cooling circuit (Fig.10.12).

### 10.3.7 Results

To investigate the effects of DDP-based control strategies for energy-thermal management (Combined-DDP), three test cases has been conceived as reported in Tab.10.5. The first test-case consider the baseline rule-based strategies for the energy and thermal management (Par.8.1.2 and Par 10.3.3). The second one, instead, considers a DDP-based controller (Energy-DDP) for the only energy management (Par.10.2.2), while the battery thermal management is still based on fixed rules. The last one, test-case 3, makes use of the results obtained with the combined optimization for the energy and battery thermal management.

From here on, all the reported results derive from the MiL, where the optimal control policies calculated with the DDP algorithm have been integrated into the controllers and the results have been corrected following the approach proposed in Par. 10.2.3.

Table 10.5 Test-cases for results comparison

Test case	Control strategy	
	Energy management	Thermal management
TC1	Rule-based	Rule-based
TC2	Energy-DDP	Rule-based
TC3	Combined DDP	

Even for this comparison, the reference cycle has been the one introduced in Chap.7.

To clearly evaluate the benefits of an optimized thermal management, different ambient temperature values have been considered, assuming that at the beginning of the driving mission the battery temperature is equal to the ambient one.

**Results @ Ambient temperature = 40°C**

The SOC trends in the case with ambient temperature equal to the maximum limit of the battery temperature range, the TC2 and TC3 are similar, since the SOC is mainly affected by the energy part of the optimization. Obviously, the TC1 has a completely different trend because of the heuristic control policy (Fig.10.13).

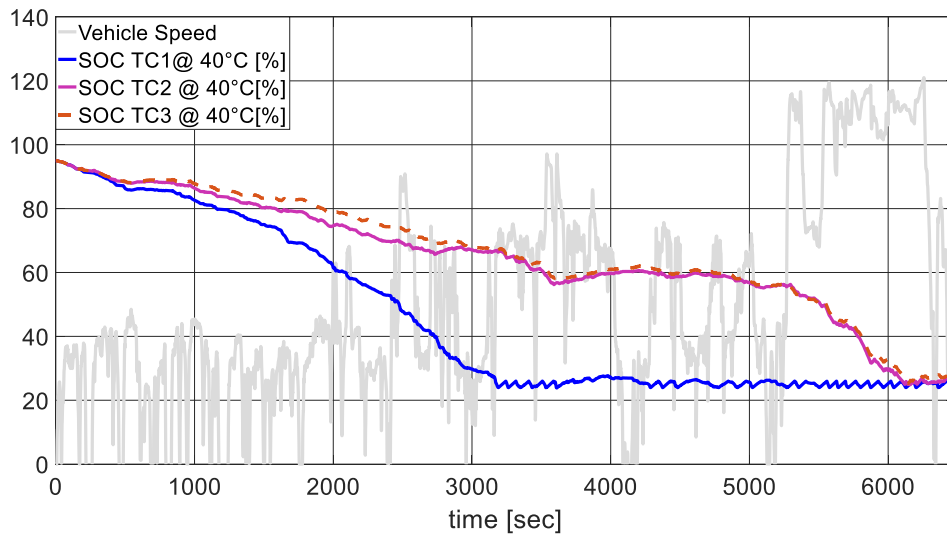


**Figure 10.13 Comparison @ Ambient Temperature =40°C – SOC**

The battery temperature trend, instead, is different for any case (Fig.10.14), since the behaviour of TC1 and TC2 are similar, but the difference in the energy management leads to different cooling phases. In the case of TC3, instead, the battery temperature trend depends on the optimal control sequence of the cooling activation variable  $u_{TM}$ .

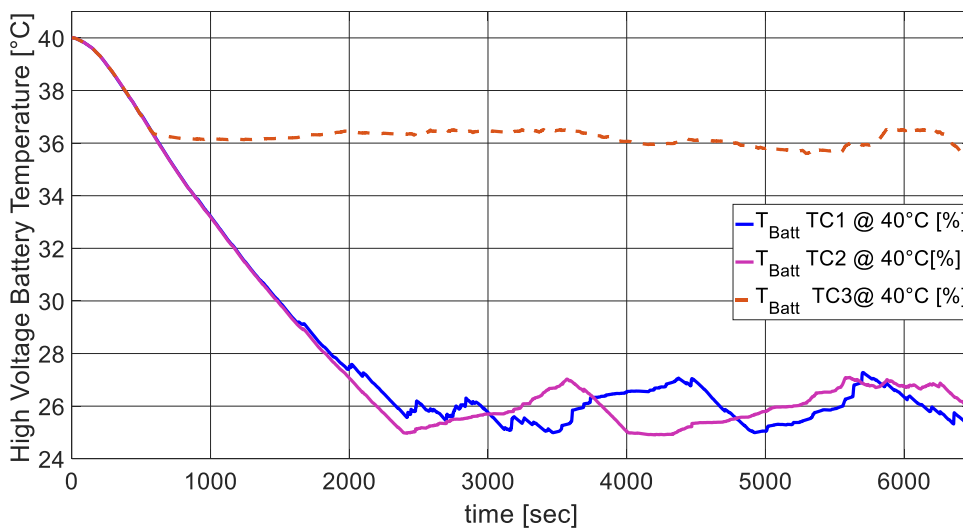


**Figure 10.14 Comparison @ Ambient Temperature =40°C – T<sub>Batt</sub>**

The main reason why the optimized thermal management keeps the battery temperature near to the higher limit of the range is related to the characteristic of the battery internal resistance with respect to its temperature,

which decreases as the temperature increases, as can be noticed in Fig. 5.6. As a result, the total energy consumption for the energy management, for each test-case is different, as Fig.10.15 depicts. Of course, another reason is related to the fact that no running and final costs have been associated to the battery thermal state within the optimization algorithm.

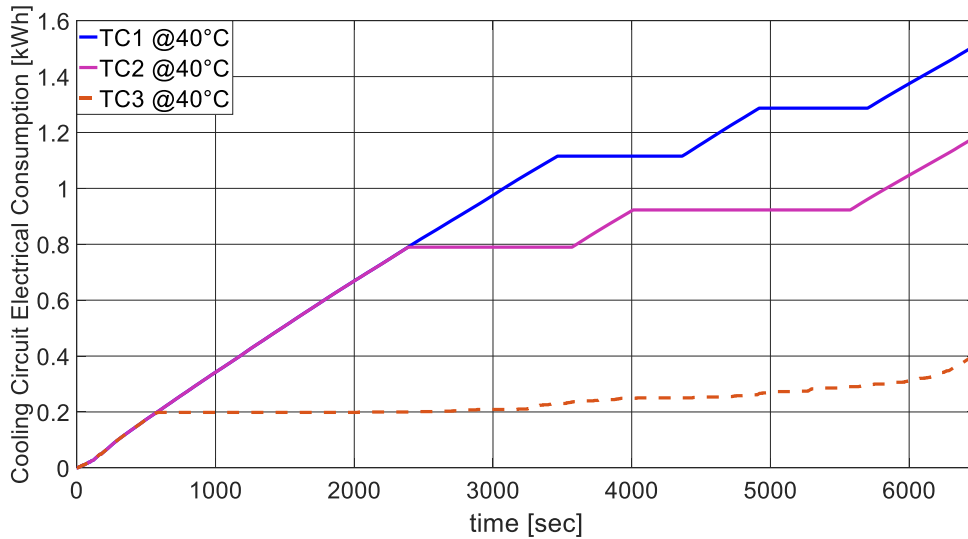


Figure 10.15 Comparison @ Ambient Temperature =40°C – Energy consumption cooling circuit

**Results @ Ambient temperature = 10°C**

When the initial temperature of the battery is low, the differences between TC2 and TC3 are barely appreciable both on the SOC (Fig.10.16) and battery temperature trends (Fig.10.17), since, in this case, even optimizing only the energy management, the battery temperature doesn't reach the activation threshold. On the contrary, if a purely heuristic powertrain control is applied, a cooling phases is needed at the end of the cycle, as confirmed by Fig.10.18.

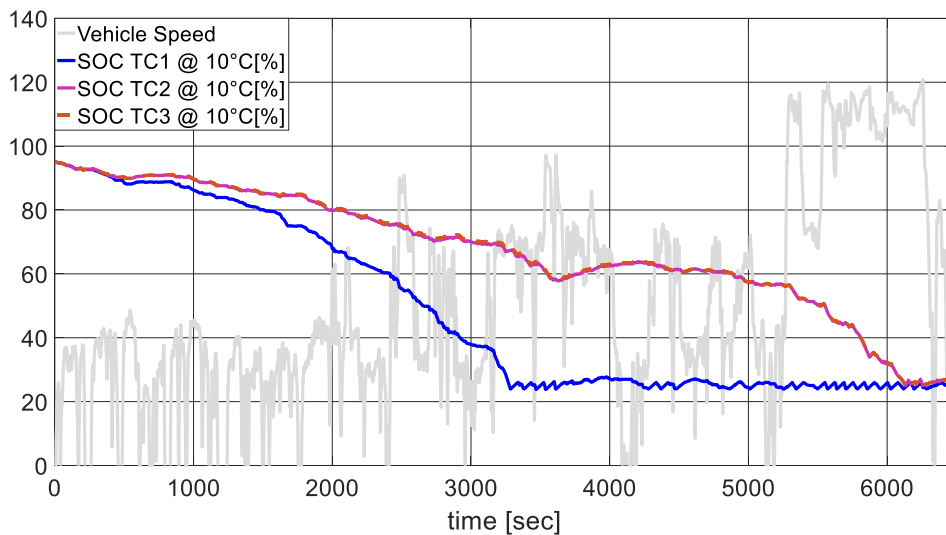


Figure 10.16 Comparison @ Ambient Temperature =10°C – SOC

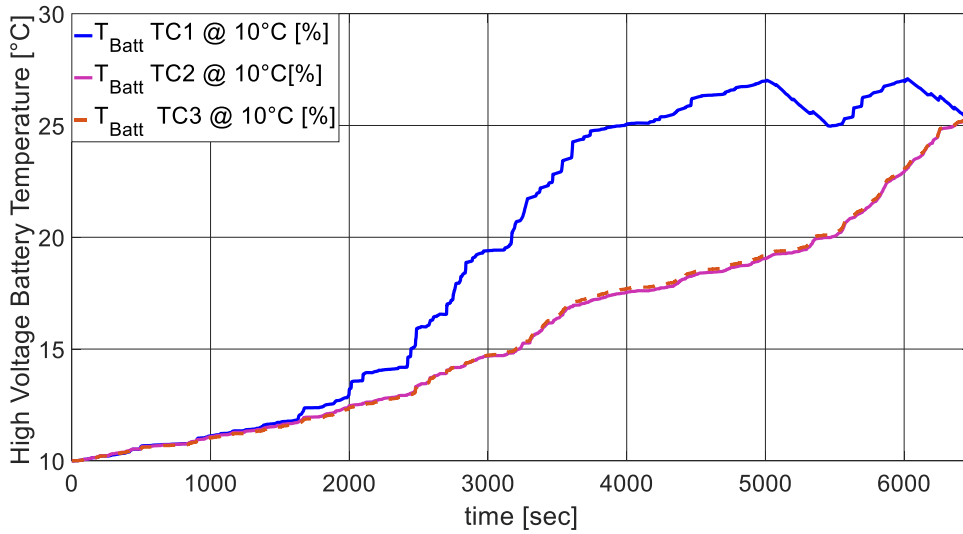


Figure 10.17 Comparison @ Ambient Temperature =10°C – T<sub>Batt</sub>

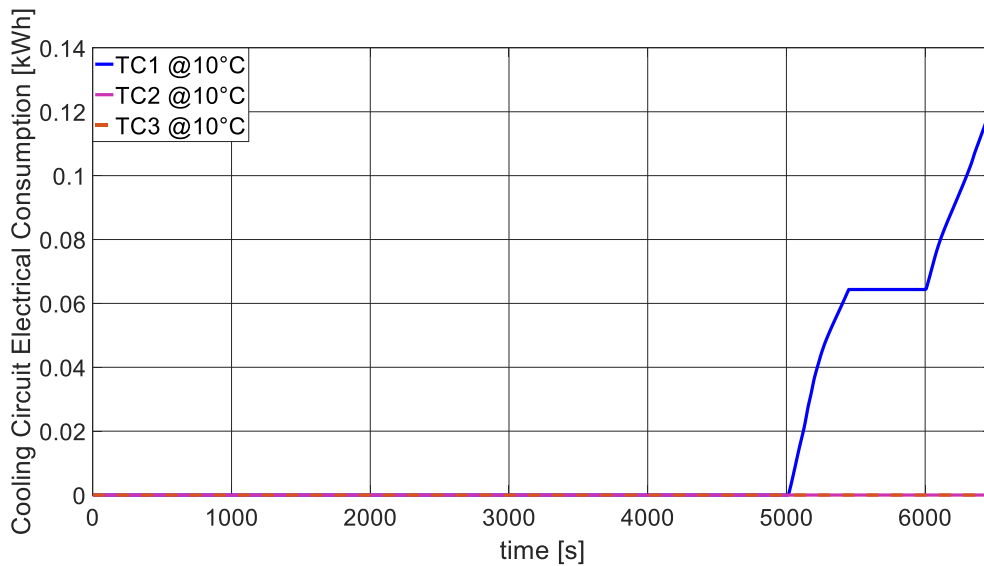


Figure 10.18 Comparison @ Ambient Temperature =10°C – Energy consumption cooling circuit

### Numerical results

As aforementioned in this paragraph, the numerical results shown in Tab. 10.6, have been corrected to estimate the controllers' performances on a single parameter. Different ambient temperature values have been simulated, in order to assess the potential of the combined-optimization approach.

Table 10.6 Test-cases results for different ambient temperatures

Test case	Ambient temperature [°C]						
	10	15	20	25	30	35	40
	Corrected CO2 production						
TC1	235.2	237.1	238.2	239.3	243.4	242.0	254.5
TC2	215.0	214.1	214.9	216.4	219.2	221.7	227.4
TC3	214.1	213.0	212.4	212.4	213.1	217.4	220.7

In general, referring to Tab. 10.6 and Fig. 10.19, for TC3 the fuel economy gain, with respect to the reference controller (Test case 1), increases with the ambient temperature.

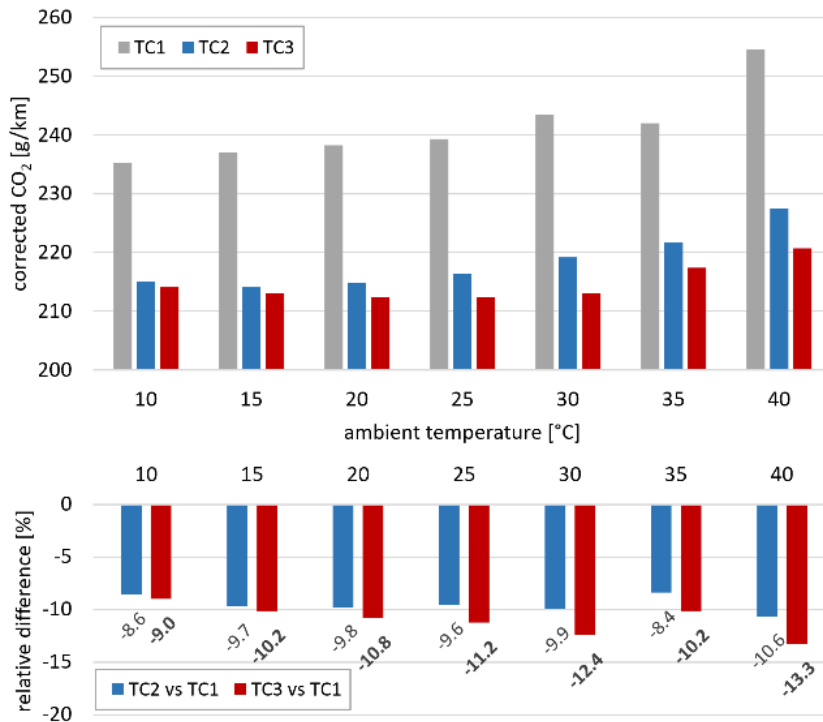


Figure 10.19 Test-cases results for different ambient temperatures - Comparison

### Comments

The simulation at ambient temperature equal to 10°C, where both TC2 and TC3 have no cooling along the whole driving mission, shows results that are slightly higher than the ones obtained at 15°C. This behaviour can be explained considering again Fig. 5.6, where the battery cell internal resistance is shown versus the battery temperature. Accordingly, at low temperature the battery power losses increase, resulting in a lower battery electrical efficiency, therefore the obtained performance is coherent with the physics of the component. From Fig.10.19 it is also possible to see a discontinuity in the increasing trend of the relative difference between TC1 and the other two test-cases when the ambient temperature is equal to 35°C. Such singularity is related to the lower CO<sub>2</sub> production obtained in TC1 (which is the reference for calculating the percentual difference). As shown in Fig. 10.20 and in detail in Fig. 10.21, in fact, at 35°C the engine is used less than at 30°C, respectively the 22.2% and the 23.2% of the mission total time, which is 6483 s. Instead, the global electrical energy usage is the same (same final state of charge), therefore the balance between the initial and final SOC is the same for both cases.

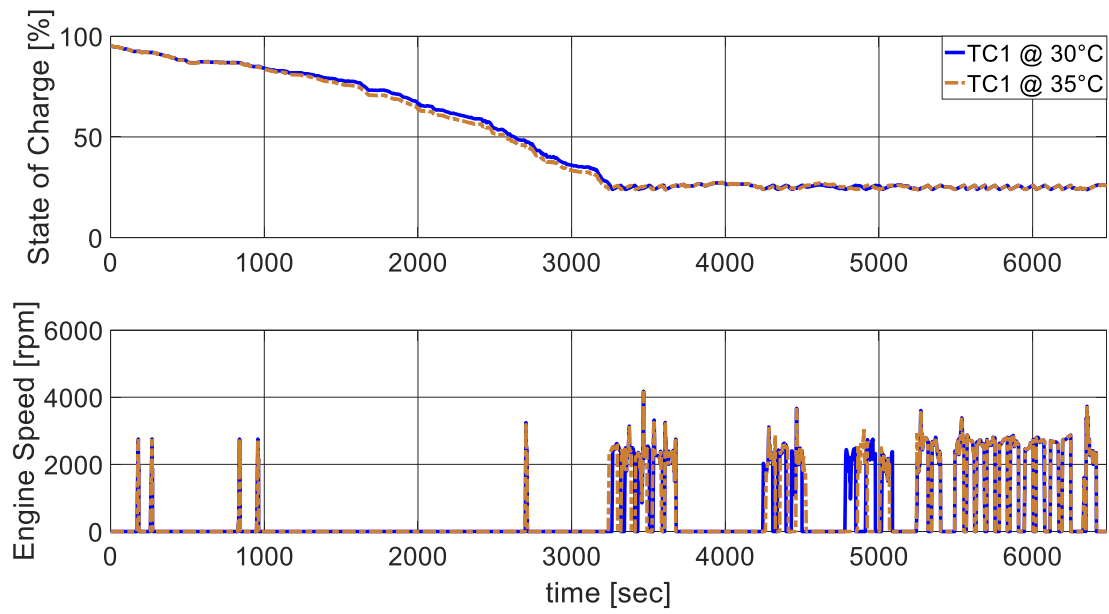


Figure 10.20 SOC and engine speed comparison at  $T_{amb}=30,35^{\circ}\text{C}$

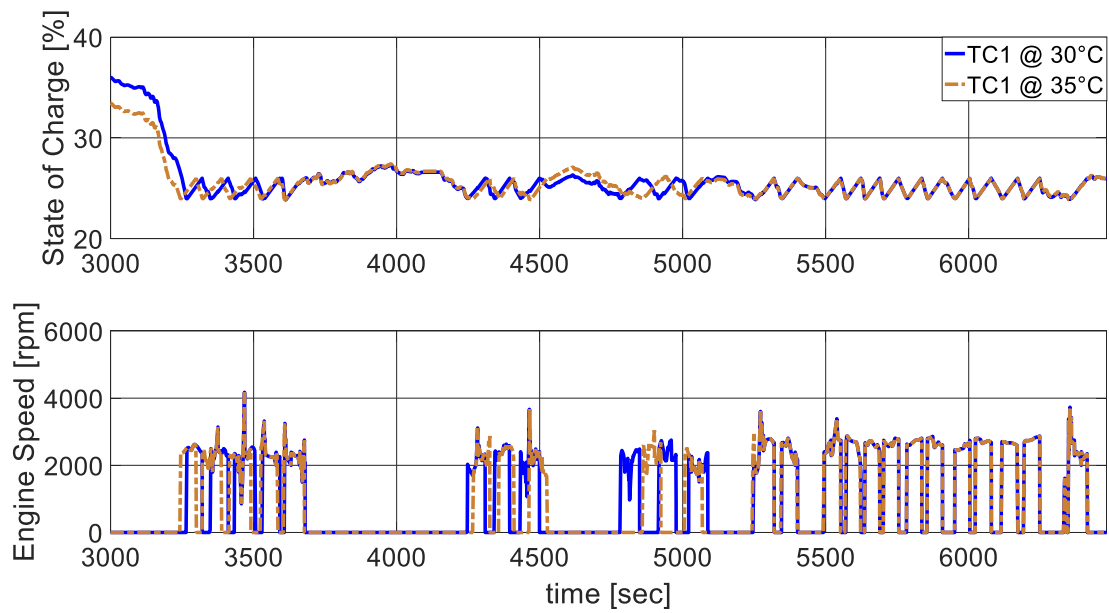


Figure 10.21 Detail of Fig. 10.20

## *V. Hardware in the Loop Implementation*

The hardware in the loop simulation environment for the vehicle has been set up as shown in Chap.6, using a rapid control prototyping unit for the supervisory controller implementation, while the rest of the vehicle, including the communication, has been simulated and implemented in real-time processing units.

Using such testing facility, it is possible to check the robustness of the developed powertrain control strategy against errors related to its real-time execution and diagnostics errors.

For the nature of the simulation, it has been only possible to test the RBS and ECMS controllers, since the optimization-based controller needs predictive information for being executed.

The aim of such additional comparison is to assess the benefits of using the proposed sub-optimal controller in working condition that are close to the in-vehicle implementation, therefore even more realistic than the model in the loop environment.

For the purpose, the reference cycle has been the RDE cycle proposed in Chap.7 and investigated in detail during this dissertation. Such choice derives from the characteristics of the powertrain, which is definitely powerful, therefore standard homologation cycles won't be representative of the reality, since they will be mainly driven in pure electric mode, given the large battery size. Instead, real driving emission tests usually consider a longer distance to be driven and, consequently, they can be more representative of common driving conditions.

### **11 HiL testing**

From the HiL simulation of the two controllers, few interesting physical quantities have been saved and shown here for the comparison, which are:

- primary vehicle parameters, such as engine and vehicle speed, accelerator pedal;
- the fuel consumption, in l/100km;
- the battery state of charge, in %;

Such trends have been considered meaningful for catching the differences between the controllers, since the SOC evolution provides an indication of the electrical energy usage along the mission, while the fuel consumption is more related to the controller performance in terms of CO<sub>2</sub> emissions. The engine speed, instead, is reported to show that the ECMS controller has a comparable behaviour with respect to the RBS one, without spikes or instability phenomena, while vehicle speed and accelerator pedal are considered representative for a correct behaviour of the vehicle in general.

The real-time control unit that performs the energy management strategy at the HiL has a complex architecture, since it uses exactly the same software architecture of the controller implemented in the prototype. Therefore, it has been chosen to replicate, for the RBS controller, the same control rules and calibrations used on-board, while the ECMS only acts on the split factor, without influencing all the other rules related to the safety of the system. Due to this particularity, the results shown in the following are different from the ones collected in the MiL comparison section (Chap.8).

#### **11.1 Real-time RBS vs Real-time ECMS**

The comparison has been made at the HiL test-bench illustrated in Chap.6, where the HCU is the hardware tested in the loop. The communication between such controller and the rest of the vehicle is simulated exactly as it is in the prototype, which means analog and digital signals, as well as CAN messages, are reproduced also in the HiL simulation environment. The clock frequency of the HCU is 100 Hz, while the rest of the system works at 1000Hz.

### 11.1.1 Vehicle parameters

As aforementioned, the comparison on the engine speed is mainly reported in order to show that the ECMS controller doesn't generate uncontrolled spikes or instability on the ICE speed when it is active. However, looking at Fig.11.1, where the trends of the engine speed in the case of heuristic and sub-optimal controller are shown, it is also possible to notice that:

- the ECMS controller allows more frequent engine on/off changes, which are 73 over the total driving mission, while the RBS one has only 25 switching phases;
- the maximum reached speed is similar for both, and it is lower than 4000 [rpm];
- when the engine is active in the same zones for both the controllers, the rotational speed is the same, meaning that the ECMS controller has no negative effects on the gear-shifting strategy.

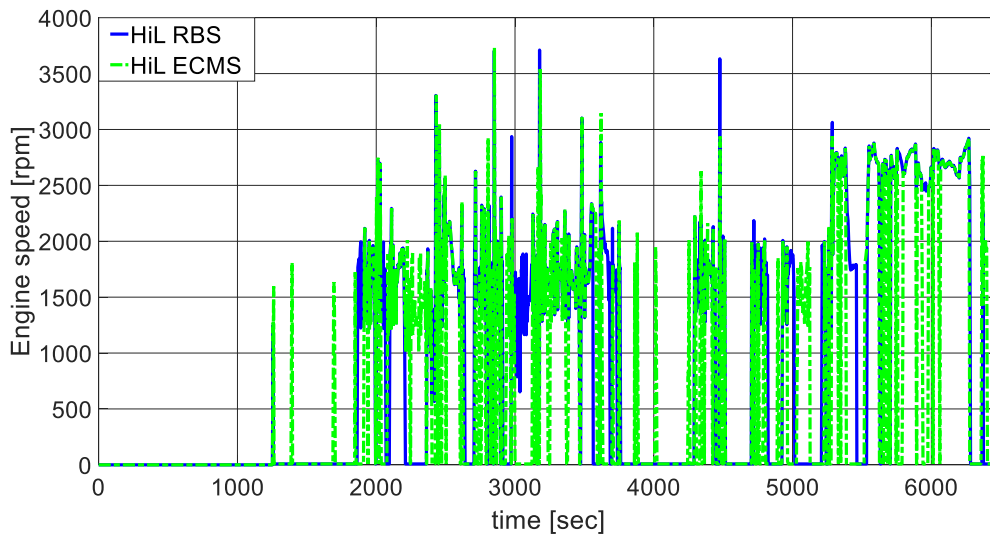


Figure 11.1 Real-time RBS vs Real-time ECMS - Engine speed

As an additional proof of the correct behavior of the sub-optimal controller during the simulation, in Fig.11.2 it is shown the actual vehicle speed calculated by the vehicle dynamics model, compared to the RBS one and the target velocity. Also in this case, there aren't particular and undesired conditions.

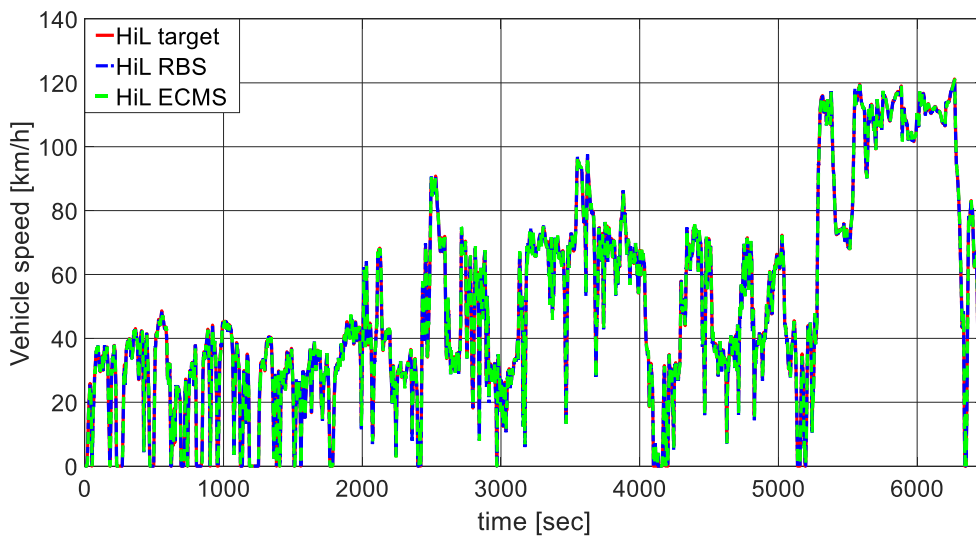


Figure 11.2 Real-time RBS vs Real-time ECMS - Vehicle speed

The accelerator pedal is considered interesting since it is strictly related to the capability of following a target vehicle speed. In fact, the driver model consists in a pre-control, which is purely open-loop and derives from an inverse longitudinal dynamic model, plus a correction coming from a PI controller that follows the target speed and close the loop with the actual vehicle speed. Accordingly, if the powertrain is not able to perform the given driving mission, the accelerator pedal reaches the request of full load in a very short time. However, nor the RBS and neither the ECMS controllers lead to this critical situation, as can be noticed in Fig.11.3.

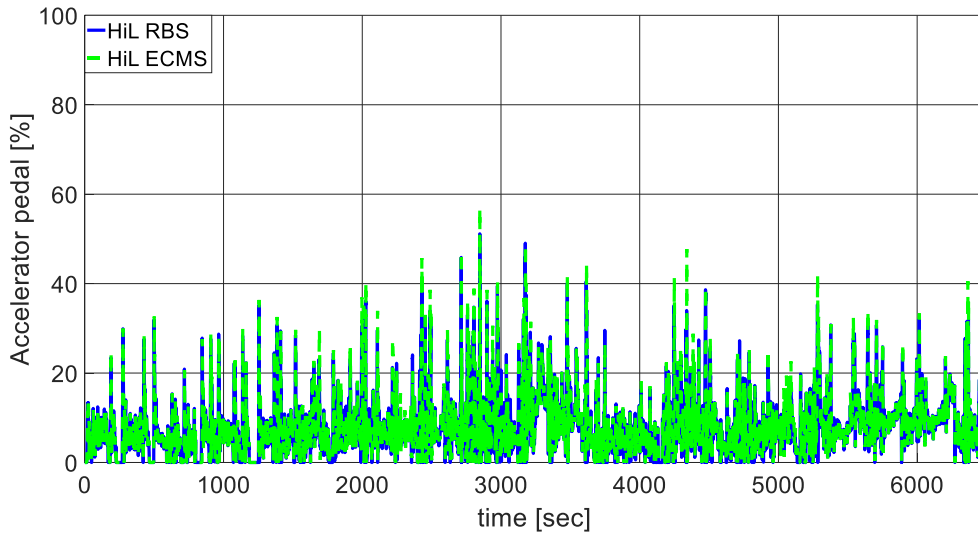


Figure 11.3 Real-time RBS vs Real-time ECMS - Accelerator pedal

### 11.1.2 Performance comparison

Once clarified the two controllers have a similar and realistic behaviour with respect to the vehicle operation, it is possible to compare the performances obtained with the real-time implementation of the controllers. The trends of the battery state of charge are reported in Fig.11.4 .

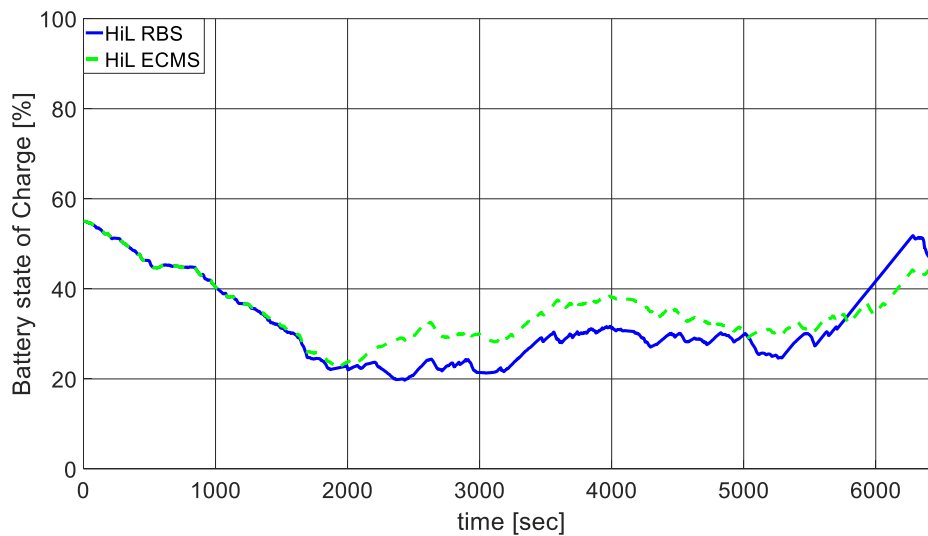


Figure 11.4 Real-time RBS vs Real-time ECMS - SOC

As a first comment, it can be said that the RBS controller implemented in the prototype vehicle, with different calibration (with respect to the MiL) and other rules related to the safety of the system and the integrity of the components, have a behaviour more similar to the sub-optimal one, since it doesn't implement exactly a charge-depleting/charge-sustaining policy. In the ECMS, instead, can be clearly seen the effect of the penalty function that effects the equivalence factor when the SOC is reaching the lower limit. While its charge-sustaining capability has been calibrated to be less influent, to have a behaviour of the battery state of charge in the middle between a charge-sustaining and a charge-depleting/charge-sustaining policy.

In general, it can be assessed that for the real-time operation, the two controllers are more similar than in the MiL environment.

Regarding the fuel consumption, the trends are reported in Fig.11.5 and, as expected from the previous analysis on the system, the ECMS controller consumes less fuel to perform the same driving mission.

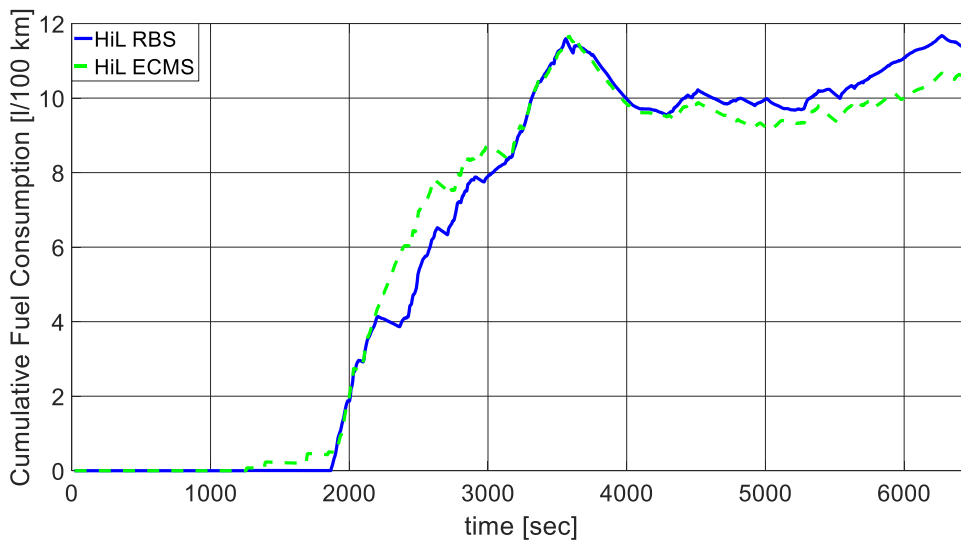


Figure 11.5 Real-time RBS vs Real-time ECMS - cFC

Since in this case the final battery state of charge is not the same for the two controllers and, in order to have a comparison on a single parameter, the same correction proposed in Par.10.2.3 has been applied and the numerical results are collected in Tab.11.1.

Table 11.1 Corrected CO2 comparison Real-time RBS vs Real-time ECMS

Strategy	SOC <sub>fin</sub>	cFC	Corrected CO <sub>2</sub>	Difference
	[%]	[l/100 km]	[g/km]	[%]
Real-time RBS	46.50	11.31	307.70	0.00
Real-time ECMS	43.44	10.53	290.00	-5.72

The real-time testing of the sub-optimal controller has shown that the potential benefits reached in the MiL simulation can be still obtained in a more detailed simulation environment, such as the HiL, by including the ECMS policy in a complex software architecture that is ready for being implemented on-board the prototype vehicle.

Even if ECMS controller has been already widely discussed in literature, almost in every case its application is limited to pure virtual simulation environment, while in this content it has been implemented in a real prototype control unit and tested in a hardware-in-the-loop simulator, confirming its maturity for online implementation.

## VI. Conclusions

As the title of the PhD project emphasises, the purpose of this three-years research activities was the modelling and optimization of energy management strategies for hybrid electric vehicles, with the aim of reducing the overall vehicle energy consumption by means of different algorithms for the powertrain control.

The reference powertrain has been a real existing prototype with a complex hybrid architecture that includes a large size engine e three additional machines. Clearly, the first challenge derives from the objective of reducing the energy consumption of such oversized powertrain in standard driving conditions.

The baseline energy management strategy was heuristic, which means that it is based on fixed rules based on logical conditions on few main vehicle parameters. No predictive or optimal control functionalities were implemented.

The first implemented energy management strategy has been a sub-optimal controller known as ECMS, for which different battery state of charge management strategies have been evaluated. In this case a fuel consumption reduction of around the 5% has been reached, mainly by better managing the recuperation phases, since the mean efficiency of the machines are similar to the baseline controller. Additional improvements in fuel economy have been possible by considering predictive information in order to optimize the energy recuperation. However, in this case, the reachable benefits are strictly related to the capacity of the electrical energy storage system since, for large battery sizes, the implemented predictive functionality may lead to limited effects on the energy consumption.

For the topic of predictive control, it has been also implemented a function to optimize the aftertreatment system of a generic Diesel-based hybrid electric vehicle. The aftertreatment temperature and NO<sub>x</sub> production are estimated over a driving horizon and used to manage the SCR system and, if needed, the engine, for being always compliant with the emission regulation, with the additional benefit of reducing the AdBlue usage, when possible.

To further improve the fuel economy of the reference vehicle, an optimal control problem has been defined for the powertrain operation over a given mission. For the purpose, it has been implemented and validated an analytic consumption model of the vehicle, used in the backward optimization. The main variables of the optimal control problem have been chosen according to the powertrain degrees of freedom. Interesting results in the achievable fuel consumption reduction (around the 9%) have been obtained with the implementation of the optimal control policy in a detailed powertrain model. As a drawback, optimization-based controllers are still not suitable for real-time operation, at least for long horizon problems, due to the large computational effort required and for the needed *a priori* knowledge of the driving mission.

The potential of optimal control applied to the powertrain has been further exploited by combining the energy management and high voltage battery thermal managements, thus considering the battery temperature as fundamental problem variable, since it influences the battery efficiency over the cycle. Moreover, also the battery cooling control has been optimized within the same loop, significantly reducing the electrical energy needed by the thermal management. In this case the maximum benefit in term of energy economy with respect to the baseline vehicle has been around the 13%.

Moreover, concerning the ECMS controller, its real-time operation at the HiL test bench has confirmed the potential benefit obtained in simulation, without undesired behaviours of the powertrain. Indeed, it is possible to assess that a big step forward to the on-board implementation has been made.

Summarizing the results collected in this dissertation, it can be assessed that, starting from the baseline vehicle, diverse energy management strategies have been modelled and implemented, increasing at each step the complexity of the algorithm from one hand, but on the other significantly reducing the vehicle overall energy consumption.

The future works for this activity will be focused on the implementation of the combined optimization-based controller in real-time and over short horizons, generating therefore a predictive powertrain control based on optimal control theory.

# References

- [1] A. Cerofolini. *Optimal Supervisory Control of Hybrid Vehicles*. PhD thesis, University of Bologna, 2014.
- [2] I. Trivic. *Comparative Analysis of Alternative Hybrid Systems for Automotive Applications*. PhD thesis, University of Bologna, 2012.
- [3] Guzzella, L. and Sciarretta, A., *Vehicle Propulsion Systems*. Springer Verlag, 3rd edition, 2012.
- [4] Zhou, S., Walker, P., Tian, Y., and Zhang, N., *Parameter Design of a Parallel Hydraulic Hybrid Vehicle Driving System Based on Regenerative Braking Control Strategy*, SAE Technical Paper, (2019-01-0368), 2019.
- [5] Huang, K., Nam-Nguyen, H., and Quang, K., *Validation of a Dynamic Model of a Hybrid Pneumatic Power System*. SAE Technical Paper, (2009-01-1304), 2011.
- [6] Huang, Y. and Wang, K., *A hybrid power driving system with an energy storage flywheel for vehicles*. SAE Technical Paper, (2007-01-4114), 2007.
- [7] DiPierro, G., Millo, F., Tansini, A., Fontaras, G. and Scassa, M., *An Integrated Experimental and Numerical Methodology for Plug-In Hybrid Electric Vehicle 0D Modelling*, SAE Technical Paper (2019-24-0072), 2019.
- [8] Böhme, T. J. and Frank, B., *Hybrid Systems, Optimal Control and Hybrid Vehicles*. Springer, 1st edition, 2017.
- [9] Jalil, N., Kheir, N. and Salman, M., *A rule-based energy management strategy for a series hybrid vehicle*, Proceedings of the 1997 American Control Conference, vol. 1, 1997.
- [10] He, X., Parten, M., and Maxwell, T., *Energy management strategies for a hybrid electric vehicle*, Proceedings of the 2005 IEEE Vehicle Power and Propulsion Conference, pp. 536–540, 2005.
- [11] Lin, C., Kang, J., Grizzle, J., and Peng, H., *Energy management strategy for a parallel hybrid electric truck*, Proceedings of the 2001 American Control Conference, vol. 4, pp. 2878–2883, 2001.
- [12] Lin, C., Peng, H., Grizzle, J., and Kang, J., *Power management strategy for a parallel hybrid electric truck*, IEEE Transactions on Control Systems Technology, vol. 11, no. 6, pp. 839–849, 2003.
- [13] Zhu, Y., Chen, Y., Tian, G., Wu, H., and Chen, Q., *A four-step method to design an energy management strategy for hybrid vehicles*, Proceedings of the 2004 American Control Conference, vol. 1, 2004.
- [14] Serrao, L., *A Comparative Analysis of Energy Management Strategies for Hybrid Electric Vehicles*. PhD thesis, Ohio State University, 2009.

- [15] Kim, N., Cha, S., and Peng, H., *Optimal Control of Hybrid Electric Vehicles Based on Pontryagin's Minimum Principle*. IEEE Transactions on Control Systems Technology, 19(5):1279–1287, 2011.
- [16] Serrao, L., Onori, S., and Rizzoni, G., *A Comparative Analysis of Energy Management Strategies for Hybrid Electric Vehicles*, ASME. *J. Dyn. Sys., Meas., Control*, 2011.
- [17] Zhang, J., Hongwen, H. and Wang, X., *Model Predictive Control Based Energy Management Strategy for a Plug-In Hybrid Electric Vehicle*, 3rd International Conference on Mechanical Engineering and Intelligent Systems, ICMEIS, 2015.
- [18] Kouvaritakis, B. and Cannon, M., *Model Predictive Control – Classical, Robust and Stochastic*, Springer, 1st edition, 2016.
- [19] Larsson, V., *Route Optimized Energy Management of Plug-in Hybrid Electric Vehicles*, PhD thesis, Chalmers University of Technology, 2014.
- [20] Murgovski, N., *Optimal Powertrain Dimensioning and Potential Assessment of Hybrid Electric Vehicles*, PhD thesis, Chalmers University of Technology, 2012.
- [21] Murgovski, N., Johannesson, L., Sjöberg, J., and Egardt, B., *Component sizing of a plug-in hybrid electric powertrain via convex optimization*, J. Mechatronics, vol. 22, no. 1, p. 106-120, 2012.
- [22] Bellman, R. E., *Dynamic Programming*, Princeton University Press, 1957.
- [23] Ambühl, D., *Energy management strategies for hybrid electric vehicles*, PhD thesis, ETH Zurich, 2009.
- [24] Varnhagen, R., *Electronic Horizon: A Map as a Sensor and Predictive Control*, L. Ray Buckendale Lecture, SAE International, (2017-01-1945), 2017.
- [25] Enzweiler, M. and Gavrilu, D.M., *Monocular Pedestrian Detection: Survey and Experiments*, IEEE Trans. Pattern Anal. Mach. Intell. 31(12):2179-2195, Dec. 2009.
- [26] Raphael, E., Kiefer, R., Reisman, P., and Hayon, G., *Development of a Camera-Based Forward Collision Alert System*, 2011.
- [27] Ruta, A., Porikli, F., Watanabe, S., and Li, Y., *In-Vehicle Camera Traffic Sign Detection and Recognition*, Mach. Vis. Appl. 22(2):359-375, 2009.
- [28] Bertozzi, M., Broggi, A., and Fascioli, A., *Vision-Based Intelligent Vehicles: State of the Art and Perspectives*, Rob. Auton. Syst. 32(1):1-16, Jul. 2000.
- [29] Wifvat, V., Shaffer, B. and Samuelson, S., *A Review of Sensor Technologies for Automotive Fuel Economy Benefits*, SAE International, (12-02-01-0001), 2019.
- [30] Kissinger, D., *Millimeter-Wave Receiver Concepts for 77 GHz Automotive Radar in Silicon-Germanium Technology*, 2012.

- [31] Beg, C., Vajedi, M., Nezhad-Ahmadi, M.R., Azad, N.L., et al., *A Cost-Effective Radar System for Automotive Powertrain Control Applications*, 15th International IEEE Conference on Intelligent Transportation Systems, 2012, 84-89.
- [32] Turner, J.D. and Austin, L., *Sensors for Automotive Telematics*, Meas. Sci. Technol. 11(2):R58-R79, Feb. 2000.
- [33] Neal, A. *Lidar vs Radar*, <https://www.fierceelectronics.com/components/lidar-vs-radar> , FierceElectronics, 2018.
- [34] Arena, F., and Pau, G., *An Overview of Vehicular Communications*, MDPI- future internet, 2019.
- [35] Gonder, J., Earleywine, M., and Sparks, W., *Analyzing Vehicle Fuel Saving Opportunities through Intelligent Driver Feedback*, SAE Int. J. Passeng. Cars - Electron. Electr.Syst. 5(2):450-461, 2012
- [36] Lang, D., Schmied, R., and Del Re, L., *Prediction of Preceding Driver Behavior for Fuel Efficient Cooperative Adaptive Cruise Control*, SAE Int. J. Engines 7(1):14-20, 2014.
- [37] Harding, J., Powell, G., Yoon, R., Joshua, F. et al., *Vehicle-to-Vehicle Communications: Readiness of V2V Technology for Application*, NHTSA, U.S. Dept of Transportation, 2014.
- [38] Raubitschek, C., Schutze, N., Kozlov, E., and Baker, B., *Predictive Driving Strategies under Urban Conditions for Reducing Fuel Consumption Based on Vehicle Environment Information*, IEEE Forum on Integrated and Sustainable Transportation Systems, 13-19, 2011.
- [39] Asadi, B. and Vahidi, A., *Predictive Cruise Control: Utilizing Upcoming Traffic Signal Information for Improving Fuel Economy and Reducing Trip Time*, IEEE Trans. Control Syst. Technol. 19(3):707-714, 2011.
- [40] Horita, Y., and Schwartz, R.S., *Extended Electronic Horizon for Automated Driving*, 14<sup>th</sup> International Conference on ITS Telecommunications (ITST), 2015.
- [41] Continental AG, <https://www.continental-automotive.com/en-gl/Passenger-Cars/Interior/Software-Solutions-and-Services/eHorizon/Static-eHorizon> , website.
- [42] OEM, off-highway, <https://www.oemoffhighway.com/electronics/sensors/press-release/12172750/continental-ehorizon-technology-provides-up-to-6-fuel-savings>, website.
- [43] Zhang, F., Hu, X., Langari, R., and Cao, D., *Energy management strategies of connected HEVs and PHEVs: Recent progress and outlook*, Progress in Energy and Combustion Science, Elsevier, 2019.
- [44] Zhang, C., Vahidi, A., Pisu, P., Li, X., and Tennant, K., *Role of terrain preview in energy management of hybrid electric vehicles*, IEEE Transactions on Vehicular Technology, 59(3), 1139-1147, 2010
- [45] Zheng, C., Xu, G., Xu, K., Pan, Z., and Liang, Q., *An energy management approach of hybrid vehicles using traffic preview information for energy saving*, Energy Conversion and Management, Volume 105, 2015.

- [46] Karbowski, D., Kim, N., and Rousseau, A., *Route-Based Online Energy Management of a PHEV and Sensitivity to Trip Prediction*, 2014 IEEE Conference on Vehicle Power and Propulsion, 2014.
- [47] Preda, I., Covaciu, D. and Ciolan, G., *Coast down test – Theoretical and experimental approach*. CONAT20104030. 2010.
- [48] Schouten, N.J., Salman, M.A. and Kehir, N.A., *Fuzzy Logic Control for Parallel Hybrid Vehicles*, IEE Transactions on Control Systems Technology, 2002.
- [49] Bianchi, D., Rolando, L., Serrao, L., Onori, S., Rizzoni, G., Al-Khayat, N., Hsieh, T.M., and Kang, P., *A Rule-Based Strategy for a Series/Parallel Hybrid Electric Vehicle: An Approach Based on Dynamic Programming*. *Proceedings of the ASME 2010 Dynamic Systems and Control Conference*. ASME 2010.
- [50] Paganelli, G., Delprat, S., Guerra, T. M., Rimaux, J., and Santin, J.-J., *Equivalent consumption minimization strategy for parallel hybrid powertrains*, in Vehicular Technology Conference, 2002. VTC Spring 2002.
- [51] Manzie, C., Dewangan, P., Corde, G., Grondin, O., and Sciarretta, A., *State of charge management for plug in hybrid electric vehicles with uncertain distance to recharge*, Control Conference (ASCC) 2013 9th Asian, pp. 1-6, 2013.
- [52] Tribioli, L., and Onori, S., *Analysis of Energy Management Strategies in Plug-in Hybrid Electric Vehicles: application to the GM Chevrolet Volt*, American Control Conference, USA, 2013
- [53] Shankar, R., Marco, J., and Assadian, F., *Design of an Optimized Charge-Blended Energy Management Strategy for a Plug-in Hybrid Vehicle*. In Proceedings of the UKACC (United Kingdom Automatic Control Council) International Conference on Control, Cardiff, UK, 3–5 September 2012; pp. 1–6.
- [54] Kural, E., and Güvenç, B.A., *Predictive-Equivalent Consumption Minimization Strategy for Energy Management of A Parallel Hybrid Vehicle for Optimal Recuperation*. Journal of Polytechnic, 2015; 18 (3): 113-124, 2015.
- [55] Onori, S., and Rizzoni, G., *Energy Management of Hybrid Electric Vehicles: 15 Years of Development at the Ohio State University*, IFP Energies nouvelles, 2014.
- [56] Serrao, L., Onori, S., and Rizzoni, G., *ECMS as a Realization of Pontryagin's Minimum Principle for HEV Control*. Proceedings of the 2009 American Control Conference, 2009.
- [57] Cervone, D., Sessa, B., Arsie, I., Pianese, C. et al., *A Comprehensive Hybrid Vehicle Model for Energetic Analyses on Different Powertrain Architectures*, SAE Technical Paper 2019-24-0064, 2019.
- [58] Guardiola, C., Dolz, V., Pla, B., and Mora, J., *Fast estimation of diesel oxidation catalysts inlet gas temperature*, Control Engineering Practice, 56(2016)148–156.
- [59] Tschopp, F., Nüesch, T., Wang, M., and Onder, C., *Optimal Energy and Emission Management of a Diesel Hybrid Electric Vehicle Equipped with a Selective Catalytic Reduction System*, SAE Technical Paper 2015-24-2548, 2015.

- [60] Salazar, M., “Time-optimal Control of the Formula 1 Hybrid Electric Power Unit”, PhD thesis, ETH Zurich, 2018.
- [61] Nüesch, T., Cerofolini, A., Mancini, G., Cavina, N., Onder, C., and Guzzella, L., *Equivalent Consumption Minimization Strategy for the Control of Real Driving NOx Emissions of a Diesel Hybrid Electric Vehicle*. *Energies* 7, no. 5: 3148-3178. 2014.
- [62] Sciarretta, A., Back, M., and Guzzella, L., *Optimal Control of Parallel Hybrid Electric Vehicles*. IEEE Transactions on Control Systems Technology, 2004.
- [63] Sciarretta, A. and Guzzella, L., *Control of Hybrid Electric Vehicles: Optimal Energy-Management Strategies*. IEEE Control Systems Magazine, 2007.
- [64] Ahmadizadeh, P., Mashadi, B., and Lodaya, D., *Energy management of a dual-mode powersplit powertrain based on the Pontryagin's minimum principle*, IET Intelligent Transport Systems, 2017.
- [65] Sharma, O., Onori, S., and Guezennec, Y. *Analysis of Pontryagin's Minimum Principle-based energy management strategy for PHEV applications*. 5th Annual Dynamic Systems and Control Conference and 11th Motion and Vibration Conference. 2012.
- [66] Hadj-Said, S., Colin, G., Ketfi-Cherif, A., and Chamaillard, Y., *Convex Optimization for Energy Management of Parallel Hybrid Electric Vehicles*, IFAC-PapersOnLine, 2016.
- [67] Nüesch, T., Elbert, P., Flankl, M., Onder, C., and Guzzella, L., *Convex Optimization for the Energy Management of Hybrid Electric Vehicles Considering Engine Start and Gearshift Costs*, MDPI-Energies, 2014.
- [68] Platt, J., Moehle, N., Fox, J. D., and Dally, W., *Optimal Operation of a Plug-In Hybrid Vehicle*, IEEE Transactions on Vehicular Technology, 2018.
- [69] Bertsekas, D., “*Dynamic Programming and Optimal Control*”. Belmont, Athena Scientific, 1995.
- [70] How, J., *Principles of optimal control*. Lecture Notes : <https://ocw.mit.edu/courses/aeronautics-and-astronautics/16-323-principles-of-optimal-control-spring-2008/lecture-notes/lec3.pdf> .
- [71] Lewis, F., and Syrmos, V., *Optimal Control*. Wiley-Interscience, 1995.
- [72] Mansour, C. and Clodic, D., *Optimized energy management control for the Toyota Hybrid System using dynamic programming on a predicted route with short computation time*, International Journal of Automotive Technologies. 2012.
- [73] Zhu, C., Lu, F., Zhang, H., Sun, J. and Mi, C. C., *A Real-Time Battery Thermal Management Strategy for Connected and Automated Hybrid Electric Vehicles (CAHEVs) Based on Iterative Dynamic Programming*, in IEEE Transactions on Vehicular Technology, 2018.
- [74] Maamria, D., Gillet, K., Colin, G., Chamaillard, Y., and Nouillant, C., *On the use of Dynamic Programming in eco-driving cycle computation for electric vehicles*, 2016 IEEE Conference on Control Applications (CCA), 2016.

- [75] D'Amato, A., Donatantonio, F., Arsie, I., and Pianese, C., *Enhancing Cruise Controllers through Finite-Horizon Driving Mission Optimization for Passenger Vehicles*, SAE Technical Paper 2018-01-1180, 2018.
- [76] Neumeister, D., Wiebelt, A. and Heckenberger, T., *Systemeinbindung einer Lithium-Ionen-Batterie in Hybrid- und Elektroautos*. ATZ - Automobiltechnische Zeitschrift , 2010.

# List of Figures

Figure 1.1. Series HEV energy flow ([8]) .....	3
Figure 1.2. Parallel HEV energy flow ([8]).....	3
Figure 1.3. Power-split HEV energy flow ([8]).....	4
Figure 1.4. Overview of HEV characteristics ([8]) .....	4
Figure 1.5. HEV's powertrain control architecture.....	5
Figure 1.6. MPC loop .....	6
Figure 2.1. Vehicle sensors integration .....	10
Figure 2.2. Vehicle communication technologies .....	11
Figure 2.3. eHorizon information example .....	12
Figure 3.1 Powertrain architecture .....	13
Figure 4.1 Longitudinal resistance forces acting on a moving vehicle .....	14
Figure 4.2 Equivalent series resistance (ESR) model for cell electrical characterization. ....	17
Figure 5.1. Engine Maximum Torque and Power vs Engine Speed.....	18
Figure 5.2 Engine efficiency map.....	19
Figure 5.3 Electric Motor Maximum Torque vs Motor Speed.....	19
Figure 5.4 Motor efficiency map.....	20
Figure 5.5 Battery Open Circuit Voltage vs SOC .....	21
Figure 5.6 Battery internal Resistance vs Battery Temperature Range.....	21
Figure 6.1 HiL setup.....	22
Figure 7.1 MiL validation.....	23
Figure 7.2 RDE cycle vehicle speed (a) and road altitude (b) profiles.....	24
Figure 7.3 Analytic model validation.....	24
Figure 8.1 ECMS controller block diagram .....	29
Figure 8.2 ECMS controller Charge-Sustaining.....	30
Figure 8.3 ECMS controller Charge-Blended .....	31
Figure 8.4 ECMS controller Charge-Depleting/Charge Sustaining .....	32
Figure 8.5 RBS results - SOC.....	33
Figure 8.6 RBS results – cFC .....	33
Figure 8.7 ECMS results - SOC .....	34
Figure 8.8 ECMS results – cFC.....	34
Figure 8.9 Average Efficiencies on RDE cycle RBS vs ECMS.....	35
Figure 8.10 Fuel Consumption RBS vs ECMS .....	35
Figure 8.11 Engine provided energy on RDE cycle RBS vs ECMS .....	36
Figure 8.12 Recovered energy on RDE cycle RBS vs ECMS .....	37
Figure 9.1 Predictive SOC target ideal modification.....	38
Figure 9.2 ECMS-CS vs ECMS-predictive_CS – SOC .....	39
Figure 9.3 ECMS-CS vs ECMS-predictive_CS – cFC .....	40
Figure 9.4 Average Efficiencies on RDE cycle ECMS-CS vs ECMS - predictive CS .....	40
Figure 9.5 15Ah-ECMS-CS vs ECMS-predictive_CS – SOC .....	41
Figure 9.6 6Ah-ECMS-CS vs ECMS-predictive_CS – SOC .....	42
Figure 9.7 SOC target modification for different battery capacities .....	42
Figure 9.8 Predictive Aftertreatment control function algorithm structure .....	43
Figure 9.9 Aftertreatment Temperature model validation.....	45
Figure 9.10 NOx production model validation.....	46
Figure 9.11 Strategy possible cases.....	46
Figure 9.12 Predictive Aftertreatment control function Input.....	48
Figure 9.13 Aftertreatment Temperature prediction.....	48
Figure 9.14 Cumulative NOx production @ engine - out estimation.....	49
Figure 9.15 Cumulative NOx production @ tailpipe estimation.....	49

Figure 9.16 Predictive emission control strategy decisions for Case2 .....	50
Figure 9.17 Predictive Aftertreatment control function Input (Case1).....	50
Figure 9.18 Predictive emission control strategy decision for Case1 .....	51
Figure 9.19 Predictive Aftertreatment control function Input (Case3).....	51
Figure 9.20 Predictive emission control strategy decision for Case3 .....	52
Figure 9.21 Torque gradient limitation (a) and consequent NOx production reduction (b) for Case3 .....	52
Figure 10.1 Generic discrete-time dynamic system .....	54
Figure 10.2 Control variable for target PHEV.....	57
Figure 10.3 Sensitivity of the Global Cost to variables discretization .....	58
Figure 10.4 Forward implementation of the optimal control policy.....	60
Figure 10.5 DDP vs ECMS-CDCS vs RBS – SOC.....	61
Figure 10.6 DDP vs ECMS-CDCS vs RBS – cFC.....	62
Figure 10.7 Average Efficiencies on RDE cycle DDP vs ECMS CDCS vs RBS.....	62
Figure 10.8 RDE3: DDP vs ECMS-CDCS vs RBS – SOC.....	63
Figure 10.9 Average Efficiencies on RDE3 cycle DDP vs ECMS CDCS vs RBS.....	64
Figure 10.10 HV Battery cooling circuit.....	64
Figure 10.11 Control variable for combined optimization of PHEV .....	69
Figure 10.12 Forward implementation of the combined-optimal control policy .....	71
Figure 10.13 Comparison @ Ambient Temperature =40°C – SOC.....	72
Figure 10.14 Comparison @ Ambient Temperature =40°C – T <sub>Batt</sub> .....	72
Figure 10.15 Comparison @ Ambient Temperature =40°C – Energy consumption cooling circuit .....	73
Figure 10.16 Comparison @ Ambient Temperature =10°C – SOC.....	73
Figure 10.17 Comparison @ Ambient Temperature =10°C – T <sub>Batt</sub> .....	74
Figure 10.18 Comparison @ Ambient Temperature =10°C – Energy consumption cooling circuit .....	74
Figure 10.19 Test-cases results for different ambient temperatures - Comparison.....	75
Figure 10.20 SOC and engine speed comparison at T <sub>amb</sub> =30,35°C.....	76
Figure 10.21 Detail of Fig. 10.20 .....	76
Figure 11.1 Real-time RBS vs Real-time ECMS - Engine speed.....	78
Figure 11.2 Real-time RBS vs Real-time ECMS - Vehicle speed.....	78
Figure 11.3 Real-time RBS vs Real-time ECMS - Accelerator pedal.....	79
Figure 11.4 Real-time RBS vs Real-time ECMS - SOC .....	79
Figure 11.5 Real-time RBS vs Real-time ECMS - cFC .....	80

## *List of Abbreviations*

<b>BMS</b>	Battery Management System
<b>CB</b>	Charge Blended
<b>CD-CS</b>	Charge-Depleting/Charge Sustaining
<b>CS</b>	Charge Sustaining
<b>DDP</b>	Discrete dynamic programming
<b>ECMS</b>	Equivalent Consumption Minimization Strategy
<b>EM</b>	Electric motor
<b>EMS</b>	Energy Management Strategy
<b>FC</b>	Fuel Consumption
<b>HEV</b>	Hybrid Electrical Vehicle
<b>ICE</b>	Internal Combustion Engine
<b>ISG</b>	Integrated Starter-Generator
<b>MiL</b>	Model in the Loop
<b>NEDC</b>	New European Driving Cycle
<b>NOx</b>	Nitrogen Oxides
<b>PHEV</b>	Plug-in Hybrid Electrical Vehicle
<b>RDE</b>	Real Driving Emission
<b>s</b>	Equivalence Factor
<b>SOC</b>	State of Charge
<b>SoCMS</b>	State of Charge Management Strategy
<b>TMS</b>	Thermal Management Strategy